UNIVERSITÀ DEGLI STUDI DI PARMA

Dipartimento di Chimica Organica ed Industriale

Ph.D. in Science and Technology of
Innovative Materials

XXII Cycle

Harnessing Cavitand Chemistry:

Polymers, Receptors and Self-Assembly on Silicon

Francesca Tancini

Coordinator: **Prof. Anna Painelli**

Supervisor: **Prof. Enrico Dalcanale**

Author: **Francesca Tancini**

Contents

CHAPTER 1

A General Introduction to Supramolecular Chemistry

CHAPTER 2

Host-Guest Supramolecular Polymers

CHAPTER 3

Dual-Coded Supramolecular Frameworks

CHAPTER 4

Cavitand-based Ion-Pair Receptors

CHAPTER 5

Calix-Pyrrole-based Receptors

CHAPTER 6

Hierarchical Self assembly on Silicon

A General Introduction to Supramolecular Chemistry

1

1.1 The "chemistry beyond the molecule".

While molecular chemistry is based on covalent interactions, supramolecular chemistry could be described as the field of molecular assemblies and of intermolecular bonding. According the definition given by Jean-Marie Lehn in 1988, it is the "*chemistry beyond the molecule*",[1] and it aims at developing highly complex chemical systems starting from molecular components held together by noncovalent forces.[2]

Based on self-assembly[3] and self-organization processes,[4] supramolecular chemistry is intrinsically dynamic, which allows the spontaneous but information-directed generation of organized structures under equilibrium conditions. Suitable manipulation of structural subunits and interaction codes gives rise to a wide and new variety of systems. Thanks to a constant and continuous development, supramolecular chemistry widens the playground for scientists. Simple systems are replaced by ever more complex ones. Building-blocks become more intricate, with respect to both structure and function. Dynamic chemical bonding range from the tiny van der Waals forces to the thermodynamically reversible covalent interactions. The attention, previously focused exclusively on the solid and solution states, is now pointing through surfaces and interfaces, tackling more complex systems, featuring multivalency and cooperativity.

With its challenges, ever more function-oriented and application driven, supramolecular science constitutes a multidisciplinary and interdisciplinary domain that provides a highly fertile ground for the creativity of scientists from all origins.

The present thesis takes its place in this context, and it shows, by harnessing noncovalent interactions within different building-blocks, how it is possible to generate functional materials, such as supramolecular polymers and ion-pair receptors, as well as to realize hierarchical self-assembly on surfaces.

1.2 Secondary Interactions: a "glue" to assemble supramolecular architectures.

G. R. Desiraju wrote *"in supramolecular chemistry, one makes higher level aggregates (supermolecules) from lower level entities (molecules) using weak intermolecular interactions as a glue"*.[5]
The term *supramolecular* refers in fact to ordered molecular aggregates, held together by noncovalent interactions, such as metal-ligand bonds, hydrogen bonds, or van der Waals' forces. Because of the weakness of such binding interactions, the formation of supramolecular assemblies is often thermodynamically dictated, and it commonly results from spontaneous self-assembly processes, rather than from sequential bond-forming strategies. In particular, if self-assembly could be simply defined as the reversible collection and aggregation of components into a confined entity, self-organization is the real driving force that leads to complex supramolecular systems. After a first step, involving the reciprocal molecular recognition among the structural subunits, thanks to selective binding motifs, the growth of a supramolecular structure progresses through sequential and eventually hierarchical interaction of multiple components, according to cooperative or linear behavior.
The choice of the interactional motifs is therefore crucial in supramolecular chemistry, because it determines the robustness of the final products, as well as their plasticity, their structure and therefore their specific physical and chemical properties.
In the following paragraphs, we will focus briefly on the binding motifs that have been exploited in this thesis.

- ***Hydrogen-Bonding.***

Hydrogen bonding is a type of attractive intermolecular force that exists between two partial electric charges of opposite polarity. As the name "hydrogen bond" implies, one part of the bond involves a hydrogen atom, which is attached to a relatively electronegative heteroatom, such as oxygen, nitrogen or fluorine, and it is called the *hydrogen-bond donor (D-H)*. The electronegative element attracts the electron cloud from around the hydrogen nucleus and, by decentralizing the cloud, leaves the atom with a positive partial charge. The hydrogen bond results when this positive charge density attracts a lone pair of electrons on another heteroatom, which becomes the *hydrogen-bond acceptor (A)*. Depending on the reciprocal location of H-donors and H-acceptors, H-bonding can be intramolecular or intermolecular, respectively if donor and acceptor are located on the same molecule or on different ones.

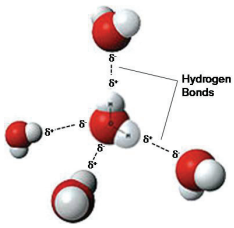

Figure 1: 3D model of hydrogen-bonds in water.

Hydrogen bonding is generally considered with a geometry D-H···A. Some of the functions commonly used to evaluate its strength involve a modified Lennard-Jones potential, with a D-H···A angle dependent term like:

$$\boldsymbol{E}_{\boldsymbol{H-Bond}}(\mathrm{R}) = \varepsilon\left[\boldsymbol{A}\left(\frac{\boldsymbol{R_0}}{\boldsymbol{R}}\right)^{\boldsymbol{12}} - \boldsymbol{B}\left(\frac{\boldsymbol{R_0}}{\boldsymbol{R}}\right)^{\boldsymbol{10}}\right](\boldsymbol{cos\theta}_{\boldsymbol{D-H\cdots A}})^{\boldsymbol{4}}$$

where R is the distance between the D and A, R_0 is the equilibrium distance, ε is the depth of the potential and A and B are adjustable parameters.[6] From the above reported equation it appears that, for single donor acceptor systems, such as D-H···A, the strongest hydrogen bonds are collinear.[7] Electrostatic calculations suggest that deviation of 20° from linearity leads to a decrease in binding energy of approximately 10%.[8] In double acceptor systems, bifurcated hydrogen

bonds with nonlinear angles are preferred. For example, in protein structures, the 90% of N-H···O bonds lie between 140° and 180°, and they are centered around 158°. For C=O···H, the range is more broadly distributed between 90° and 160° and centered around 129°.[9]
Although stronger than most other intermolecular forces, the hydrogen bond is much weaker than both the ionic bond and the covalent bond. Namely it can vary in strength from very weak (1-2 kJ mol^{-1}) to extremely strong (higher than 155 kJ mol^{-1}), as in the ion [HF_2^-].[10] Typical values include:

F-H···F (155 kJ/mol)

O-H···N (29 kJ/mol)

O-H···O (21 kJ/mol)

N-H···N (13 kJ/mol)

N-H···O (8 kJ/mol)

In contrast to covalent bonds, which once formed are stable under normal conditions, hydrogen bonds are reversible and their strength depends on the chemical environment. Therefore, a suitable tuning of the external parameters allows the direct control of the physical properties of supramolecular assemblies based on this kind of interaction. For example, the well known solvent dependence of H-bonded complex stability in solution, can be exploited to obtain robust systems in apolar, aprotic solvents, or to reduce the association, by moving to polar solvents, which can act as competitive H-bond acceptor or donor.
Stable supramolecular assemblies can also be obtained by a combination of multiple hydrogen bonds. In this case, not only the primary hydrogen bonds play a role in the stability of the final complexes, but also the secondary electrostatic interactions, which can act according to a repulsive or attractive fashion.[11] These effects have been quantified by Sartorius and Schneider[12] for the prediction of multiple H-bonded complex stability in chloroform.
The length of hydrogen bonds depends on the interaction strength, as well as on temperature and pressure. Namely it can range from 1.2 Å, when the interaction features a strong covalent character, to values

higher than 2.2 Å, when the binding features a more dispersive nature.[10]
As a consequence of their specificity, directionality, and versatility[13] hydrogen bonds have been widely exploited in supramolecular chemistry, giving rise to dynamic and tunable materials, such as polymers, dendrimers, or molecular containers.

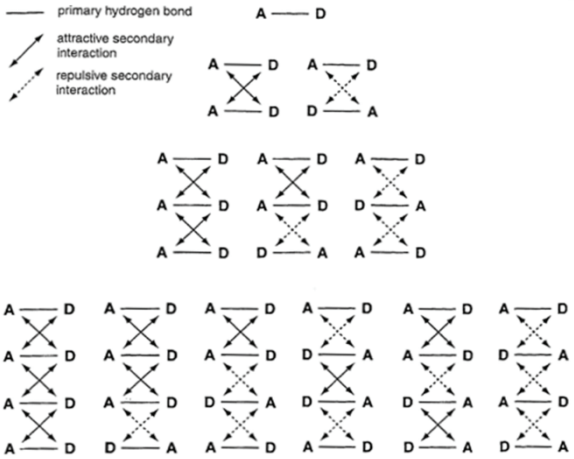

Figure 2: Schematic representation of complexes containing one to four H-bond together with the secondary attractive or repulsive electrostatic interactions.[11]

- ***Metal-Ligand Coordination.***

Coordinative metal-bonds feature a great versatility, thanks to the large number of structural motifs and bond energies that are available through coordination chemistry. Moreover, the high directionality displayed by coordinative bonds is particularly appealing for supramolecular chemists, allowing the rational design of the structural subunits to bind together, as well as the structural control of the entities formed by self-assembly.
The energy bond related to metal-ligand interactions ranges from the strong value of covalent binding, in carbon-based molecules, to the weak one, characterizing biological systems.
When the energy required to induce a geometrical distortion around the metal center is relatively low, dynamic coordination complexes can be

obtained, able to give ligand exchange or pseudorotation around the bond axes, resulting in the tuning of the final shape of the self-assembled entities. Also, the availability of a wide variety of metals, bearing different coordination numbers and different coordination geometries, as well as the chance to act on the orientation of the ligand binding sites, provide powerful means to model the structure of supramolecular architectures.
The most common potential building-blocks embrace nitrogen-containing molecules, cyano-substituted ligands and phosphorous-containing ligands.
The most used metals are zinc and palladium, which form labile reversible complexes, or ruthenium, rhenium and platinum, whose adducts are very stable or become reversible only by addition of competitive adducts.

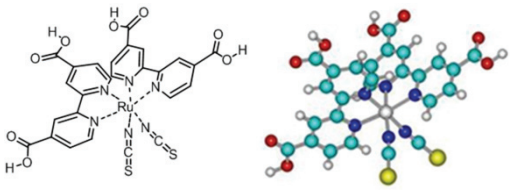

Figure 3: An example of transition metal complex comprising a Ru-centre and polypyridine ligands.

Metal-ligand motifs have been frequently used to extend covalent oligomers or polymers, and to improve their initial structural and mechanical properties. Also the cross-link of polymers bearing multiple metal-coordination sites is quite common in supramolecular chemistry, as well as the induction of such redox or thermo-reversibility by exploiting metals properties.

- ***Ion–Dipole Interactions.***

Numerous supramolecular complexes owe their stability and function to electrostatic forces between a permanent charge and neutral species featuring a dipole.

Ion-dipole interactions occur with a strength ranging between 50 and 200 kJmol^{-1}, and they became stronger as either the charge on the ion increases, or as the magnitude of the dipole of the polar molecule increases. The interaction energy depends also upon the distance from the center of the ion to the midpoint of the dipole. Said that, temperature changes can be used to enhance or to decrease the binding strength.

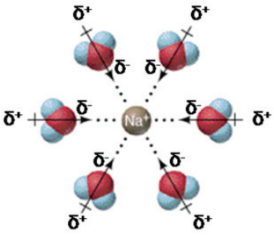

Figure 4: Ion-dipole interaction between Na^+ and H_2O molecules.

Host-guest chemistry displays a huge number of complexes based on ion-dipole interactions. For example, the binding of protonated amines in cucurbituril macrocycle[14] is largely attributable to ion–dipole forces, as well as the inclusion of alkali-metal and alkaline-earth cations by crown ethers[15] and related compounds.

- ***CH-π Interactions.***

Even if weaker than the ordinary hydrogen-bonds, the CH-π interactions (2 ~ 8 kJ mol^{-1}), were shown to play a substantial role in a variety of chemical and biological phenomena. They can be described as the interactions occurring between soft acids (CHs in an alkyl group) and soft bases (π-systems). Suggestion for the presence of attractive interactions between C-H groups and π-electron systems came from studies on conformational problems of a series of compounds bearing an aliphatic group on one side of the molecule and a phenyl group at the other terminus.[16] Stabilization of this bond comes essentially from the dispersion forces and charge-transfer interactions, while contribution from the electrostatic energy is relatively unimportant.

Orientation dependent and additive in enthalpy, CH-π bonds can act in a cooperative fashion when multiple CH groups participate simultaneously in interactions with π-groups.

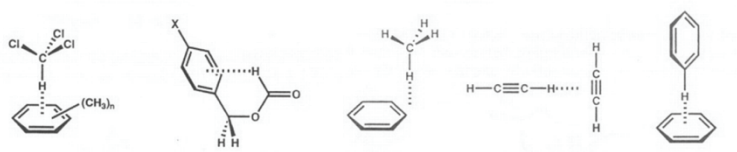

Figure 5: Examples of CH-π interactions.

A relevant feature of this kind of interaction is that it is effective in water as well as in nonpolar media, with significant consequences on molecular recognition in biological environments.
In any case, CH-π interacting species were found to become more favored as the π-electron density of the involved aromatic system increases, and, at the same time, the hydrogens of the partner molecule become more acidic.
CH-π interaction plays a crucial role in determining the selectivity of organic reactions, the properties of solid materials, such as graphite and fullerene, as well as the specificity of substrate and biologically important macromolecules.

- ***π-π Interactions.***

Weak electrostatic π-π interactions occur between aromatic moieties, because of the intermolecular overlapping of p-orbital in π-conjugated systems.[17] Accordingly, more π-electrons are involved in the interaction, the stronger is the bonding.
The stabilizing energy of π−π interactions also includes induced dipole and dispersion contributions.
Aromatic interactions are intriguing in molecular recognition processes, since they are expected to be strong in water (because of the hydrophobic component of the interaction), and at the same time, selective, if the electrostatic component is significant. Consequently they provide the best features of both hydrophobic interactions and hydrogen bonding.
Two general types of aromatic π−π interactions are face-to-face and edge-to-face. The latter is actually a C−H···π interaction (the C−H bond

generally having a small dipole moment). The attraction in these two orientations comes from the interaction between positively charged hydrogen atoms and negatively charged π-face of aromatic system. The perfect facial alignment of face-to-face orientation is unlikely because of the electrostatic repulsion between the two negatively charged π-systems of the aromatic rings. The distance between the aromatic π−π faces is about 3.3−3.8 Å.

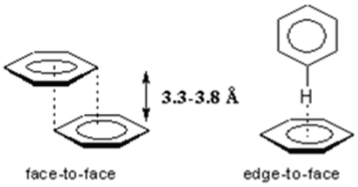

Figure 6: The limiting types of aromatic π −π interactions: face-to-face and edge-to-face orientations.

π-π interactions are one of the principal noncovalent forces governing supramolecular organization and recognition processes. They are key interactions influencing the tertiary structure of proteins[18] and the vertical base stacking in DNA.[19] Moreover they also play a major role in stabilizing host-guest complexes[20] and in self-assembly based on synthetic molecules.[21]

- ***Host-Guest Complexation.***

Host-guest complexation involves receptor molecules containing hollow and enforced spaces, and smaller species that can be located inside them.
In a kind of designer-chemistry, different functional groups are incorporated into the host molecules, so that their orientation facilitates strong binding to corresponding fragments in the guest.
A variety of forces, such as electrostatic interaction, hydrophobic interaction and hydrogen bonding, are utilized to achieve higher affinity and selectivity in the binding processes.
Particular attention is focused not only on the structure of the interacting units, but also on the thermodynamics that control the inclusion phenomena. Namely, host and guest are devised in order to

maximize favorable enthalpic and, when possible, entropic contributions during the complexation processes.
Based on structurally well-defined pattern of intermolecular interactions, host-guest chemistry leads to a huge variety of supramolecular architectures, embracing polymers and sensors, molecular machines and functional surfaces.

1.3 Structural Subunits to build Supramolecular Frameworks.

If secondary interactions are the "glue" to assemble supramolecular architectures, macromolecules such as crown-ethers, cavitands, velcrands, cryptands, spherands, calixarenes, porphyrins, pyrroles, and so on, are the structural subunits which forms these higher level aggregates.

In the following paragraph we will describe briefly the structural properties and the most important association features for the macromolecules exploited in this thesis as building-blocks.

- **Cavitands.**

Cavitands have been defined by Cram[22] as *"synthetic organic compounds with enforced cavities large enough to complex complementary organic molecules or ions."* Because of their versatile behavior as molecular receptors, these compounds are extremely interesting in host-guest chemistry and they have been extensively studied in the solid state,[23] in solution[24] and in the gas phase.[25]
Suitable scaffolds for the construction of cavitands are resorcin[4]arenes.

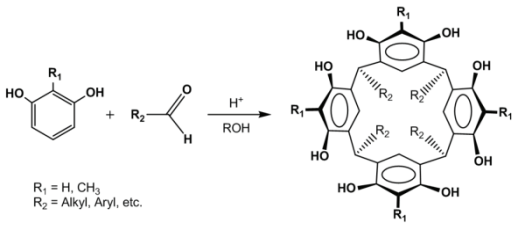

Figure 7: Synthesis of resorcin[4]arenes.

They can be easily prepared by the acid-catalyzed condensation between resorcinol and either aliphatic or aromatic aldehydes.[26]
A further functionalization of the resulting macrocycles can be achieved by means of bridging reactions on the four couples of adjacent phenolic oxygens. The choice of the bridging groups is pivotal to determine shape, dimensions and complexation properties of the final cavitand.

Tetraphosphonate-bridged Cavitands.

Tetraphosphonate cavitands are resorcinarene-based molecular receptors presenting four P(V) moieties as bridging units.[27] The introduction of phosphonate groups imparts to these systems special complexing properties toward positively charged species, such as alkali-metal and alkaline-earth cations,[28] or ammonium and N-methylpyridinium salts.[29]
The presence of four stereogenic centers in the tetraphosphonate cavitands gives rise to six possible diasteromeric isomers, differing from each other for the orientation of the P=O moieties, inward (i) or outward (o) the cavity.[30]

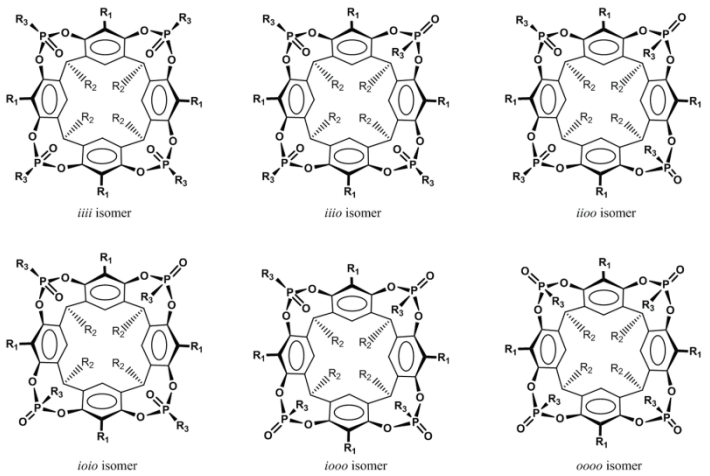

Figure 8: Tetraphosphonate cavitand isomers.

Stereochemistry is pivotal to determine the cavitand complexing capability. The higher binding has been observed for the isomer featuring four P=O groups converging toward the center of the cavity.

The main specific interactions responsible for recognition processes are H-bonding, CH-π, and cation-dipole forces.[31] Namely, a multiple ion-dipole interaction occurs between the inward facing P=O groups and the positively charged guest moieties; directional H-bonding involve two adjacent P=O groups in presence of H-donor species; CH-π interaction acts between guest acidic protons (e.g. CH_3 group in N-methylpyridinium salts) and the π-basic cavity. All these forces operate in a synergistic fashion, assuring high association constant[29] for the complex formation (for example, in the order of 10^7 M^{-1} for N-methylpyridinium guests, and exceeding 10^9 M^{-1} for methyl ammonium species).
When the P=O moieties are replaced by the P=S ones, by means of oxidation reaction with sulfur on P(III) precursor,[29b] the structurally related tetrathiophosphonate cavitands are obtained.
These compounds feature ionophoric properties toward soft metals,[32] such as Ag^+, Hg^{2+}, Tl^+, but result inefficient in pyridinium or ammonium binding, because of the weaker H-bonding and ion-dipole interactions that they can form with these guests.[29b]

In this thesis, host-guest properties of tetraphosphonate cavitands have been exploited to form supramolecular polymers, and to develop hierarchical self-assembly protocols on surface (Chapter 2 and Chapter 6).

Tetraquinoxaline-bridged Cavitands.

Tetraquinoxaline cavitands result from nucleophilic aromatic substitution with 2,3-dichloroquinoxaline on the phenolic oxydryl moieties of a resorcin[4]arene.
As reported by Cram,[33] in solution, quinoxaline-cavitands act as flaps: when they are in the fully axial conformation (*aaaa*) resemble a *vase,* with a large interior cavity, while, when they are in the fully equatorial conformation (*eeee*), the model looks like a *kite*.[34] In compounds without methyl groups in apical position at the resorcinarene, the *vase* and *kite* forms are equilibrating. At room temperature, in apolar solvents, only the close *vase* conformation is present. Upon cooling, the population of the open and less symmetric *kite* form increases, until all cavitands are transformed at ≈ 230 K. This behavior is due to the

different solvation of the cavitand in its two geometrically conformations.[35] In the open *kite* form, the solvent-accessible surface is much larger than in the close state, so that much more solvent molecules can stabilize this species by noncovalent interactions. This kind of stabilization is effective only at low temperature. In fact, interactions between solvent and cavitand result in a reduced solvent translational freedom, which determines an entropic loss that becomes too unfavorable at higher temperatures ($\Delta G = \Delta H - T\Delta S$).
Changing the pH is another effective method to exert dynamic control over the *kite-vase* equilibrium.[36] Since the quinoxaline nitrogen atoms are weakly basic ($pK_{a\ 293\ K} = 0.56$),[37] addition of a strong acid, such as CF_3COOH ($pK_{a\ 293\ K} = 0.52$)[37] protonates them, inducing repulsive forces that lead the cavitand to assume the *kite* conformation, where the positive charges are moved apart from each other.

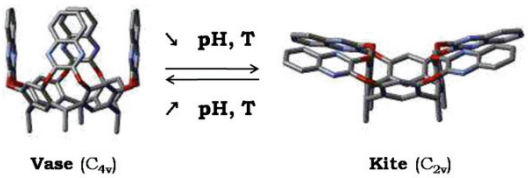

Figure 9: *Kite-vase* equilibrium for quinoxaline-cavitands.

A totally different behavior was observed when cavitands present methyl groups in apical position. In this case, the substituents sterically inhibit formation of the *vase* species, allowing the *kite* one only.[38]

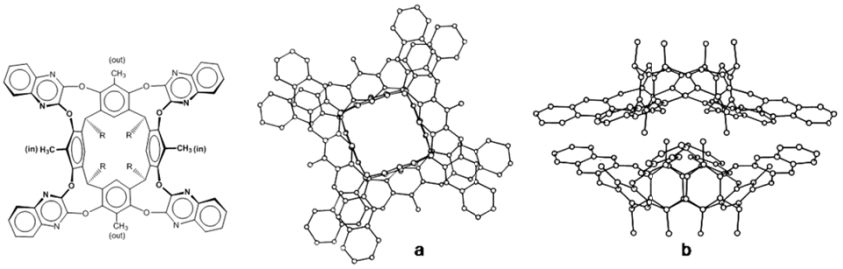

Figure 10: *Kite-kite* quinoxaline-cavitand dimers: a) top and b) side view.

When two molecular models are fitted to one another, they share a large common surface composed of the tetramethyl lock and their large rectangular areas in roughly parallel planes: in particular, in the X-ray crystal structure, four sets of quinoxaline "wings" contact one another, with their inner six-membered rings lying face-to-face.
Differently, quinoxaline-cavitands with four H instead of CH_3 in the apical position show no tendency to dimerize both in the kite and vase forms.[38]
The best criterion of determining the cavitand structure in solution came from ^1H NMR spectroscopy.[38] In fact the signals for 'up' methyls in the dimer are all upfield of those of the monomer, because located in the shielding region of the tilted benzene ring pointing out. On the contrary, the 'out' CH_3 protons in the dimer are all downfield of those of monomer, because lying in the deshielding region of the complexing partners.

δ of protons	**Dimer**	**Monomer**
$ArCH_3$ *out*	3.16 ppm	2.66 ppm
$ArCH_3$ *in*	2.23 ppm	2.52 ppm

Table 1: Monomer *versus* dimer chemical shifts for ArCH_3 protons.

Dipole-dipole, van der Waals attractions and solvophobic effects are the driving forces for dimerization.

In this thesis, dimerization capability of quinoxaline-bridged cavitands have been exploited, in combination with H-bonding, to assemble dual-coded supramolecular polymers (Chapter 3).

Tetramethylene-bridged Cavitands.

Conformationally mobile resorcinar[4]arenes can be converted to bowl-shaped cavitands by fourfold ring closures, which introduce methylene bridges anchored by the four sets of proximate oxygens.[23]

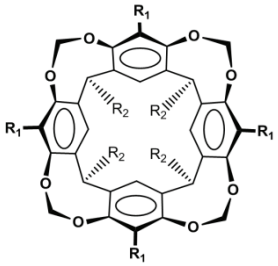

Figure 11: Tetramethylene-bridged cavitands.

Cavitand depth and shape vary with the character of the R_1 substituents (H, CH_3, Br, I, etc.).
These compounds possess enforced concave surfaces of molecular dimensions and form solvates with simple guest molecules, most of which are complementary to their cavities, such as CH_2Cl_2, $CHCl_3$, SO_2, CH_3CN, $C_6H_5CH_3$, and C_6H_6.[37] Methylene-bridged cavitands stand at the lower end of complexation ability, as they bind the guest only through CH_3-π interaction.
Even if, recently, Schalley and coworkers demonstrated that these cavitands are able to complex anionic species in gas phase,[39] in solution, where the solvent effect cannot be neglected, no evidences have ever been shown of such affinity neither for anions nor for cations.

Accordingly, in this thesis, we exploited methylene-bridged cavitand simply as preorganized inert scaffold to realize organic soluble molecules, to which we imparted ion-pair recognition capability, by introduction of further suitable functional groups at the lower rim (Chapter 4).

- **Calix[4]pyrroles.**

Calix[4]pyrrole belongs to the family of hetero-calixarene macrocycles,[40] which have four pyrrole units instead of the phenolic ones.
They are generally prepared in one step, by acid-catalyzed condensation between pyrrole and a symmetric or asymmetric ketones.[41]

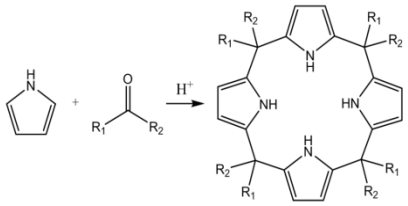

Figure 12: Synthesis of calix[4]pyrroles.

They can also be obtained by mixed condensations,[42] involving a specific pyrrole with more than one type of ketone, or a specific ketone and more than one type of pyrrole. Otherwise, [2+2] and [1+3] condensations[42] are possible, occurring respectively between two dipyrromethane units, or between a tripyrrane and a pyrrole. All these procedures, generally, show a lower yield than the one-pot homocondensation, due to the fact that a mixture of product is formed.
In any case tetrapyrrolic macrocycles, structurally similar, but electronically different than porphyrins, are obtained in such a way that the 18π-electron aromatic structure cannot be formed. Thus each pyrrole results electronically independent and, consequently, it can donate one hydrogen bond. Because of that, these compounds are able to bind small anions, such as fluoride and chloride, with good affinity in aprotic solvents.
Calix[4]pyrroles can adopt four limiting conformations: 1,3-alternate, 1,2-alternate, partial cone and cone. The form predicted to be the most stable, and experimentally lowest energetic, is the first one, in which adjacent pyrrole rings are pointing in opposite directions.[43]

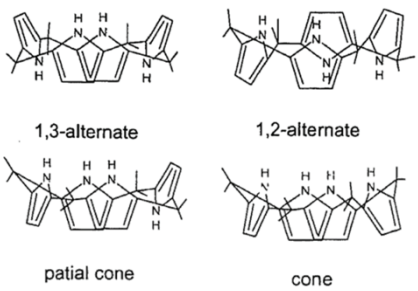

Figure 13: Possible conformations for calix[4]pyrroles.

However, the cone conformation is the most stable upon anion binding, due to the formation of four NH-halide hydrogen bonds.
In order to improve the complexation capability of these systems, they can be functionalized at either the β-position (C-rim) or meso position (bridge position).[42] The latter approach serves not only to change the intrinsic anion selectivity of calix[4]pyrrole skeleton, but also, in appropriate cases, to induce secondary binding sites that may allow selective recognition of cationic, anionic, or neutral guests.
A further option comes from modifying the calix[4]pyrrole at the N-rim, performing alkylation reactions.[44] By changing the number of NH moieties available for H-bonding, the binding capability of the whole system is tuned.
Calixpyrroles have been exploited for a multitude of applications,[42] among which as optical and electrochemical sensors, HPLC supports, anion transporting agents, chelating polymers and nonlinear optical materials.

In this thesis we exploited these compounds to realize ion-pairs receptors, performing suitable meso-position modifications, which allowed us to expand the original cavity and to introduce further binding sites (Chapter 5).

1.4 Functional Supramolecular Materials.

Supramolecular materials are by nature dynamic materials, whose constituents are linked through reversible connections and may undergo assembly/disassembly processes under specific conditions.
In principle they can select their constituents in response to external stimuli or environmental factors. Instructed, dynamic, and combinatorial, they behave as complex adaptive systems.[45]
Supramolecular chemistry, by means of the explicit manipulation of the noncovalent forces binding structural components, opens new perspectives toward “smart objects”, whose features depend on molecular information.

- ***Supramolecular Polymers.***

A rich domain emerges from the combination of polymer chemistry with supramolecular chemistry, defining a new field that involves the designed manipulation of molecular interactions and recognition processes to generate main-chain or side-chain supramolecular polymers, featuring unprecedented and highly useful functional properties.

According the definition proposed by E. W. Meijer, "*supramolecular polymers are polymeric arrays of monomeric units held together by reversible and highly directional secondary interactions, resulting in polymeric properties in diluted and concentrated solution as well as in the bulk".*[46]

Polymers based on this concept potentially combine many of the attractive features of conventional polymers with properties that result from the dynamic nature of non-covalent interactions between monomeric units. Made up of small molecules, they can, for example, flow like small molecules at elevated temperatures or in dilute solution.[47] Also, they might respond differently to high levels of stress, since the interactions holding the chains together are constantly being broken and reformed. Because of that, they can behave as self-healing materials,[48] able to repair damages occurring during their service lifetime.

In general, supramolecular polymers, can be classified into two classes:[49] main-chain and side-chain. Main-chain polymers are divided into linear main-chain polymers, networks and linear-main chain polymers based on bidirectional units. On the other hand, side-chain polymers can be of two types: polymers bearing binding motifs in the side-chain, and polymers bearing binding motifs in the main chain.

The design of supramolecular polymers has several elements to it. Using a directional self-complementary units (A-A) or complementary couples (A-B, or A-A + B-B), it is possible to form all known structures of polymers, including linear homo- and copolymers, cross-linked networks and branched structures.[50]

The most important aspect is the choice of the interactions that will hold the monomers together. The interactions must be stronger than the van der Waal's forces between the polymer chains, but weak enough to allow reversible dissociation under a reasonable stress. Moreover, it

has to be taken in mind, that high association constants are required to obtain significant polymerization degree.

The use of each noncovalent interaction has its own set of advantages and limitations. For example, while metal coordination is directional, the strength of the interaction often restricts its dynamic nature and, consequently, its reversibility. Coulombic interactions between ionic groups, on the other hand, suffer from the fact that these forces are non-directional in many cases, giving rise to ill-defined aggregation. Hydrogen bonding is strong and highly directional, but binding in aqueous solution without the additional aid of hydrophobic interactions still remains a challenge.

Meijer and co-workers exploited the self-complementary DDAA (donor-donor-acceptor-acceptor) array of four hydrogen bonds of 2-ureido-4-pyrimidone derivatives to realize supramolecular polymers, featuring great stability at elevated temperatures and under high levels of strain.[51]

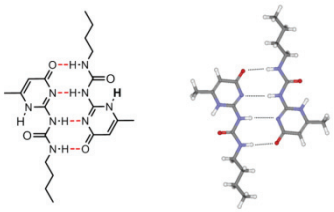

Figure 14: Homodimer of ureido-pyrimidone units.

Host-guest based supramolecular polymers were prepared by Harada and co-workers using two covalently linked α-cyclodextrins and ditopic guest bearing adamantyl groups.[52]

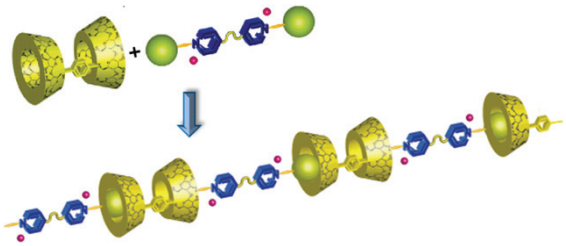

Figure 15: Schematic depiction of cyclodextrins-based supramolecular polymers.

Rebek used the strong association between urea substituted calix[4]arenes to design “policaps” (polymeric capsules), formed from monomers based on two calix[4]arene tetraurea units covalently attached at their lower rims.[53]

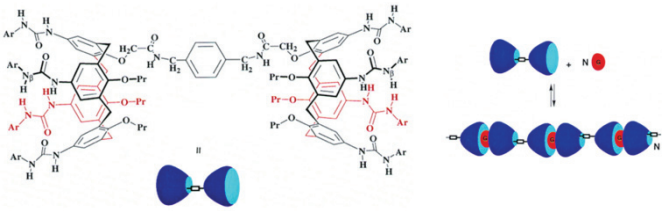

Figure 16: Benzene-tuned polymeric capsule (polycaps) formation.

These are only few examples among the numerous ones that could be found in recent literature concerning supramolecular science.
Three are the major growth mechanisms by which a monomer can polymerize into a supramolecular polymer, namely, isodesmic, ring-chain, and cooperative/anticooperative growth.[54]

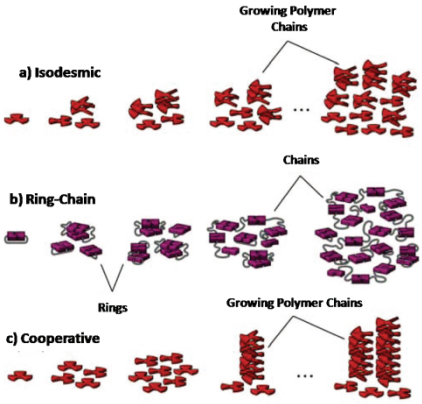

Figure 17: Graphical representation of (a) isodesmic (b) ring-chain (c) cooperative supramolecular polymerization.

The isodesmic polymerization is similar to the step polymerization of polyesters and is characterized by a single binding constant for each reversible step in the assembly pathway. The second class of

supramolecular polymerizations is represented by linear oligomers and polymers in equilibrium with their cyclic counterpart. The tendency for reversible intramolecular cyclization is largely determined by the conformational properties of the linker separating the two reversibly associating end groups in the monomer, and only above an effective concentration, formation of chain-polymers results favored.
Finally, the third mechanism of supramolecular polymerization is characterized by a nonlinear and often nucleated growth. In the case of a cooperative mechanism, in the initial stages of the polymerization the Gibbs free energy of the oligomers increases with respect to the monomer. The polymerization process continues until a maximum of free energy, own by a nucleus of degree of polymerization *n*; then polymerization becomes energetically favorable. On the contrary, for anticooperative supramolecular polymerization, the initial formation of oligomers occurs with a higher association constant than subsequent elongation. Anticooperative growth in supramolecular polymerizations has received much less attention than cooperative growth, even if it could be really interesting, resulting in the formation of discrete objects with low polydispersities.

In Chapters 2 and 3, we introduce two new classes of supramolecular polymers. The first one is based on host-guest driven self-assembly, while the second one exploits the combination of solvophobic interactions and hydrogen bonding to generate multifunctional frameworks.

- ***Ion-Pair Receptors.***

The development of synthetic receptors for ionic species have played an important role in the growth of supramolecular chemistry.
Whereas cation receptors started to develop in 1967, thanks to Pedersen's research on the complexation of alkali metal ions by crown ethers,[55] interest in anion receptors was born much later, in 1976, when Graf and Lehn reported that protonated cryptate encapsulates F^-, Br^- and Cl^- anions.[56]
Since then, synthesis and design of specific anionic or cationic receptors received a growing attention, and several host species were developed. Recently, attention turned on ion-pair complexation, which

are heteroditopic systems, capable of simultaneous coordination of both anionic and cationic guest species.
In these systems, anion and cation can be bound separately within the receptor, or as a single moiety. Particularly, the latter approach is noteworthy as it avoids the energetically unfavorable separation of the two ions.[57]
While cation complexation may occur by means of Lewis bases, the anion coordination can exploit Lewis acidic, electrostatic, or hydrogen bonding interactions.
In the case of contact ion-pair complexation, the geometry of the ditopic receptor must be optimized so that the anion and cation binding sites are located in close proximity, in order to avoid incorrect orientation, that could lead to the ion-pair association outside of the receptor, or solvent-separated ion binding.
In order to complex ion-pairs successfully, Smith and co-workers have synthesized a variety of macrobicyclic compounds, including crown-ether diamide based receptors, which are able of binding solvent separated ion-pairs.[58]

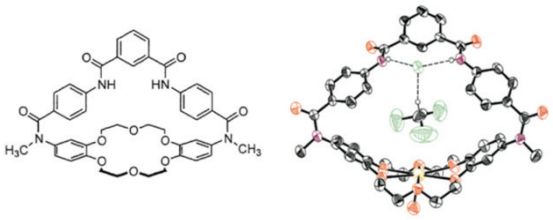

Figure 18: Solvent ion-pair inclusion (Na^+, $CHCl_3$, Cl^-) in a dibenzo-18-crown-6-ether covalently linked to a bridging 1,3-phenyldicarboxamide.

Beer and co-workers recently reported the synthesis of a heteroditopic calix[4]diquinone receptor, capable of binding contact ion-pairs, such as KCl.[59]

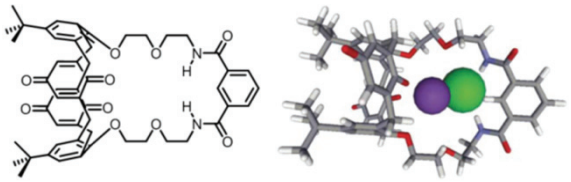

Figure 19: Contact ion-pair inclusion (K^+, Cl^-) in a calix[4]diquinone receptor.

Sessler devised a receptor for solvent separated CsF ions, based on a crown-6-calix[4]arene capped with a calix[4]pyrrole.

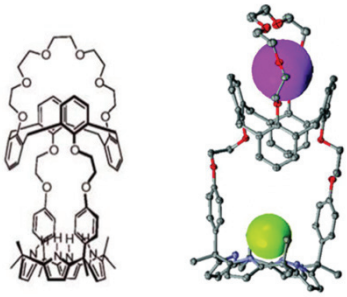

Figure 20: CsF in a crown[6]calix[4]arene capped calix[4]pyrrole receptor.

In Chapters 4 and 5 we report the synthesis and design of two ion-pair receptors. The first one is a cavitand-based host, featuring suitable phosphonate groups at the lower rim, imparting complexing properties toward guest species, such as the ammonium salts. The second one is based on a calix[4]pyrrole scaffold, implemented with phosphonate motifs at the upper rim, in order to achieve complexation of both cations and anions.

1.5 Supramolecular Chemistry on Surfaces.

A great number of functional hybrid systems, based on the attachment of chemical units on the surface of nanoparticles or nanostructured solids, have been developed in the last few years. Whereas, traditionally, the functionalization of surfaces was used to modulate adhesion characteristics or to improve the dispersion of particles in liquids, with the advent of supramolecular chemistry, the introduction of specific groups on nanostructured solids was exploited to enhance active functions, such as the recognition of guests, or to switch surface properties.[60]

Moving from a one-dimensional molecule in solution, to a 2D or 3D-arrangement in the hetero-supramolecular ensemble, one can achieve unique properties which often are not simply an extrapolation of the solution conduct to the surface.

Such materials, with a high and readily accessible specific surface, can amplify certain functional chemical processes, as a consequence of collective phenomena between the preorganized functional units. In other cases, entropic factors associated with the restriction of movement or the proximity of molecular entities on the surface, lead to an enhancement of classical recognition features.

In this perspective, metal nanoparticles, self-assembled monolayers, and more complex structures formed via layer-by-layer techniques, have recently attracted considerable attention.

For example, hybrid frameworks that involve the use of gold nanoparticles (AuNPs) cofunctionalized with guest-responsive sulfur-containing compounds have been recently reported for anion sensing. These systems display size- and shape dependent plasmon absorption bands and show strong optical changes upon guest induced aggregation processes, because of the mutual induction of dipoles which varies with the aggregate size and interparticle distance.

Hupp and co-workers[61] exploited these features, to realize simple colorimetric receptors, for the detection of low concentrations of heavy metal ions (Pb^{2+}, Cd^{2+}, Hg^{2+}) in aqueous solution. The ensemble in this case consisted of AuNPs functionalized with alkanethiol chains carrying carboxylate functions at the distal terminal end. Similarly Murphy and co-workers[62] functionalized gold nanoparticles with 1,10-phenanthroline for the detection of Li^{+} ions. Again, Chen[63] reported an efficient recognition of K^{+} ions by colloidal AuNPs functionalized with [15]crown-5-ethers.

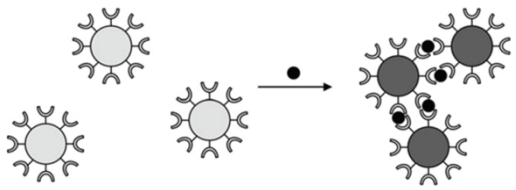

Figure 21: Aggregation of AuNPs induced by coordination.

A different aim has been pursued by Kaifer and co-workers,[64] which exploited supramolecular recognition to induce NPs aggregation, in order to create assemblies for electronic circuit components with extraordinarily high degrees of integration.

Self- assembled monolayers (SAMs) have been probably the first hybrid frameworks investigated by supramolecular scientists years before the advent of metal nanoparticles. From the beginning, SAMs resulted particularly intriguing because able to introduce an unprecedented flexibility in tailoring interfaces and generating patterned surfaces.
In this context, the pioneering role of Reinhoudt's research dominates, aimed to generate cyclodextrin-functionalized gold or silicon oxide surfaces, as hybrid scaffolds for recognition processes. By suitable choices of interacting species, fully controlled assembly/disassembly has been achieved, with the consequent tuning of surface properties.
For example, strong hydrophobic cyclodextrin–adamantane interaction has been exploited for the formation of complex structures via layer-by-layer techniques.[65] CD-functionalized gold surfaces, adamantyl-terminated dendrimers, and gold nanoparticles functionalized with cyclodextrins were the three components used for multilayer devices.

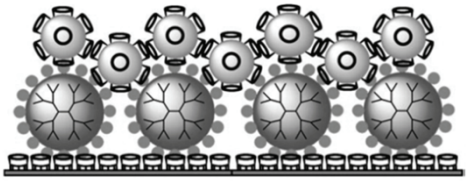

Figure 22: Representation of layer-by-layer assembly of adamantly-terminated dendrimers and cyclodextrins-functionalized AuNPs on a CD-SAMs.

Another interesting example of layer-by-layer assembly based on supramolecular interactions was developed by Kobuke and co-workers[66] to generate the first hybrid layer structure able to enhance the generation of photocurrent.

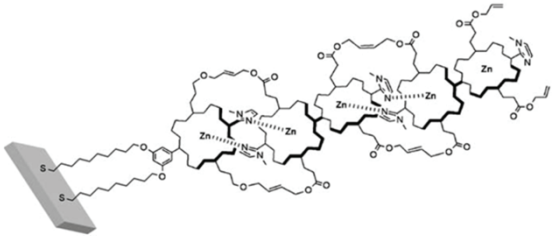

Figure 23: Imidazolyl-substituted porphyrinatozinc complexes onto a gold surface.

They deposited onto a gold surface imidazolyl-substituted porphyrinatozinc complexes, cross-linked pairwise by a metathesis reaction, in order to form rigidly fixed multiporphyrin arrays. In presence of viologen, as an electron carrier, this nanomaterial revealed outstanding "light-harvesting" properties, leading to photocurrent amplification.

These few examples highlight the growing interest, in materials chemistry, for flexible and efficient methods for creating ordered structures, with functional properties and tunable behaviors.
Accordingly, in Chapter 6 we report the hierarchical self-assembly of supramolecular architectures on silicon surface, achieved by exploiting orthogonal binding motifs, namely hydrogen-bonding and host-guest interactions.

1.6 References and Notes.

[1] J.-M. Lehn, *Angew. Chem. Int. Ed.* **1988**, *27*, 89-112.

[2] J.-M. Lehn, *Proc. Natl. Acad. Sci. U.S.A.* **2002**, *99*, 4763-4768.

[3] G. M. Whitesides, B. Grzybowoski, *Science* **2002**, *295*, 2418-2421.

[4] J.-M. Lehn, *Science* **2002**, *295*, 2400-2403.

[5] G. R. Desiraju, *Curr. Sci.* **2005**, *88*, 374-380.

[6] F. Jensen, in *Introduction to Computational Chemistry*, Wiley, Chichester, **1999**.

[7] T. Steiner, *Angew. Chem. Int. Ed.* **2002**, *41*, 48-76.

[8] M. Akke, S. Forsen, *Proteins: Struct. Funct. Genet.* **1990**, *8*, 23-29.

[9] E. Baker,R. Hubbard, *Prog. Biophy. Mol. Biol.* **1984,** *44***,** 97-179.

[10] G.A. Jeffrey, in *An Introduction to Hydrogen Bonding*, Oxford University Press, Oxford, **1997**.

[11] (a) W. L. Jorgensen, J. Pranata, *J. Am. Chem. Soc.* **1990**, *112*, 2008-2010; (b) J. Pranata, S. G. Wierschke, W. L. Jorgenseng, *J. Am. Chem. Soc.* **1991**, *113*, 2810-2819.

[12] J. Sartorius, H.-J. Schneider, *Chem. Eur. J.* **1996**, *2*, 1446-1452.

[13] L. J. Prins, D. N. Reinhoudt, P. Timmerman, *Angew. Chem. Int. Ed.* **2001**, *40*, 2382-2426.

[14] (a) J. Lagona, P. Mukhopadhyay, S. Chakrabarti, L. Isaacs, *Angew. Chem. Int. Ed.* **2005**, *44*, 4844-4870; (b) J. W. Lee, S. Samal, N. Selvapalam, H. J. Kim, K. Kim, *Acc. Chem. Res.* **2003**, *36*, 621-630.

[15] K. A. Nielsen, W. S. Cho, J. O. Jeppesen, V. M. Lynch, J. Becher, J. L. Sessler, *J. Am. Chem. Soc.* **2004**, *126*, 16296-16297.

[16] M. Nishio, M. Hirota, Y. Umezawa, *The CH-π Interactions*, Wiley-VCH, New York, **1998**; M. Nishio, Y. Umezawa, M. Hirota, Y. Takeuchi, *Tetrahedron* **1995**, *51*, 8665-8700.

[17] C. A. Hunter, K. R. Lawson, J. Perkins, C. J. Urch, *J. Chem. Soc., Perkin Trans. 2* **2001**, 651-669.

[18] S. K. Burley, G. A. Petsko, *Science* **1985**, *229*, 23-28.

[19] W. Seanger, *Principles of Nucleic Acid Structure*, Springer-Verlag, New York, **1984**.

[20] (a) C. A. Hunter, *Chem. Soc. Rev.* **1994**, *23*, 101-109; (b) E. A. Meyer, R. K. Castellano, F. Diederich, *Angew. Chem. Int. Ed.* **2003**, *42*, 1211-1250.

[21] C. G. Claessens, J. F. Stoddart, *J. Phys. Org. Chem.* **1997**, *10*, 254-272.

[22] D. J. Cram, J. M. Cram, in *Container Molecules and Their Guests* (Ed.: J. F. Stoddart), **1994**, The Royal Society of Chemistry, Cambridge, Chap. 5.

[23] D. J. Cram, S. Karbach, H.-E. Kim, C. B. Knobler, E. F. Maverick, J. L. Ericson, R. C. Helgeson, *J. Am. Chem. Soc.* **1988**, *110*, 2229-2237.

[24] (a) J. A. Tucker, C. B. Knobler, K. N. Trueblood, D. J. Cram, *J. Am. Chem. Soc.* **1989**, *111*, 3688-3699 ; (b) P. Soncini, S. Bonsignore, E. Dalcanale, F. Ugozzoli, *J. Org. Chem.* **1992**, *57*, 4608-4612; (c) T. Haino, D. M. Rudkevich, A. Shivanyuk, K. Rissanen, J. Rebek, Jr., *Chem. Eur. J.* **2000**, *6*, 3797-3805; (d) K. Paek, J. Cho, *Tetrahedron Lett.* **2001**, *42*, 1927-1929.

[25] (a) M. Vincenti, E. Dalcanale, P. Soncini, G. Guglielmetti, *J. Am. Chem. Soc.* **1990**, *112*, 445-447; (b) M. Vincenti, E. Pelizzetti, E. Dalcanale, P. Soncini, *Pure Appl. Chem.* **1993**, *65*, 1507-1512.

[26] L. M. Tunstad, J. A. Tucker, E. Dalcanale, J. Weiser, J. A. Bryant, J. C. Sherman, R. C. Helgeson, C. B. Knobler, D. J. Cram, *J. Org. Chem.* **1989**, *54*,1305-1312.

[27] R. Pinalli, M. Suman, E. Dalcanale, *Eur. J. Org. Chem.* **2004**, *3*, 451-462.

[28] P. Delangle, J.-C. Mulatier, B. Tinant, J.-P. Declercq, J.-P. Dutasta, *Eur. J. Org. Chem.* **2001**, 3695–3704; (b) J.-P. Dutasta, *Top. Curr. Chem.* **2004**, *232*, 55-91.

[29] (a) E. Biavardi, G. Battistini, M. Montalti, R. M. Yebeutchou, L. Prodi, E. Dalcanale, *Chem. Commun.* **2008**, 1638–1640; (b) R. M. Yebeutchou, F. Tancini, N. Demitri, S. Geremia, R. Mendichi, E. Dalcanale, *Angew. Chem., Int. Ed.* **2008**, *47*, 4504–4508.

[30] (a) T. Lippmann, E. Dalcanale, G. Mann, *Tetrahedron Lett.* **1994**, *35*, 1685-1688; (b) T. Lippmann, H. Wilde, E. Dalcanale, L. Mavilla, G. Mann, U. Heyer, S. Spera, *J. Org. Chem.* **1995**, *60*, 235-242; (c) P. Delangle, J.-P. Dutasta, *Tetrahedron Lett.* **1995**, *36*, 9325-9328.

[31] R. M. Yebeutchou, E. Dalcanale, *J. Am. Chem. Soc.* **2009**, *131*, 2452–2453.

[32] B. Bibal, J.-P. Declercq, J.-P. Dutasta, B. Tinant, A. Valade, *Tetrahedron* **2003**, *59*, 5849-5854.

[33] D. J. Cram, J. M. Cram, in *Container Molecules and Their Guests* (Ed. J. F. Stoddart), **1994**, Royal Society of Chemistry, Cambridge, Chap. 6.

[34] J. R. Moran, J. L. Ericson, E. Dalcanale, J. A. Bryant, C. B. Knobler, D. J. Cram, *J. Am. Chem. Soc.* **1991**, *113*, 5707-5714.

[35] (a) V. A. Azov, B. Jaun, F. Diederich, *Helv. Chim. Acta* **2004**, *87*, 449-462; (b) P. Roncucci, L. Pirondini, G. Paderni, C. Massera, E. Dalcanale, V. A. Azov, F. Diederich, *Chem. Eur. J.* **2006**, *12*, 4775-4784.

[36] P. J. Skinner, A. G. Cheetham, A. Beeby, V. Gramlich, F. Diederich, *Helv. Chim. Acta* **2001**, *84*, 2146-2153.

[37] *CRC Handbook of Chemistry and Physics* (Ed. D. R. Lide), **2005**, Taylor& Francis, Boca Raton, FL, USA.

[38] D. J. Cram, H. J. Choi, J. A. Bryant, C. B. Knobler, *J. Am. Chem. Soc.* **1992**, *114*, 7748-7765.

[39] S. S. Zhu, H. Staats, K. Brandhorst, J. Grunenberg, F. Gruppi, E. Dalcanale, A. Lützen, K. Rissanen, C. A. Schalley, *Angew. Chem. In. Ed.* **2008**, *47*, 788-792.

[40] W. Sliwa, *Chemistry of Heterocyclic Compounds* **2004**, *40*, 683-700.

[41] (a) A. Baeyer, *Ber. Dtsch. Chem. Ges.* **1886**, *19*, 2184-2185; (b) M. Dennstedt, J. Zimmermann, *Chem. Ber.* **1887**, *20*, 850-857; (c) M. Dennstedt, *Ber. Dtsch. Chem. Ges.* **1890**, *23*, 1370-1374; (d) P. Rothemund, C. L. Gage, *J. Am. Chem. Soc.* **1955**, *77*, 3340-3342; (e) W. H. Brown, B. J. Hutchinson, M. H. MacKinnon, *Can. J. Chem.* **1971**, *49*, 4017-4022.

[42] V. K. Jain, H. C. Mandalia, *Heterocycles*, **2007**, *71*, 1261-1313.

[43] W. P. van Hoorn, W. L. Jorgensen, *J. Org. Chem.* **1999**, *64*, 7439-7444.

[44] Y. Furusho, H. Kawasaki, S. Nakanishi, T. Aida, T. Takata, *Tetrahedron Lett.* **1998**, *39*, 3537-3540.

[45] J.-M. Lehn, *Supramolecular Science: Where It Is and Where It Is Going* (Eds. R. Ungaro & E. Dalcanale), **1999**, Kluwer, Dordrecht, 287–304.

[46] L. Brunsveld, b. J. B. Folmer, E. W. Meijer, R. P. Sijbesma, *Chem. Rev.* **2001**, *101*, 4071-4097.

[47] C. B. St Pourcain, A. C. Griffin, *Macromolecules*, **1995**, *28*, 4116-4121.

[48] (a) M. W. Keller, B. J. Zlaiszik, S. R. White, N. R. Sottos, *Adaptive Structures* **2007**, 247-260; (b) R. P. Wool, *Soft Matter* **2008**, *4*, 400-418.

[49] G. B. W. L. Ligthart, O. A. Scherman, R. P. Sijbesma, E. W. Meijer, *Macromolecular Engeneering. Precise Synthesis, Materials Properties, Application* (Eds. K. Matijaszewski, Y. Gnanou, L. Liebler), **2007**, Whiley-VCH, Weinhaim, 351-398.

[50] *Supramolecular Polymers, Second Edition* (Ed. A. Ciferri) **2005**, Francis & Taylor, New York.

[51] R. P. Sijbesma, F. H. Beijer, L. Brunsveld, B. J. B. Folmer, J. H. K. K. Hirschberg, R. F. M. Lange, J. K. L. Lowe, E. W. Meijer, Science, **1997**, *278*, 1601-1604.

[52] (a) K. Ohga, Y. Takashima, H. Takahashi, Y. Kawaguchi, H. Yamaguchi, A. Harada *Macromolecules* **2005**, *38*, 5897-5904; (b) M. Miyauchi, Y. Takashima, H. Yamaguchi, A. Harada, *J. Am. Chem. Soc.* **2005**, *127*, 2984-2989; (c) M. Miyauchi, T. Hoshino, H. Yamaguchi, S. Kamatori, A. Harada, *J. Am. Chem. Soc.* **2005**, *127*, 2034-2035; (d) H. Takahashi, Y. Takashima, A. Harada, *J. Org. Chem.* **2006**, *76*, 4878-

4883; (e) *Cyclodextrins and their complexes: chemistry, analytical methods, applications* (Ed. Helena Dodziuk), **2006**, Wiley-VCH, Weinheim; (f) P. Kuad, A. Miyawaki, Y. Takashima, A. Harada, *J. Am. Chem. Soc.* **2007**, *42*, 12630-12631.

[53] R. K. Castellano, D. M. Rudkevich, J. Rebek, Jr, *Proc. Natl. Acad. Sci. U.S.A.* **1997**, *94*, 7132-7137.

[54] T. F. A. De Greef, M. M. J. Smulders, M. Wolffs, A. P. H. J. Schenning, R. P. Sijbesma, E. W. Meijer, *Chem. Rev.* **2009**, *109*, 5687-5754.

[55] C. J. Pedersen, *J. Am. Chem. Soc.* **1967**, *89*, 7017-7036.

[56] E. Graf, J.-M. Lehn, *J. Am. Chem. Soc.* **1976**, *98*, 6403-6405.

[57] (a) J. M. Mahoney, A. M. Beatty, B. D. Smith, *Inorg. Chem.* **2004**, *43*, 7617-7621; (b) M. Cametti, M. Nissinen, A. Dalla Cort, L. Mandolini, K. Rissanen, *J. Am. Chem. Soc.* **2005**, *127*, 3831-3837.

[58] M. J. Deetz, M. Shang, B. D. Smith, *J. Am. Chem. Soc.* **2000**, *122*, 6201-6207.

[59] M. D. Lankshear, A. R. Cowley, P. D. Beer, *Chem. Commun.* **2006**, *39*, 612-614.

[60] A. B. Descalzo, R. Martìnez-Màñez, F. Sancenòn, K. Hoffmann, K. Rurack, *Angew. Chem. Int. Ed.* **2006**, *45*, 5924-5948.

[61] Y. Kim, R. C. Johnson, J. T. Hupp, *Nano Lett.* **2001**, *1*, 165–167.

[62] S. O. Obare, R. E. Hollowell, C. J. Murphy, *Langmuir* **2002**, *18*, 10407–10410.

[63] S.-Y. Lin, S.-W. Liu, C.-M. Lin, C.-H. Chen, *Anal. Chem.* **2002**, *74*, 330–335.

[64] J. Liu, J. Alvarez,W. Ong, A. E. Kaifer, *Nano Lett.* **2001**, *1*, 57–60.

[65] O. Crespo-Biel, B. Dordi, D. N. Reinhoudt, J. Huskens, *J. Am. Chem. Soc.* **2005**, *127*, 7594–7600.

[66] M. Morisue, S. Yamatsu, N. Haruta, Y. Kobuke, *Chem. Eur. J.* **2005**, *11*, 5563 – 5574.

Host-Guest Supramolecular Polymers

2

2.1 Introduction.

Based on modular components reversibly linked through noncovalent interactions, supramolecular polymers are constitutionally dynamic materials,[1] which fully meet the quest for adaptability, currently a must in materials science.

In a previous work,[2] we have reported synthesis and design of self-complementary heteroditopic monomers (A-B), that exploited the outstanding complexing properties[3] of tetraphosphonate cavitands towards N-methylpyridinium guests to form supramolecular arrays, by isodesmic polymerization. In particular, the designed monomers were cavitands bearing four inward facing P=O groups at the upper rim, and a single N-methylpyridinium unit at the lower rim. The corresponding polymers featured guest-triggered reversibility,[2] responsiveness to electrochemical stimuli,[4] and template-driven conversion from linear into star-branched forms.[2]

The growing interest in this field has prompted us to devise new component units, with structural and functional properties ready to be integrated in covalent polymeric networks. As self-assembly motif, we have decided to exploit the previously investigated host-guest interaction, featuring the high complexation constants ($K_{ass} \approx 10^7\ M^{-1}$) needed to realize truly polymeric materials.[5] Ditopic complementary partner molecules, splitting the host and guest functionalities on two different species, were designed: ditopic hosts (A-A) have been prepared

from two tetraphosphonate cavitands covalently attached at their lower rim, while ditopic guests (B-B) have been obtained from flexible alkyl chains functionalized with two N-methylpyridinium end-groups.

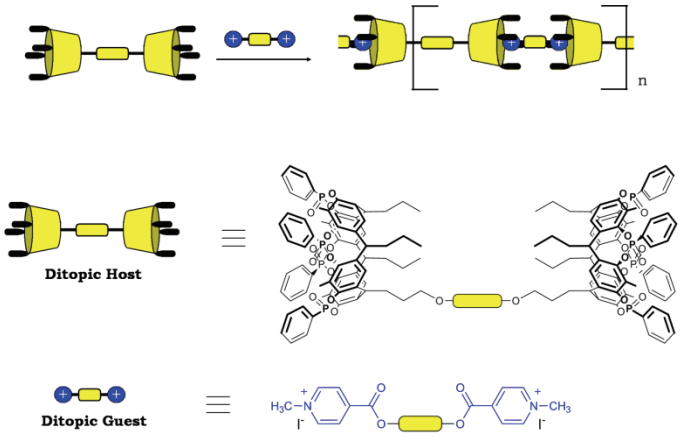

Figure 1: Host-guest polymerization scheme.

This AA BB copolymerization mode is best suited to explore the viability of non-covalent interactions among end-groups or side chain groups in covalent polymers.
While ^{1}H-NMR studies confirmed the effectiveness of the selected self-association process, microcalorimetric analyses (ITC) clarified the binding thermodynamics, revealing the possibility to tune entropic contributions, by acting on the flexibility of the guest spacing chain. Finally, viscosity measurements indicated the presence of a concentration-dependent ring-chain equilibrium, showing to be a useful means to elucidate the polymerization mechanism.
Metal-driven cross linking was also achieved by addition of labile $(CH_3CN)_2PdCl_2$ complexes.

2.2 Results and Discussion.

2.2.1 Synthesis of the Building-Blocks.

Synthesized hosts and guests differ from each other for the linkers unit connecting their complexing moieties units. Spacer of different length

and flexibility have been selected, in order to evaluate how these features affect self-association processes.
In the host case, methylenic (**1a**), adipic (**1b**) and isonicotinoyl (**1c**) spacers have been introduced.
In the guest case, one long and two short linkers have been chosen, namely a polyethylenglycol chain, and an ethyl and hexyl spacers.
The target hosts **1a**, **1b**, **1c** were synthesized in three steps, starting from the known monohydroxy footed silylcavitand **I** (Scheme 1).[2]

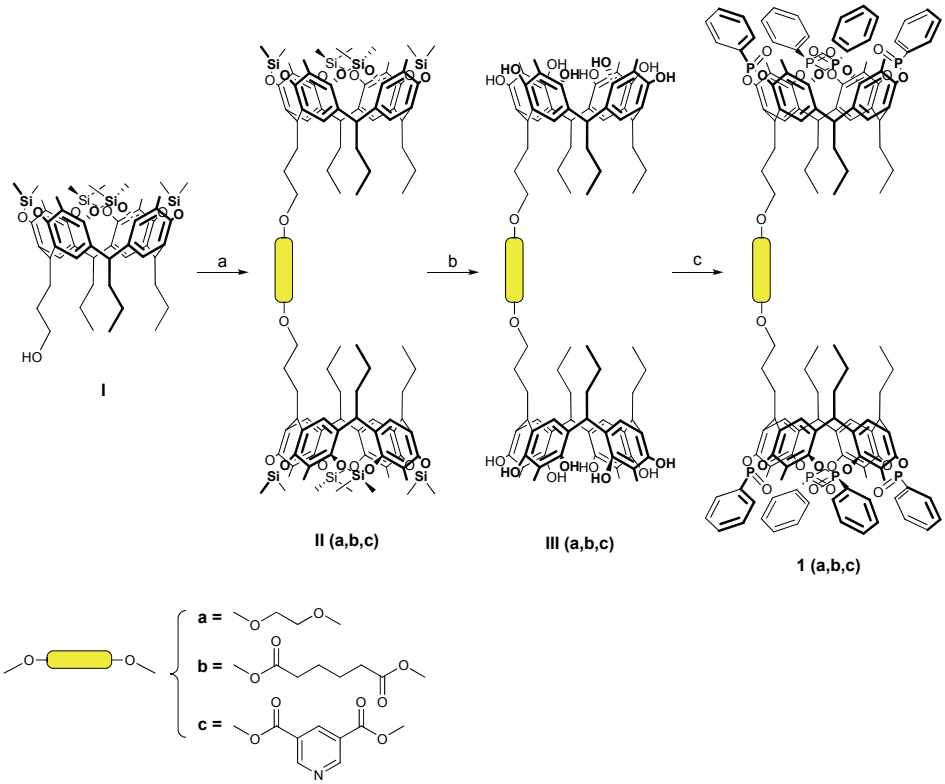

Scheme 1: Target hosts synthesis: a) dry CH_2Cl_2, DCC/DMAP, overnight, r.t.; b) DMF/$CHCl_3$, HF, overnight, 45 °C; c) dry pyridine, $PhPCl_2$, 3 h, 80 °C; H_2O_2, 30 min, r.t.

Different dimerization protocols were followed to bind together two units of **I**. Esterification reactions with adipic acid and 3,5-pyridinedicarboxylic acid, in presence of 1,3-dichlorohexylcarbodiimide (DCC) and 4-dimethylaminopyridine (DMAP), were exploited respectively in the case of **IIb** and **IIc**. In order to obtain **IIa**, silylcavitand **I** was

instead reacted with dimethoxymethane, in presence of p-toluenesulfonic acid monohydrate.
Treatment of the resulting products **II** (a,b,c) with an aqueous 36% HF solution caused the selective removal of the dimethylsilyl bridges, affording the corresponding resorcinarenes **III** (a,b,c), ready for the functionalization with dichlorophenylphosphine. This latter reaction gave rise to a tetraphosphonite intermediate, which was in situ oxidized by addition of H_2O_2,[2] to give tetraphosphonate cavitands **1** (a,b,c). Thanks to the stereospecificity of this reaction only the isomers featuring four inward-facing phosphonate bridges were formed.
The target guests **2a**, **2b**, **2c** were prepared in two steps, by reaction of isonicotinoyl chloride hydrochloride respectively with ethylene glycol, 1,6-hexandiol and polyethylenglycol. The subsequent methylation with iodomethane, afforded the desired products in quantitative yield.

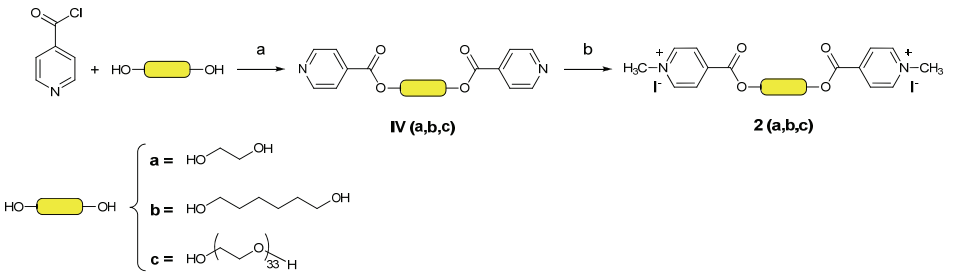

Scheme 2: Target guests synthesis: a) pyridine, 3 h, 100 °C; b) acetonitrile, CH_3I, overnight, under reflux.

2.2.2 Host-Guest driven Complexation.

The complexation of N-methylpyridinium-based guests inside the host cavity was first confirmed by a simple ^1H NMR titration.
In Figure 2, we report sections of ^1H NMR spectra monitoring the system formed by **1b** and **2c**. Diagnostic up-field shift of the guest signals are observed, as expected for included species that experience the shielding effect of the cavity. The CH_3-pyridinium moiety (blue circle) moves more than 3 ppm up-field; ortho and meta pyridinic protons feature a lower shift in the same direction, respectively from 8.60 to 8.39 ppm (magenta circle) and from 8.51 to about 7.98 ppm (green circle).

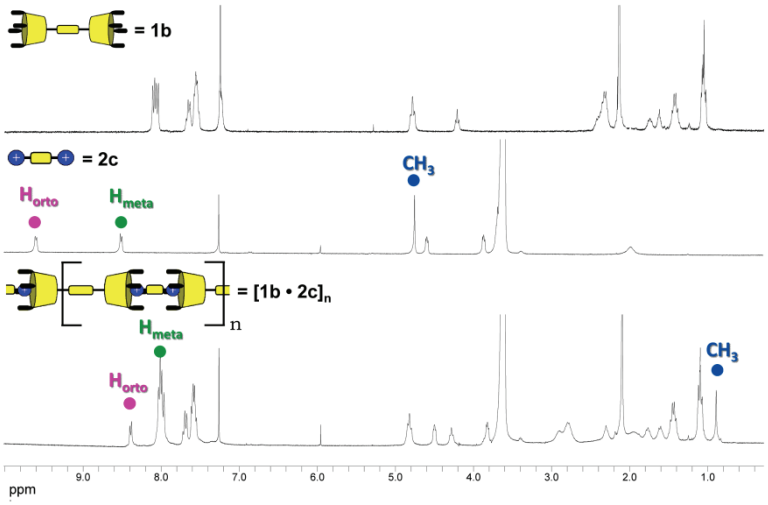

Figure 2: Section of ^{1}H NMR spectra ($CDCl_3$) monitoring host-guest complexation: from the top i) free host; ii) free guest; iii) host-guest complex.

Shifts for the cavitand signals are less obvious and consequently not highlighted in Figure 2.

The presence of complexed species has been confirmed also by ESI-MS spectroscopy.

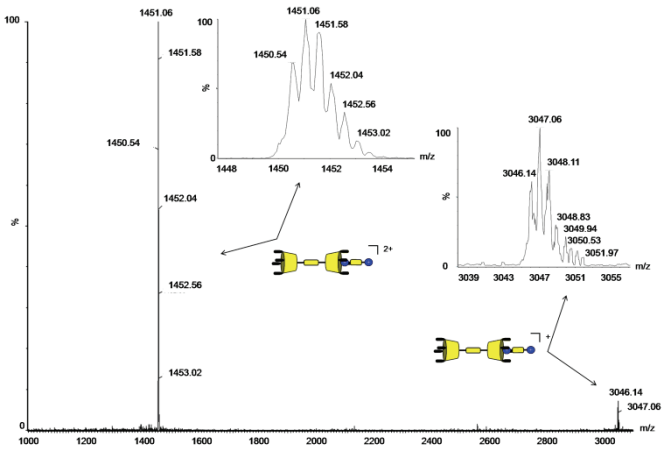

Figure 3: ESI-MS spectrum of 1:1 mixture of **1b•2b***.

Short ditopic guest **2b***, structurally equivalent to **2b**, with six carbon atoms in the linking chain, but bearing PF_6^- as counter ion instead of I^-, was chosen in order to have a suitable mass range for ESI analysis.
The ESI-MS spectrum in acetone/methanol of a 1:1 mixture of **1b** and **2b*** showed two main peaks at 1451.1 and 3047.1 *m/z*, respectively due to double and mono charged ions of **1b•2b*** species.

2.2.3 Thermodynamics Investigations by ITC measurements.

ITC experiments[6] were carried out to quantify the thermodynamic parameters associated with the inclusion process, $\Delta H°$, K_{ass}, $\Delta G°$, $\Delta S°$.
Enthalpies of dilution of the hosts and guests, determined in separate experiments, were negligible. All the measurements were performed at 298 K, and repeated at least three times, in order to obtain coherent data.
The studied molecules are depicted in Figure 4.

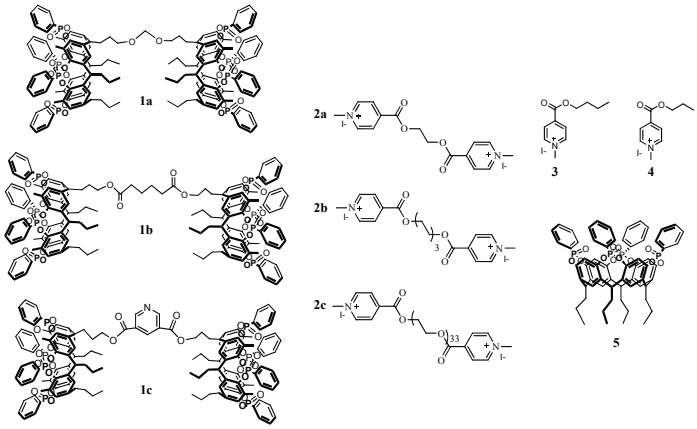

Figure 4: Host and guest for ITC experiments.

Hosts (in the calorimeter cell) were always titrated by guests (in the syringe). Typical concentrations were 0.3-0.5 mM and 2.5-8 mM, respectively. The choice of these concentrations was determined by the high value expected for the association constant. In fact, very large K_{ass} values, require very low concentration regimes to obtain isotherms with a suitable shape for the determination of the thermodynamic parameters.

It can immediately be noticed that, in this low concentration regime, only oligomeric species can form when ditopic guests are complexed by cavitand dimers, because in supramolecular polymers the average degree of polymerization is directly proportional to the concentration.[5] Thus, in that case, the reported association constants K_{ass} correspond to an average value for the formation of 1:1 oligomers (not truly polymeric materials).
Said that, a first set of experiments were performed in degassed methanol, using both monotopic and ditopic species, in order to evaluate if such cooperativity is present in trimerization/oligomerization events. The average values for the thermodynamic parameters are given in Table 1.

MeOH	**5•3**	**1b•4**	**1b•2a**
K_{ass} (M^{-1})	$(8.7 \pm 0.7)\cdot10^4$	$(6.6 \pm 0.1)\cdot10^4$	$(1.3 \pm 0.1)\cdot10^5$
ΔH (KJ mol^{-1})	-17.2 ± 0.1	-17.2 ± 0.2	-34.8 ± 0.6
$T\Delta S$ (KJ mol^{-1})	11.0 ± 0.2	10.3 ± 0.3	-5.6 ± 0.5
ΔG (KJ mol^{-1})	-28.2 ± 0,2	-27.5 ± 0.1	-29.2 ± 0.2

Table 1: Thermodynamic parameters for host-guest complexation via ITC.

Comparing the K_{ass} values recorded in the three cases, it appears that the complexation processes can always be considered as independent (no cooperativity, either positive or negative).
Observing Table 1, we notice that self-association between monotopic guests and mono or ditopic hosts, is both enthalpy and entropy driven. Whereas this result, in terms of enthalpy, is well understandable, from the entropic point of view, it turns out unexpected. Probably, the decrease in the components freedom that occurs during complexes formation, is compensated to large extent by the desolvation of the involved species, justifying the positive value which is recorded. However, also the conformational freedom of the final products have to be taken into account. In fact, in the oligomerization case, where the pre-organization of the final adducts is much larger, the entropic loss is not longer balanced by the desolvation, resulting on the whole unfavorable.
In order to have favorable entropy also in the oligomerization process, we moved to more flexible guests. Therefore we performed new titrations

using **1b**, as ditopic host, and **2a**, **2b** and **2c** as ditopic guests. Table 2 summarizes the obtained results.

MeOH	**1b•2a** 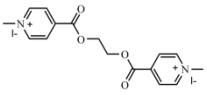	**1b•2b** 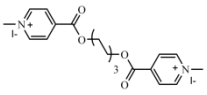	**1b•2c** 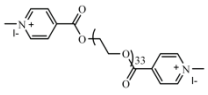
K_{ass} (M^{-1})	(1.3 ± 0.1)•10^5	(8.4 ± 0.6)•10^4	(4.9 ± 0.2)•10^5
ΔH (KJ mol^{-1})	-34.8 ± 0.6	-26.7 ± 0.3	-25.4 ± 0.1
TΔS (KJ mol^{-1})	-5.6 ± 0.5	1.5 ± 0.4	7.1 ± 0.3
ΔG (KJ mol^{-1})	-29.2 ± 0,2	-28.2 ± 0.2	-32.5 ± 0.1

Table 2: Comparison of thermodynamic data for **1a** complexation by **2a**, **2b**, **2c** guests.

Looking at the collected data, the entropic influence of the guest spacer clearly appears. Namely, moving from the short ethyl linker to longer and flexible ones, we turn negative entropic contribution in neutral or positive ones. In particular, the system formed by **1b** and **2c** results specially promising for polymers formation, because of the favorable thermodynamics that it features. In this case, the high flexibility of the guest polyethylenglycol spacer imparts such conformational freedom at the final complex, reducing the entropy loss that generally occurs during self-association.

In order to verify if other ditopic hosts could operate with higher efficiency, we repeated titrations exploiting **2c**, as ditopic guest, and **1a**, **1b** and **1c** as ditopic hosts.

MeOH	**1a•2c** 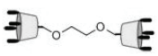	**1b•2c** 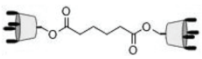	**1c•2c** 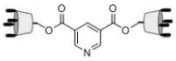
K_{ass} (M^{-1})	(2.3 ± 0.2)•10^5	(4.9 ± 0.2)•10^5	(3.9 ± 0.2)•10^5
ΔH (KJ mol^{-1})	-25.4 ± 0.5	-25.4 ± 0.1	-23.9 ± 0.2
TΔS (KJ mol^{-1})	5.1 ± 0.3	7.1 ± 0.3	8.0 ± 0.2
ΔG (KJ mol^{-1})	-30.6 ± 0,2	-32.5 ± 0.1	-31.9 ± 0.1

Table 3: Comparison of thermodynamic data for **2c** complexation by **1a**, **1b**, **1c** hosts.

As highlighted in Table 3, no significant differences are observed using the three hosts. Enthalpy values are very close, because the interactions involved in the complexation events are unchanged.
On the other hand, entropy appears mainly related to the guest capability to keep conformational freedom in the complexed form, so that, since the same, very flexible guest is employed, the entropic contribution is comparable in all cases.
The most relevant result enucleated from ITC measurements is the solvent effect. When the titration between **1b** and **2c** is repeated in dichloromethane, a gain of two orders of magnitude for the K_{ass} value is recorded by moving from MeOH to CH_2Cl_2 (Table 5).

1b•2c	*MeOH*	*CH_2Cl_2*
K_{ass} (M^{-1})	$(4.9 \pm 0.2) \bullet 10^5$	$(1{,}8 \pm 0{,}5) \bullet 10^7$
ΔH (KJ mol^{-1})	-25.4 ± 0.1	-35,3 ± 0,2
$T\Delta S$ (KJ mol^{-1})	7.1 ± 0.3	6,0 ± 0,5
ΔG (KJ mol^{-1})	-32.5 ± 0.1	- 41,2 ± 0,6

Table 4: Comparison of thermodynamic data for host-guest complexation in MeOH and CH_2Cl_2.

In first instance, this gain can be attributed to the better solvation of the methyl pyridinium cation by methanol. In other words, in methylenchloride the guest prefer cavity inclusion to CH_2Cl_2 solvation.
However, also the host affinity for the alcohols has to be taken into account, when measurements are performed in MeOH. While in dichloromethane pyridinium guests are directly bound by the cavitands, in methanol they compete with the solvent for the inclusion in the cavity, with a consequent decrease of the binding effectiveness in this latter media.

In conclusion, from the performed ITC analysis, we inferred that:

i) Self-association events are always independent. No cooperativity is observed when oligomers form.

ii) Entropy can be tuned, by acting on the flexibility of the guest spacing chain. In particular, favourable contributions are achieved by employing flexible guests, able to retain most of

the conformational freedom in the final complexation products.

iii) When flexible guests are employed, the entropic influence of the host spacer is negligible.

iv) In dichloromethane very high K_{ass} values can be achieved, making this solvent the eligible media to create polymeric arrays.

2.2.4 Polymerization Mechanism.

When supramolecular polymers are created from complementary homoditopic monomers featuring reactive end-groups linked by hydrocarbon chains, formation of cyclic species cannot be excluded.[7]
In particular, the tendency for reversible cyclization is largely determined by the conformational properties of the linker separating the complexation active moieties.
In the early 1930s Kuhn[8] introduced the concept of effective concentration c_{eff}, for self-complementary bifunctional AB type monomer. In that case, he defined c_{eff} as the local concentration of one chain-end in the vicinity of the other chain-end of the same molecule. This definition can be applied also to AA-BB systems, which can be assimilated to AB systems if dimeric species AA•BB are thought as a single AB entity.
The theoretical concept of effective concentration was often replaced by the identical, but empirical, concept of effective molarity *EM*,[9] indicating the ratio of the intra- and intermolecular equilibrium constant:

$$\boldsymbol{EM = \frac{K_{intra}}{K_{inter}}}$$

in which K_{inter} (M^{-1}) is the association constant for an intermolecular model reaction and K_{intra} is the dimensionless equilibrium constant for the intramolecular reaction.
Even if this definition too was coined for AB type monomers, it can be extended to AA-BB systems, making the above said assumption.

In supramolecular polymerization *EM* represents the limit concentration below which cyclization is more favored than linear oligomerization.
The parameters that can affect the ring-chain equilibrium are mainly four:

i) the length of the spacing chain in the monomers;
ii) the linker flexibility in the structural units;
iii) the monomer concentration;
iv) the pre-organization grade of the constituent building-blocks.

It was experimentally demonstrated[10] that, as the linker length in the monomers is increased, the effective molarity is lowered and the formation of cyclic species is suppressed. In fact, as Ercolani[11] reported in his recent work about ring-opening polymerization, for sufficiently long chains undergoing theta conditions (according which polymers form coils and can be treated as spherical particles), the mean square end-to-end distance is proportional to the number of skeletal bonds.
Dormidontova and co-workers[12] investigated the influence of the spacer rigidity. According their studies, when all other factors such as spacer length and interaction energy between the end-groups are considered to be constant, the critical concentration decreases moving from flexible to rigid linkers. That is because, for rigid polymers, the probability of finding spacer-ends within a bonding distance is smaller than for flexible polymers, which results in a decrease in the total fraction of rings.
Since this probability is obviously influenced also by the conformational properties of the linker connecting the two reactive end-groups, it follows that selective pre-organization toward cyclic or linear species can be achieved by structural tuning of the spacing chain.[7]
A further aspect, firstly presented by Jacobson and Stockmayer in their theory of macrocyclization equilibria,[13] is that for chains obeying Gaussian statistics (i.e. theta condition assumed), *EM* varies inversely to the 5/2 power of the polymerization degree *DP*. Since for supramolecular polymers the *DP* is proportional to the concentration, in diluted solutions, rings are more favored than chains.
Moving from this considerations, we studied two borderline AA-BB systems: a rigid one and a very flexible one.

- **AA-BB systems: the rigid case.**

For this study, we chose to exploit the self-assembly between commercially available methyl viologen $2PF_6^-$ and ditopic host **1c**.
In collaboration with prof. Geremia of the university of Trieste, a mixture 1:1 of homoditopic host **1c** and methyl viologen hexafluorophosphate was crystallized from a mixture 9:1 of acetonitrile and water, and the crystal structure was solved.

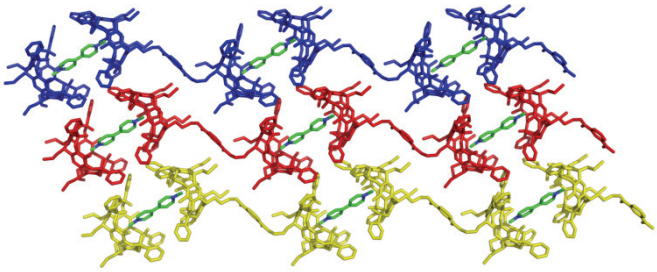

Figure 5: X-Ray crystal structure of the linear polymer formed by self-assembly between methyl viologen $2PF_6^-$ and **1c**.

The X-Ray analysis clearly shows the formation of linear polymeric chains, in which monomers units are held together by ion-dipole and CH-π interactions.
A section of the crystal packing highlights the eight P=O groups facing inward the cavity and making ion-dipole interaction with the positive charged nitrogen of methyl viologen guest. The measured average distance N^+-O=P is 3.04 ± 0.03 Å (green arrows, Figure 6). On the other hand, the average distance between the protons of the CH_3-pyridinium moiety and the plane of the aromatic rings is 3.60 ± 0.02 Å (blue arrows, Figure 6).
The PF_6^- counter ion is located at the bottom of the cavity, interacting with the alkyl chains at the lower rim of the cavitand (red arrows). Moreover, the P-F bond points toward the center of the cavity, stabilizing the ion-pair with the complexed methyl-pyridinium moiety.

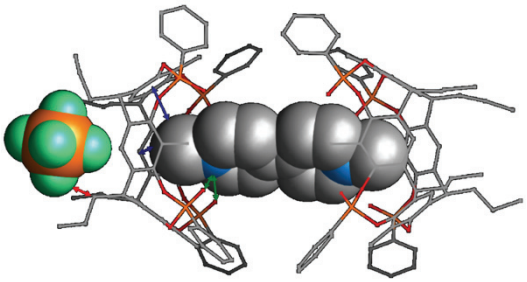

Figure 6: Section of the linear polymer featuring ion-dipole and CH-π interactions, and the fitting of the PF_6^- counterion among the alkyl chains of the cavitands.

Isonicotinoyl spacer in host **1c** could feature a relative conformational freedom, theoretically allowing both *cis* and *trans* reciprocal positioning of the cavitand units. The *trans* geometry is the favored-one in the solid state. This result can be explained taking into account the steric hindrance of the cavitand units, which leads the system to adopt the more strainless conformation.
A further contribution in this direction, probably comes from the repulsive interaction between the negative charged counterions positioned at the lower rim of the cavity. By minimizing this repulsive effect, the *trans* geometry results again the favored-one.
This feature, combined with the rigidity of the selected ditopic guest, imparts at the system a prominent pre-organization which plays a key role toward formation of linear polymers.

- **AA-BB systems: the flexible case.**

In this case we studied the system formed by self-assembly of ditopic host **1b**, featuring an adipic spacer connecting the cavitand units, and ditopic guest **2c**, bearing a very flexible polyethylenglycol linker between the two pyridinium moieties.
Since in this case we were not able to obtain suitable crystals, we turned to viscometry investigation for direct physical evidence of the formation of linear supramolecular polymers.
Initially, specific viscosities of chloroform solutions of 1:2 mixtures of **1b** and monotopic pyridinium guest **4** were measured as a function of concentration.

The curve obtained by plotting the resultant data, shows a linear relationship between concentration and viscosity, which is characteristic for non-interacting species of constant size (Figure 7).[14] This result is in agreement with the expected formation of **4•1b•4** trimers.

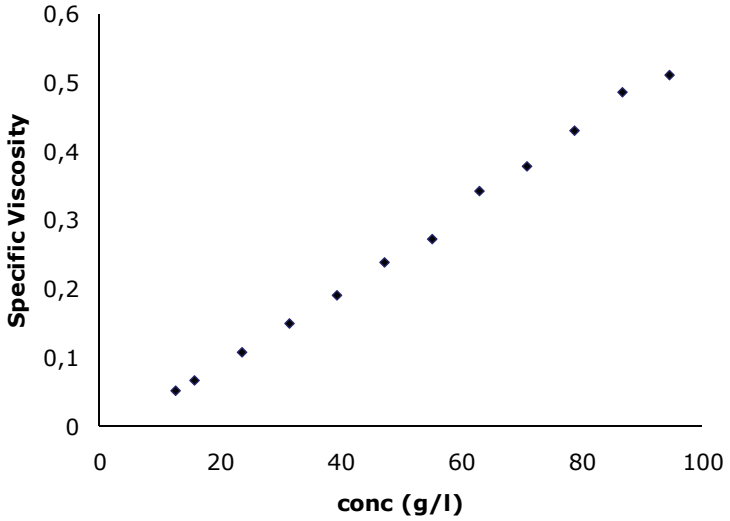

Figure 7: Specific viscosity of chloroform solution of 1:2 mixtures of **1b** and **4** as a function of concentration.

When the same measurement is repeated on 1:1 mixtures of **1b** and **2c**, a completely different behavior was observed.
As depicted in Figure 8, in the low concentration range (1.8-31.5 g/l-0.4-7 mM), a linear relationship between concentration and viscosity is recorded again. Nevertheless, with increasing concentration, a sharp rise in the viscosity is observed.
In order to exclude that this enhancement is due to the polyethylenglycol (PEG) spacer in the guest, we measured the specific viscosity of a 40 mM PEG solution (average M_n:1500 Da). From the recorded value (η = 0.41), we inferred that PEG alone cannot affect the solution viscosity, but that the observed exponential trend indicates the formation of supramolecular polymers of increasing size.

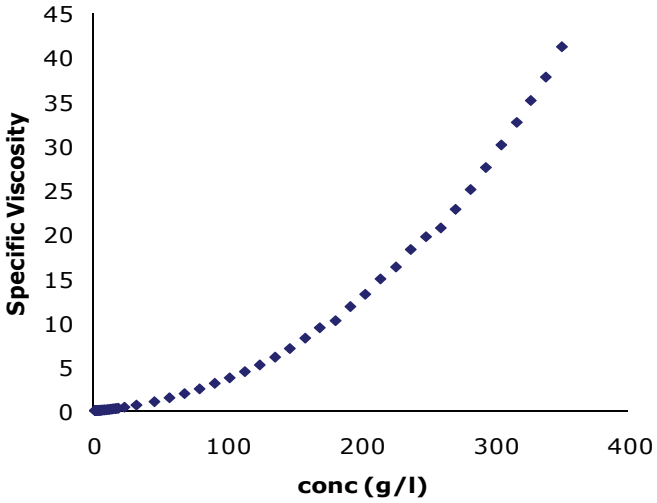

Figure 8: Specific viscosity of chloroform solution of 1:1 mixtures of **1b** and **2c** as a function of concentration.

Reporting the collected data in a log-log plot, three regions can be identified (Figure 9).

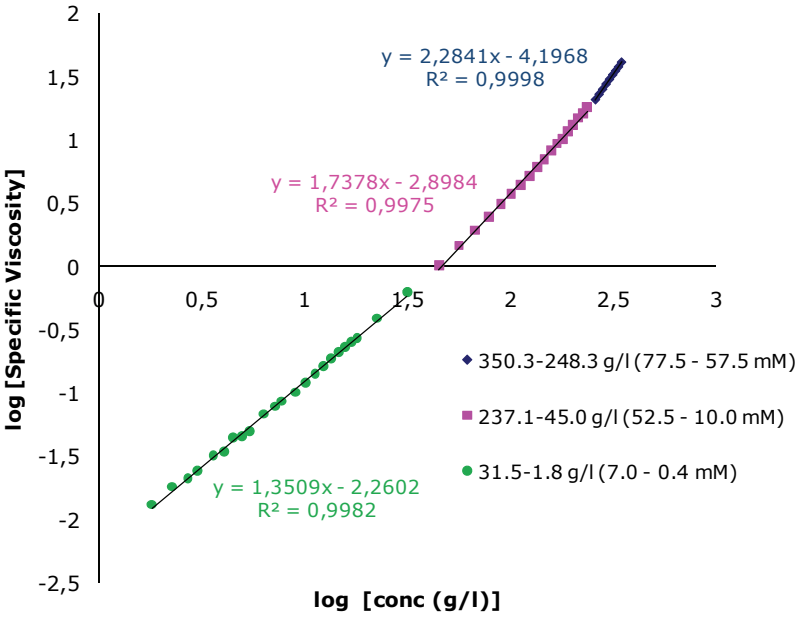

Figure 9: Log-log plot of specific viscosity of chloroform solution of 1:1 mixtures of **1b** and **2c** as a function of concentration.

In the first region, corresponding to the low concentration regime, the curve has a slope of 1.35, demonstrating that all compounds form cyclic species in solution.
This hypothesis finds confirmation in static light scattering measurements. The weight-average molecular weight M_w of 1:1 mixtures of **1b** and **2c** was experimentally determined in chloroform, in batch off-line mode, in a concentration range between 7 and 18.5 g/l (1.5-4.0 mM). Beyond this latter concentration the SLS signal was saturated, depending on both concentration and molecular weight. For the data in Table 5, the recorded M_w corresponds to dimeric or tetrameric species, consistent with the expected cyclic adducts evidenced by viscometry analysis.

conc g/l	*M_w (g/mol)*	*Aggregation*
7 (1.5 mM)	4500	AA•BB
7.8 (1.7 mM)	4500	AA•BB
8.8 (1.9 mM)	4700	AA•BB
16.6 (3.6 mM)	8700	$(AA•BB)_2$
18.5 (4.0 mM)	9500	$(AA•BB)_2$

Table 5: SLS data recorded for 1:1 mixtures of **1b** and **2c** at different concentrations (dn/dc: 0.102).

The second region highlighted in viscosity log-log plot, corresponds to a situation where the fraction of cyclic adducts decreases, whereas the fraction of material in linear chains increases (slope = 1.73).
Above a total concentration of 248.3 g/l (57.5 M) a further increase in viscosity is observed as the slope increases to 2.28. This stronger concentration dependence is indicative of the formation of linear supramolecular polymers of increasing degree of polymerization.
The lower slope above critical concentration compared to those of other systems present in literature (slopes 3-6)[15] is consistent with the fact that in our case the exact 1:1 ratio between host and guest is difficult to obtain. Since the guest results from polyethylenglycol reactant with a distribution of MW, its exact dosing is impossible. On the other hand, it is well known that deviation from 1:1 ratio has detrimental effects on the polymerization degree.[5]

In order to evaluate how significant is the presence of cycles in the medium concentration regime, we performed viscometry measurements at different temperatures, on a tetrachloroethane 1:1 solution of **1b** and **2c** featuring a total concentration of 184.6 g/l (40 mM). If cycles were present in large amount, the viscosity should magnify with temperature increasing, because of the opening ring to form linear chains induced by heating.[7]
In our case a strange behavior is observed, suggesting that more than one phenomena occurs (Figure 10).

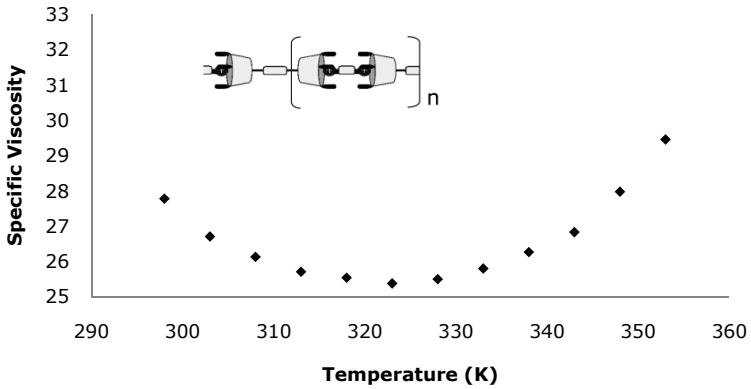

Figure 10: Specific viscosity of tetrachloroethane solution of 1:1 mixtures of **1b** and **2c** as a function of temperature.

Initially a viscosity decrease is observed with temperature. This result is in line with the thermodynamics driving the self-association process. As it has been discussed in the ITC section, **1b•2c** complexation is favored both enthalpically and entropically. However, enthalpy is more effective. Said that, it is reasonable that a temperature increase, affects negatively the polymerization, probably inducing reversible formation of smaller oligomeric and cyclic species.
Nevertheless, by heating solutions again, a kind of critical temperature is reached (323 K), above which viscosity sharply magnifies.
At this temperature, sufficient energy is provided at the system to break the rings, and to elongate the polymeric chains, promoting the approach of the reactive end-groups of different oligomers, which results in a polymerization degree increment. In fact, by cooling the solution, and measuring its viscosity at 298 K, a higher value than the starting one is

recorded (34.8 versus 26.7). This is consistent with the removal of the cyclic adducts, and the formation of higher MW species.
When the same experiment is repeated for a tetrachloroethane 40 mM solution of standard PEG (average M_n:1500 Da), a similar increase in viscosity is observed above 323 K. However in that case, the enhancement is definitely less marked, and probably simply due at the elongation of the PEG chains. Moreover, when the solution is cooled at room temperature, its initial viscosity is restored.

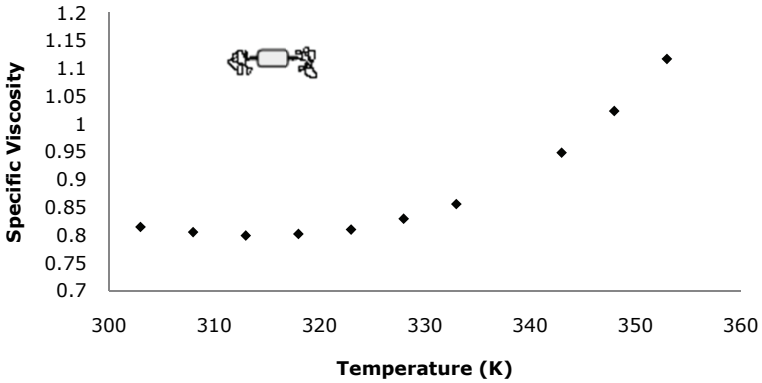

Figure 11: Specific viscosity of tetrachloroethane solution of PEG (average M_n:1500 Da) as a function of temperature.

In conclusion, viscometry investigations provide evidences of the formation of (**1b•2c**)$_n$ linear supramolecular polymers, in a medium-high concentration regime, in agreement with our expectations.

2.2.5 Polymer Metal-directed Cross-Link.

Cross-linking is a powerful tool to modify chemical, physical, and mechanical properties of polymers.[16] In particular, in supramolecular systems, where reversible cross-linking is possible, this feature results extremely interesting, because of the potential applications for self-healing materials.
Moving from these considerations, we thought to exploit the complexation capability of ditopic host **1c** to realize cross-linked polymeric networks.

As shown in 2.2.2 section, this molecule forms linear supramolecular architectures in presence of rigid ditopic guests, such as methyl viologen. Moreover it features an additional free pyridine moiety in the linker, which can act as ligand toward metal species, suitable to promote cross-linking between host-guest-based polymeric chains.
Starting from an equimolar solution of **1c** and methyl viologen hexafluorophosphate, we generated linear chains in solution. Then we induced the cross-link between the formed polymers, by addition of $(CH_3CN)_2PdCl_2$. The whole process was monitored by ^1H NMR (Figure 12)

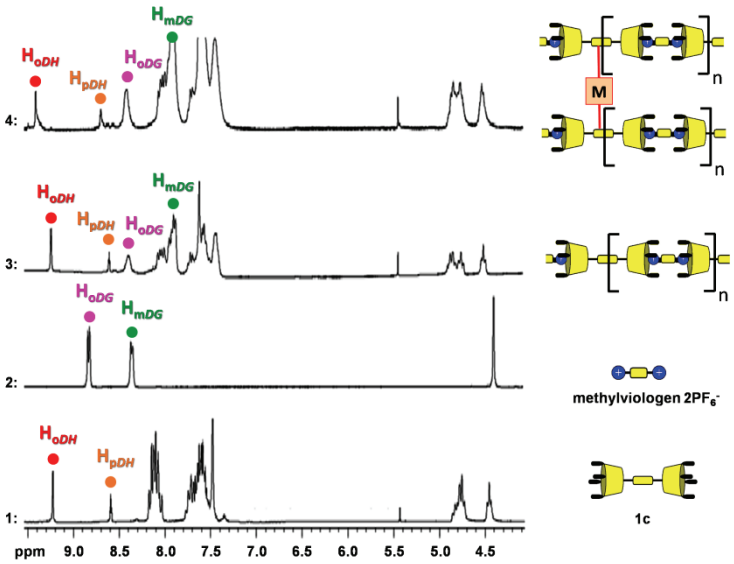

Figure 12: Section of ^1H NMR spectra (CD_3CN) monitoring host-guest complexation, and metal-driven cross-link; from the bottom 1) free **1c** host; 2) free guest; 3) host-guest complex; 4)cross-linked polymer chains.

Owing to the low solubility of the methyl viologen in apolar solvents, acetonitrile was used as solvent. The ^1H NMR spectra, shows the up-field shift of methyl-pyridinium signals (H_{oDG} and H_{mDG}), due to the inclusion inside the cavity. Moreover the observed broadening of the signals after addition of the ditopic guest indicates the formation of oligomeric/polymeric species.
The addition of $(CH_3CN)_2PdCl_2$ led to a down-field shift of the pyridine signals (H_{oDH} and H_{pDH}) in the host, demonstrating the interaction with

the Pd center, and the resulting polymer cross-link. The extension of the polymer network is also confirmed by the further broadening of the signals in the NMR spectrum.

2.3 Conclusions.

A set of complementary homoditopic molecules, able to self-assemble in polymeric chains thanks to host-guest interactions, has been designed and synthesized.
The thermodynamics of the association process has been studied via ITC measurements. Complexation resulted both enthalpy and entropy driven. In particular, the use of monomers featuring very flexible linkers, able to retain conformational freedom in the final complexes, led to favorable entropic contributions. Moreover, a significant solvent effect has been observed. Namely, a gain of two order of magnitude in the K_{ass} value was recorded moving from CH_3OH to CH_2Cl_2.
X-Ray crystal structure has been obtained for the more rigid system, formed by methyl viologen and ditopic host **1c**, bearing two cavitand units linked through an isonicotinoyl spacer. The following metal-directed cross-link of the formed linear chains was achieved by addition of $(CH_3CN)_2PdCl_2$, and the whole process was monitored by ^1H NMR.
Viscosity measurements were carried out on the more flexible system, where the ditopic guest **2c** features a PEG linking chain and the ditopic host **1b** presents two cavitand moieties joined through an adipic spacer.
A concentration-dependent ring-chain equilibrium was proved, in agreement with SLS data. Particularly significant is the considerable increase in specific viscosity observed at high concentration, demonstrating the formation of polymeric chains of increasing size.
Viscosity dependence on temperature was also evaluated in tetrachloroethane. The observed behavior suggested the presence of a critical temperature, above which rings are broken and linear chains stretch them out, promoting the approach of the reactive end-groups of different oligomers, with a consequent increase in the polymerization degree.

2.4 Experimental Section.

Bis-silylcavitand with methylenic spacer IIa.
To a solution of silylcavitand **I** (2.06 g, $2.16 \cdot 10^{-3}$ mol) in dry CH_2Cl_2 (25 mL), dimethoxymethane (0.86 mL, $9.72 \cdot 10^{-3}$ mol) and p-toluenesulfonic acid monohydrate (0.02 g, $1.26 \cdot 10^{-4}$ mol) were added. The reaction was refluxed overnight under nitrogen using a modified Soxhlet, filled with molecular sieves (type 3Å). The mixture was allowed to cool, and washed with 0.3 M NaOH, to neutralize the acid catalyst. Concentration to dryness of the organic phase afforded the crude product, that was purified by silica column chromatography (CH_2Cl_2/MeOH 99:1) to give pure **IIa** (0.66 g, $3.44 \cdot 10^{-4}$ mol, 32%).
^{1}H NMR ($CDCl_3$, 300 MHz): δ = 7.19 (s, 4H, Ar**H**); 7.18 (s, 4H, Ar**H**); 4.71 (s, 2H, OC**H**$_2$O); 4.61 (t, 8H, ArC**H**, J=8.0 Hz); 3.76 (m, 2H, OC**H**$_2$O); 3.62 (bt, 4H, CH_2C**H**$_2$O); 2.27 (m, 4H, C**H**$_2CH_2CH_2O$); 2.17 (m, 12H, C**H**$_2CH_2CH_3$); 1.91 (s, 24H, ArC**H**$_3$); 1.58 (m, 4H, CH_2C**H**$_2CH_2O$); 1.30 (m, 12H, CH_2C**H**$_2CH_3$); 0.98 (t, 18H, CH_2CH_2C**H**$_3$, J=6.6 Hz); 0.71 (s, 24H, SiC**H**$_{3OUT}$); -0.69 (s, 24H, SiC**H**$_{3IN}$). **ESI-MS:** *m/z* calcd. for $C_{105}H_{144}O_{18}Si_8$ (1918.9 Da), $[M+Na]^+$: 1941.8; found: 1941.5 $[M+Na]^+$.

Bis-silylcavitand with adipic spacer IIb.
To a solution of adipic acid (0.03 g, $1.79 \cdot 10^{-4}$ mol) in 15 mL of a dry 95:5 mixture of CH_2Cl_2 and DMF, silylcavitand **I** (0.34 g, $3.57 \cdot 10^{-4}$ mol) DCC (0.07 g, $3.57 \cdot 10^{-4}$ mol) and DMAP (0.02 g, $1.18 \cdot 10^{-4}$ mol) were added. The resulting suspension was stirred overnight at room temperature. The mixture was filtered, and the crude, recovered by solvent evaporation, was purified by silica column chromatography (CH_2Cl_2) affording pure **IIb** (0.15 g, $7.50 \cdot 10^{-5}$ mol, 42%).
^{1}H NMR ($CDCl_3$, 300 MHz): δ = 7.16 (s, 4H, Ar**H**); 7.14 (s, 4H, Ar**H**); 4.59 (t, 8H, ArC**H**, J=7.9 Hz); 4.12 (t, 4H, C**H**$_2$OC(O)CH_2, J=6.6 Hz); 2.30 (m, 4H, CH_2OC(O)C**H**$_2$); 2.16 (m, 16H, ArCHC**H**$_2$); 1.89 (s, 24H, ArC**H**$_3$); 1.64 (m, 4H+4H, OC(O)CH_2C**H**$_2$C**H**$_2CH_2$C(O)O) + CH_2C**H**$_2CH_2O$); 1.28 (m, 12H, CH_2C**H**$_2CH_3$); 0.96 (m, 18H, CH_2CH_2C**H**$_3$); 0.50 (s, 24H, SiC**H**$_{3OUT}$); -0.70 (s, 24H, SiC**H**$_{3IN}$). **ESI-MS:** *m/z* calcd. for $C_{110}H_{150}O_{20}Si_8$ (2017.0 Da), $[M+Cl]^-$: 2052.5; found: 2052.3 $[M+Cl]^-$.

Bis-silylcavitand with isonicotinoyl spacer IIc.

To a solution of 3,5-pyridinedicarboxylic acid (0.02 g, $1.20 \cdot 10^{-4}$ mol) dissolved in 9 mL of a dry 8:1 mixture of CH_2Cl_2 and DMF, DCC (0.05 g, $2.61 \cdot 10^{-4}$ mol) and DMAP (0.01 g, $8.73 \cdot 10^{-5}$ mol) were added. The resulting suspension was stirred at room temperature until complete dissolution. Silylcavitand **I** (0.25 g, $2.61 \cdot 10^{-4}$ mol) was added. The reaction mixture was stirred at room temperature for 24 h and finally quenched by solvent removal. The crude was suspended in water (10 mL) and filtered. Purification by silica column chromatography (CH_2Cl_2/EtOH 99:1) yielded the desired product **IIc** (0.11 g, $5.40 \cdot 10^{-5}$ mol, 41%).

^{1}H NMR ($CDCl_3$, 300 MHz): δ = 9.32 (d, 2H, **H_{mpy}**, J=2.0 Hz); 8.81 (d, 1H, **H_{opy}**, J=2.0 Hz); 7.16 (s, 4H, Ar**H**); 7.14 (s, 4H, Ar**H**); 4.62 (t, 8H, ArC**H**, J=8.1 Hz); 4.45 (t, 4H, C**H_2**OC(O), J =6.7 Hz); 2.32 (m, 4H, C**H_2**CH_2CH_2OC(O)); 2.17 (m, 12H, ArCHC**H_2**); 1.87 (s, 24H, ArC**H_3**); 1.82 (m, 4H, CH_2C**H_2**CH_2OC(O)); 1.27 (m, 12H, ArCHCH_2C**H_2**); 0.94 (m, 18H, CH_2CH_2C**H_3**); 0.51 (s, 24H, SiC**H_{3OUT}**); -0.68 (s, 24H, SiC**H_{3IN}**). **ESI-MS:** *m/z* calcd. for $C_{111}H_{145}NO_{20}Si_8$ (2038.0 Da), $[M+Na]^+$: 2061.0; found: 2060.8 $[M+Na]^+$.

Bis-resorcinarene with methylenic spacer IIIa.

An aqueous 36% HF solution (1.3 mL) was added to **IIa** (0.66 g, $3.44 \cdot 10^{-4}$ mol) dissolved in 30 mL of a 1:1 mixture of $CHCl_3$ and DMF. The mixture was heated at 45 °C overnight. The solvent was removed in vacuo and the product was suspended in water. Vacuum filtration afforded pure **IIIa** (0.46 g, $3.10 \cdot 10^{-4}$ mol, 91%).

^{1}H NMR (acetone-*d_6*, 300 MHz): δ = 7.95 (s, 16H, ArO**H**), 7.44 (s, 4H, Ar**H**); 7.43 (s, 4H, Ar**H**); 4.64 (s, 2H, OC**H_2**O); 4.41 (t, 8H, ArC**H**, J=7.5 Hz); 3.57 (t, 4H, CH_2C**H_2**O, J=6.6 Hz); 2.35 (m, 4H, C**H_2**CH_2CH_2O); 2.28 (m, 12H, C**H_2**CH_2CH_3); 2.05 (s, 24H, ArC**H_3**); 1.56 (m, 4H, CH_2C**H_2**CH_2O); 1.31 (m, 12H, CH_2C**H_2**CH_3); 0.95 (m, 18H, CH_2CH_2C**H_3**). **ESI-MS:** *m/z* calcd. for $C_{89}H_{112}O_{18}$ (1468.8 Da), $[M-H]^-$: 1967.8; found: 1467.9 $[M-H]^-$.

Bis-resorcinarene with adipic spacer IIIb.

An aqueous 36% HF solution (0.4 mL) was added to **IIb** (0.42 g, $2.33 \cdot 10^{-4}$ mol) dissolved in 16 mL of a 1:1 mixture of $CHCl_3$ and DMF. The mixture was heated at 45 °C overnight. The solvent was removed in

vacuo and the product was suspended in water. Vacuum filtration afforded pure **IIIb** (0.37 g, $2.33 \cdot 10^{-4}$ mol, quantitative yield).
^{1}H NMR (DMSO-d_6, 300 MHz): δ = 8.63 (s, 16H, ArO**H**); 7.25 (s, 8H, Ar**H**); 4.19 (t, 8H, ArC**H**, J=7.3 Hz); 4.01 (t, 4H, C**H$_2$**OC(O)CH_2, J=6.2 Hz); 2.21 (m, 4H+16H, CH_2OC(O)C**H$_2$** + ArCHC**H$_2$**); 1.90 (s, 24H, ArC**H$_3$**); 1.47 (m, 4H+4H, OC(O)CH_2C**H$_2$**C**H$_2$**CH_2(O)CO + CH_2C**H$_2$**CH_2O); 1.17 (m, 12H, CH_2C**H$_2$**CH_3); 0.88 (m, 18H, CH_2CH_2C**H$_3$**). **ESI-MS:** *m/z* calcd. for $C_{94}H_{118}O_{20}$ (1567.9 Da), $[M-H]^-$: 1566.8; found: 1467.0 $[M-H]^-$.

Bis-resorcinarene with isonicotinoyl spacer IIIc.
An aqueous 36% HF solution (0.8 mL) was added to **IIc** (1.0 g, $4.90 \cdot 10^{-4}$ mol) dissolved in 30 mL of a 1:1 mixture of $CHCl_3$ and DMF. The mixture was heated at 45 °C overnight. The solvent was removed in vacuo and the product was suspended in water. Vacuum filtration afforded pure **IIIc** (0.75 g, $4.72 \cdot 10^{-4}$ mol, 96%).
^{1}H NMR (DMSO-d_6, 300 MHz): δ = 9.25 (d, 2H, **H$_{mpy}$**, J=2.0 Hz); 8.63 (s, 16H, ArO**H**); 7.93 (d, 1H, **H$_{opy}$**, J=2.0 Hz); 7.25 (s, 8H, Ar**H**); 4.37 (t, 8H, ArC**H**, J=8.1 Hz); 4.19 (t, 4H, C**H$_2$**OC(O), J= 6.7 Hz); 2.35 (m, 4H, C**H$_2$**CH_2CH_2OC(O)); 2.18 (m, 12H, ArCHC**H$_2$**); 1.91 (s, 24H, ArC**H$_3$**); 1.80 (m, 4H, CH_2C**H$_2$**CH_2OC(O)); 1.20 (m, 12H, ArCHCH_2C**H$_2$**); 0.87 (m, 18H, CH_2CH_2C**H$_3$**). **ESI-MS:** *m/z* calcd. for $C_{95}H_{113}NO_{20}$ (1588.9 Da), $[M-H]^-$: 1587.8; found: 1587.8 $[M-H]^-$.

Bis-tetraphosphonatecavitand with methylenic spacer 1a.
To a solution of **IIIa** (0.46 g, $3.10 \cdot 10^{-4}$ mol) in fresh distilled pyridine (20 mL), dichlorophenylphosphine (0.36 mL, $2.64 \cdot 10^{-4}$ mol) was added slowly, at room temperature, under argon atmosphere. After 3 hours of stirring at 70 °C, the solution was allowed to cool at room temperature and 12 mL of a 1:1 mixture of aqueous 35% H_2O_2 and $CHCl_3$ were added. The resulting mixture was stirred for 30 minutes at room temperature, then the solvent was removed in vacuo. Addition of water resulted in the precipitation of a white powder, which was filtered to give pure **1a** (0.74 g, $3.02 \cdot 10^{-4}$ mol, 97%).
^{1}H NMR (acetone-d_6, 300 MHz): δ = 8.12 (m, 16H, P(O)Ar**H$_o$**); 7.74 (m, 8H, P(O)Ar**H$_p$**); 7.64 (m, 8H + 8H, Ar**H** + P(O)Ar**H$_m$**); 4.88 (t, 8H, ArC**H**, J=7.6 Hz); 4.71 (s, 2H, OC**H$_2$**O); 3.64 (bt, 4H, CH_2C**H$_2$**O); 2.47 (m, 16H, ArCHC**H$_2$**); 2.10 (s, 24H, ArC**H$_3$**); 1.65 (m, 4H, CH_2C**H$_2$**CH_2O); 1.42 (m, 12H, CH_2C**H$_2$**CH_3); 1.00 (m, 18H, CH_2CH_2C**H$_3$**). **^{31}P NMR ($CDCl_3$, 172**

MHz) δ = 5.64 (s, **P**(O)). **HR-ESI-MS:** *m/z* calcd. for $C_{137}H_{136}O_{26}P_8$ (2446.3 Da), $[M+NH_4]^+$: 2462.75590; found: 2462.76380.

Bis-tetraphosphonatecavitand with adipic spacer 1b.
To a solution of **IIIb** (0.35 g, $2.23 \cdot 10^{-4}$ mol) in fresh distilled pyridine (10 mL), dichlorophenylphosphine (0.25 mL, $1.83 \cdot 10^{-3}$ mol) was added slowly, at room temperature, under argon atmosphere. After 3 hours of stirring at 70 °C, the solution was allowed to cool at room temperature and 10 mL of a 1:1 mixture of aqueous 35% H_2O_2 and $CHCl_3$ were added. The resulting mixture was stirred for 30 minutes at room temperature, then the solvent was removed in vacuo. Addition of water resulted in the precipitation of a white powder, which was filtered to give pure **1b** (0.55 g, $2.16 \cdot 10^{-4}$ mol, 97%).
^{1}H NMR ($CDCl_3$, 300 MHz): δ = 8.08 (m, 16H, P(O)Ar**H$_o$**); 7.68-7.52 (m, 8H+16H, P(O)Ar**H$_p$** + P(O)Ar**H$_m$**); 7.25 (s, 8H, Ar**H**); 4.78 (t, 8H, ArC**H**, J= 7.8 Hz); 4.21 (t, 4H, C**H$_2$**OC(O), J=6.0 Hz); 2.46-2.27 (m, 4H+16H, $CH_2OC(O)C$**H$_2$** + ArCHC**H$_2$**); 2.13 (s, 24H, ArC**H$_3$**);1.74 (m, 4H, CH_2C**H$_2$**CH_2O); 1.62 (m, 4H, $OC(O)CH_2C$**H$_2$**C**H$_2$**$CH_2(O)CO$); 1.42 (m, 12H, CH_2C**H$_2$**CH_3); 1.06 (m, 18H, CH_2CH_2C**H$_3$**). **^{31}P NMR ($CDCl_3/D_2O$, 172 MHz)** δ = 6.59 (s, **P**(O)). **HR-ESI-MS:** *m/z* calcd. for $C_{142}H_{142}O_{28}P_8$ (2542.8 Da), $[M+H]^+$: 2543.76613; found: 2543.77453.

Bis-tetraphosphonatecavitand with isonicotinoyl spacer 1c.
To a solution of **IIIc** (0.20 g, $1.26 \cdot 10^{-4}$ mol) in fresh distilled pyridine (10 mL), dichlorophenylphosphine (0.14 mL, $1.03 \cdot 10^{-3}$ mol) was added slowly, at room temperature, under argon atmosphere. After 3 hours of stirring at 70 °C, the solution was allowed to cool at room temperature and 8 mL of a 1:1 mixture of aqueous 35% H_2O_2 and $CHCl_3$ were added. The resulting mixture was stirred for 30 minutes at room temperature, then the solvent was removed in vacuo. Addition of water resulted in the precipitation of a white powder, which was filtered to give pure **1c** (0.31 g, $1.21 \cdot 10^{-4}$ mol, 90%).
^{1}H NMR ($CDCl_3$, 300 MHz): δ = 9.25 (d, 2H, **H$_{mpy}$**, J=2.0 Hz); 8.80 (d, 1H, **H$_{opy}$**, J=2.0 Hz); 8.05 (m, 16H, P(O)Ar**H$_o$**); 7.63-7.53 (m, 8H+16H, P(O)Ar**H$_p$** + P(O)Ar**H$_m$**); 7.24 (s, 8H, Ar**H**); 4.80 (t, 8H, ArC**H**, J=7.4 Hz); 4.53 (t, 4H, C**H$_2$**OC(O), J = 6.3 Hz); 2.50 (m, 4H, C**H$_2$**$CH_2CH_2OC(O)$); 2.33 (m, 12H, ArCHC**H$_2$**); 2.20 (s, 24H, ArC**H$_3$**); 1.92 (m, 4H, CH_2C**H$_2$**$CH_2OC(O)$); 1.20 (m, 12H, $ArCHCH_2C$**H$_2$**); 1.00 (m, 18H,

$CH_2CH_2C\mathbf{H_3}$). **^{31}P NMR ($CDCl_3$, 172 MHz)** δ = 4.02 (s, **P**(O)). **HR-ESI-MS:** *m/z* calcd. for $C_{143}H_{137}NO_{28}P_8$ (2563.4 Da), $[M+H]^+$: 2564.73008; found: 2564.73965.

Diisonicotinic ester with ethyl spacer IVa.
To a solution of isonicotinoyl chloride hydrochloride (1.50 g, $8.42 \cdot 10^{-3}$ mol) in pyridine (15 mL), ethylenglycol (1.16 mL, $2.81 \cdot 10^{-3}$ mol) was added. The reaction mixture was stirred at 100 °C for 3h and the solvent was removed under vacuum. 20 mL of a solution of potassium carbonate in water were added and extracted with CH_2Cl_2. Concentration to dryness of the organic phase afforded pure **IVa** (0.82 g, $3.01 \cdot 10^{-3}$ mol, 71%).
^{1}H NMR ($CDCl_3$, 300 MHz): δ = 8.79 (d, 4H, $\mathbf{H_{orto}}$, J=6.1 Hz); 7.85 (d, 4H, $\mathbf{H_{meta}}$, J=6.1 Hz); 4.71 (s, 4H, $C\mathbf{H_2}$). **GC-MS:** calcd. for $C_{14}H_{12}N_2O_4$ (272.2 Da), found: $[M]^+$: 272.

Diisonicotinic ester with hexyl spacer IVb.
To a solution of isonicotinoyl chloride hydrochloride (1.00 g, $5.62 \cdot 10^{-3}$ mol) in pyridine (10 mL), 1,6-hexandiol (1.22 g, $1.87 \cdot 10^{-3}$ mol) was added. The reaction mixture was stirred at 100 °C for 3h and the solvent was removed under vacuum. The crude was washed with aqueous solution of K_2CO_3. Vacuum filtration afforded pure **IVb** (0.65 g, $1.98 \cdot 10^{-3}$ mol, 70%).
^{1}H NMR ($CDCl_3$, 300 MHz): δ = 8.75 (d, 4H, $\mathbf{H_{orto}}$, J=6.0 Hz); 7.82 (d, 4H, $\mathbf{H_{meta}}$, J=6.0 Hz); 4.35 (t, 4H, $C\mathbf{H_2}O$, J=6.6 Hz); 1.80 (m, 4H, $C\mathbf{H_2}CH_2O$); 1.51 (m, 4H, $C\mathbf{H_2}CH_2CH_2O$). **GC-MS:** calcd. for $C_{18}H_{20}N_2O_4$ (328.4 Da), found: $[M]^+$: 328.

Diisonicotinic ester with PEG spacer IVc.
To a solution of isonicotinoyl chloride hydrochloride (0.60 g, $3.35 \cdot 10^{-3}$ mol) in pyridine (25 mL), PEG (average M_n=1500 Da) (1.26 g, $8.43 \cdot 10^{-3}$ mol) was added. The reaction mixture was stirred at 100 °C for 3h and the solvent was removed under vacuum. The crude was washed with water and extracted with CH_2Cl_2. Concentration to dryness of the organic phase afforded pure **IVc** (2.06 g, $1.16 \cdot 10^{-3}$ mol, 69%).
^{1}H NMR ($CDCl_3$, 300 MHz): δ = 8.72 (d, 4H, $\mathbf{H_{orto}}$, J=6.0 Hz); 7.80 (d, 4H, $\mathbf{H_{meta}}$, J=6.0 Hz); 4.45 (t, 4H, $C\mathbf{H_2}OCC(O)$, J=4.8 Hz); 3.78 (m, 4H, $C\mathbf{H_2}CH_2OC(O)$); 3.58 (m, 116H, $O(C\mathbf{H_2}C\mathbf{H_2}O)_{29}$).

Ditopic Guest with ethyl spacer 2a.
To a solution of **IVa** (0.82 g, $2.99 \cdot 10^{-3}$ mol) dissolved in a 2:1 mixture of $CHCl_3$ and acetonitrile (21 mL), CH_3I (0.8 mL, $1.28 \cdot 10^{-2}$ mol) was added. The reaction mixture was stirred under reflux overnight. The solvent was removed in vacuo and the crude was recrystallized from diethyl ether to give pure **2a** (1.40 g, $2.51 \cdot 10^{-3}$ mol, 84%).
^{1}H NMR (DMSO-d_6, 300 MHz): δ = 9.18 (d, 4H, **H_{orto}**, J=6.1 Hz); 8.51 (d, 4H, **H_{meta}**, J=6.1 Hz); 4.78 (s, 4H, C**H_2**); 4.43 (s, 6H, NC**H_3**). **HR-ESI-MS:** *m/z* calcd. for $C_{16}H_{18}I_2N_2O_4$ (556.1 Da), $[M\text{-}2I]^{2+}$: 151.06278; found: 151.06267.

Ditopic Guest with hexyl spacer 2b.
To a solution of **IVb** (0.40 g, $1.22 \cdot 10^{-3}$ mol) dissolved in acetonitrile (10 mL), CH_3I (0.33 mL, $5.34 \cdot 10^{-3}$ mol) was added. The reaction mixture was stirred under reflux overnight. The solvent was removed in vacuo and the crude was recrystallized from CH_3CN/EtOAc (1:1) to give pure **2b** (0.57 g, $9.31 \cdot 10^{-4}$ mol, 76%).
^{1}H NMR (DMSO-d_6, 300 MHz): δ = 9.17 (d, 4H, **H_{orto}**, J=6.5 Hz); 8.49 (d, 4H, **H_{meta}**, J=6.5 Hz); 4.43 (s, 6H, NC**H_3**); 4.40 (t, 4H, C**H_2**O, J=6.6 Hz); 1.79 (m, 4H, C**H_2**CH_2O); 1.49 (m, 4H, C**H_2**CH_2CH_2O). **HR-ESI-MS:** *m/z* calcd. for $C_{20}H_{26}I_2N_2O_4$ (612.2 Da), $[M\text{-}2I]^{2+}$: 179.09408; found: 179.09427.

Ditopic Guest with hexyl spacer 2b*.
To a solution of **2b** (0.56 g, $9.26 \cdot 10^{-3}$ mol) in water (10 mL), NH_4PF_6 was added (0.45 g, $2.78 \cdot 10^{-3}$ mol). The mixture was stirred at room temperature for 1h. Vacuum filtration afforded pure **2b*** (0.53 g, $8.18 \cdot 10^{-3}$ mol, 88%).
^{1}H NMR (DMSO-d_6, 300 MHz): δ = 9.11 (d, 4H, **H_{orto}**, J=6.5 Hz); 8.45 (d, 4H, **H_{meta}**, J=6.5 Hz); 4.39 (s, 6H, NC**H_3**); 4.37 (t, 4H, C**H_2**O, J=6.5 Hz); 1.75 (m, 4H, C**H_2**CH_2O); 1.45 (m, 4H, C**H_2**CH_2CH_2O). **^{31}P NMR (DMSO-d_6, 172 MHz)** δ = -141.2 (s, **P**F_6). **HR-ESI-MS:** *m/z* calcd. for $C_{20}H_{26}F_{12}N_2O_4P_2$ (648.4 Da), $[M\text{-}2I]^{2+}$: 179.09408; found: 179.09375.

Ditopic Guest with PEG spacer 2c.
To a solution of **IVc** (2.06 g, $1.16 \cdot 10^{-3}$ mol) dissolved in acetonitrile (10 mL), CH_3I (0.32 mL, $5.06 \cdot 10^{-3}$ mol) was added. The reaction mixture was stirred under reflux overnight. The solvent was removed in vacuo

and the crude was taken up with diethyl ether (3 x 20mL) to give pure **2c** (1.86 g, $9.40 \cdot 10^{-4}$ mol, 81%).
^{1}H NMR ($CDCl_3$, 300 MHz): δ = 9.52 (d, 4H, **H_{orto}**, J=6.5 Hz); 8.51 (d, 4H, **H_{meta}**, J=6.0 Hz); 4.73 (s, 6H, NC**H_3**); 4.58 (t, 4H, C**H_2**OCC(O), J=4.9 Hz); 3.68 (m, 4H, C**H_2**CH_2OC(O)); 3.69-3.58 (m, 116H, O(C**H_2**C**H_2**O)$_{29}$).
HR-ESI-MS: *m/z* calcd. for $C_{80}H_{146}I_2N_2O_{36}$ (1964.8 Da), $[M-2I]^{2+}$: 855.48222; found: 855.48242.

2.5 References and Notes.

[1] (a) J.-M. Lehn, in *Supramolecular Science: Where It Is and Where It Is Going* (Eds.: R. Ungaro, E. Dalcanale), **1999**, Kluwer Academic Publishers, Dordrecht, 287–304; (b) J.-M. Lehn, *Chem. Eur. J.* **1999**, *5*, 2455–2463.

[2] R. M. Yebeutchou, F. Tancini, N. Demitri, S. Geremia, R. Mendichi, E. Dalcanale, *Angew. Chem. Int. Ed.* **2008**, *47*, 4504–4508.

[3] E. Biavardi, G. Battistini, M. Montalti, R. M. Yebeutchou, L. Prodi, E. Dalcanale, *Chem. Commun.* **2008**, 1638–1640.

[4] B. Gadenne, M. Semeraro, R. M. Yebeutchou, F. Tancini, L. Pirondini, E. Dalcanale, A. Credi, *Chem. Eur. J.*, **2008**, *14*, 8964-8971.

[5] L. B. Brunsveld, B. J. B. Folmer, E.W. Meijer, R. P. Sijbesma, *Chem. Rev.* **2001**, *101*, 4071–4097.

[6] A. Cooper, C. M. Johnson, in *Microscopy, Optical Spectroscopy, and Macroscopic Techniques*, (Eds. C. Jones, B. Mulloy, A. H. Thomas), **1994**, Humana Press, Totowa, New Jersey, 137-150.

[7] T. F. A. de Greef, M. M. J. Smulders, M. Wolffs, A. P. H. J. Schenning, R. P. Sijbesma, E. W. Meijer, *Chem. Rev.* **2009**, *109*, 5687-5754.

[8] W. Kuhn, *Kolloidn. Zh.* **1934**, *68*, 2-15.

[9] L. Mandolini, *Adv. Phys. Org. Chem.* **1986**, *22*, 1-111.

[10] (a) H. W. Gibson, N. Yamaguchi, J. W. Jones, *J. Am. Chem. Soc.* **2003**, *125*, 3522-3533; (b) F. Huang, D. S. Nagvekar, X. Zhou, H. W. Gibson, *Macromolecules* **2007**, *40*, 3561-3567.

[11] G. Ercolani, S. Di Stefano, *J. Phys. Chem. B* **2008**, *112*, 4662-4665.

[12] C.-C. Chen, E. E. Dormidontova, *Macromolecules* **2004**, *37*, 3905-3917.
[13] H. Jacobson, W. H. Stockmayer, *J. Chem. Phys.* **1950**, *18*, 1600-1606.

[14] A. Einstein, *Ann. Phys.* **1906**, *19*, 289-306.

[15] (a) R. P. Sijbesma, F. H. Beijer, L. Brunsveld,; B. J. B. Folmer, J. H. K. K. Hirshberg, R. F. M. Lange, J. K. L. Lowe, E. W. Meijer, *Science* **1997**, *278*, 1601-1604; (b) S. H. M. Soöntjens, R. P. Sijbesma, M. H. P. van Genderen, E. W. Meijer, *Macromolecules* **2001**, *34*, 3815-3818; (c) A. T. ten Cate, H. Kooijman, A. L. Spek, R. P. Sijbesma, E. W. Meijer, *J. Am. Chem. Soc.* **2004**, *126*, 3801-3808; (d) M. F. Mayer, S. Nakashima, S. C. Zimmerman, *Org. Lett.* **2005**, *7*, 3005-3008; (e) T. Park, E. M. Todd, S. Nakashima, S. C. Zimmerman, J. *Am. Chem. Soc.* **2005**, *127*, 18133-18142; (e) O. A. Scherman, G. B. W. L. Ligthart, R. P. Sijbesma, E. W. Meijer, *Angew. Chem. Int. Ed.* **2006**, *45*, 2072-2076; (f) O. A. Scherman, G. B. W. L. Ligthart, H. Ohkawa, R. P. Sijbesma, E. W. Meijer, *Proc. Natl. Acad. Sci. U.S.A.* **2006**, *103*, 11850-11855; (g) H. C. Ong, S. C. Zimmerman, *Org. Lett.* **2006**, *8*, 1589-1592; (h) T. Park, S. C. Zimmerman, *J. Am. Chem. Soc.* **2006**, *128*, 11582-11590; (i) T. Park, S. C. Zimmerman, *J. Am. Chem. Soc.* **2006**, *128*, 13986-13987; (j) T. Park, S. C. Zimmerman, *J. Am. Chem. Soc.* **2006**, *128*, 14236-14237.

[16] (a) D. I. Pererad, R. A. Shanks, *Polym. Int.* **1996**, *39*, 121-127; (b) H. Schmid, B. Michel, *Macromolecules* **2000**, *33*, 3042-3049; (c) S. A Visser, *J. Appl. Polym. Sci.* **1997**, *63*, 1.

Dual-Coded Supramolecular Frameworks[*] 3

3.1 Introduction.

Responsive materials, i.e. functional materials capable of predictable and reversible responses to precise external stimuli,[1] require the mastering of weak interactions for both their formation and function. So far the focus in supramolecular materials has been mainly on the implementation of a single interaction mode.[2,3,4] Inspired by Nature, which widely exploits multifunctionality to realize large supramolecular architectures,[5] the combination of different interaction motifs is receiving a growing attention.[6]

Until now, only few examples of multifunctional supramolecular polymers have been reported in the literature,[7] due to the difficulty in finding robust and orthogonal self-assembly modes. In particular, attention has to be paid to the geometry of the monomers, in order to control the structural growth of polymers, and to the strength of the selected binding motifs, in order to assure an high degree of polymerization.[8] Moreover, high fidelity of the orthogonal recognition units to their complementary counterparts is demanded, in order to achieve well-defined multifunctionalization.[7]

In a previous work,[9] we reported the synthesis and design of dynamic materials based on metal-directed and solvent-driven self-assembly of cavitands. In particular, solvophobic interactions of a quinoxaline kite velcrand were combined with metal-coordination capability of two pyridine ligands, introduced at the lower rim of the cavitand.[10] Only

[*] The work reported in this chapter has been accepted for publication.

oligomers could be formed by following that approach, because of the weakness of the solvophobic interaction (K_{ass}^{273K} = 1.91•10^3 M^{-1}). Namely, the introduction of two pyridyl-based connecting units at the lower rim rigidified the velcrand structure, affecting the spatial orientation of the quinoxaline wings and therefore reducing the dimerization capability.

To overcome this problem, we devised a different combination of orthogonal interactions, substituting the metal coordination with a robust multiple H-bonding. The H-bonding interaction chosen is the ureidopyrimidone unit, capable of homodimerizing with high fidelity.[2a,d] Along this line, we report here the synthesis and the association properties of a new quinoxaline kite velcrand, bearing a single ureidopyrimidone moiety at the lower rim, and able to combine multiple hydrogen bonding with solvophobic interactions to generate a dual-coded supramolecular structure. This change in the monomer allows the retention of the natural spatial orientation for the quinoxaline wings, preserving unchanged their tendency to dimerize under solvophobic conditions.[11]

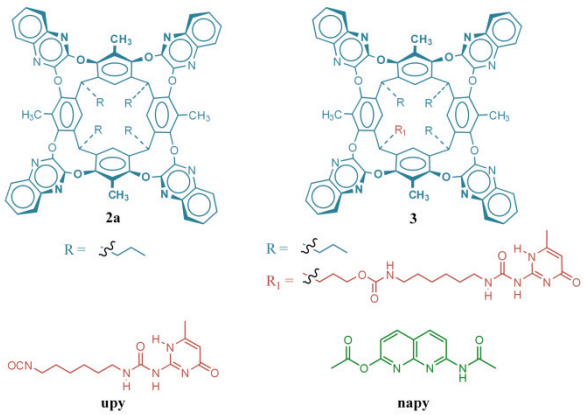

Scheme 1: Synthesized molecules.

3.2 Results and Discussion.

The target cavitand 3, which features an ureidopyrimidone moiety at the lower rim and four quinoxaline wings in kite conformation at the

upper rim, was synthesized in two steps starting from the monohydroxy resorcinarene[6d] **1b** (Scheme 2). Condensation with 2,3-dichloroquinoxaline afforded the corresponding quinoxaline-bridged cavitand **2b**, which was then reacted with 2(6-isocyanatohexylaminocarbonylamino)-6-methyl-4[1H]pyrimidinone[12] to afford the kite velcrand **3**. The methyl groups in the apical positions of the resorcinarene skeleton freeze the molecule in kite conformation, allowing kite-to-kite dimerization at the upper rim, while the ureidopyrimidone unit controls the dimerization at the lower rim.
The structurally related quinoxaline kite cavitand **2a** was synthesized as solvophobic dimerization model. This molecule, bearing four alkyl feet, is unable to undergo H-bonded dimerization, but it can form the kite-kite homodimer **2a•2a**, as well as heterodimer **2a•3**, if mixed with a solution of **3•3**. Both monomeric and dimeric species were detected in methanol solution via HR-ESI MS (see Experimental Section).

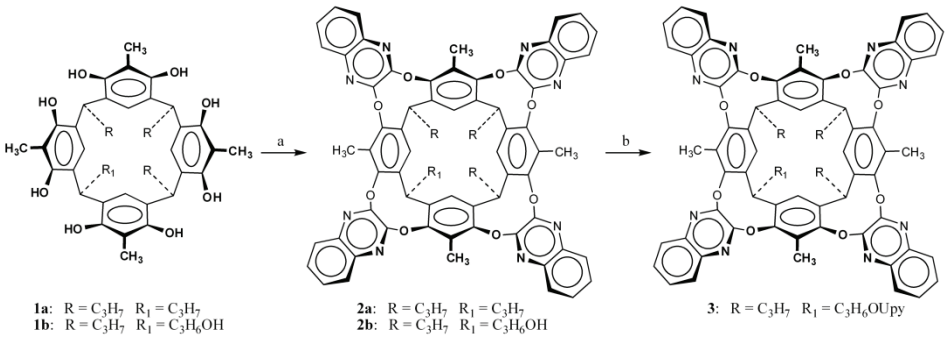

Scheme 2: Synthesis of kite velcrand **2a** and **3**: (a) 2,3-dichloroquinoxaline, K_2CO_3, 80 °C, DMF; (b) 2(6-isocyanatohexylaminocarbonylamino)-6-methyl-4[1H]pyrimidinone, toluene, reflux.

A simple ^{1}H NMR experiment was devised to prove that the chosen binding interactions are selective and orthogonal: equimolar amounts of quinoxaline velcrand 2a and 2(6-isocyanatohexylaminocarbonylamino)-6-methyl-4[1H]pyrimidinone (upy)[12] were mixed in $CDCl_3$. As shown in Figure 1, the spectrum of this solution resulted the sum of the spectra of the two components, as expected for non interacting species. In particular, the signals at 13.1, 11.9 and 10.2 ppm, diagnostic for the H-bonded N*H* protons in **upy•upy** homodimers, did not feature any

chemical shift. In the same manner, the signals at 3.16 and 2.26 ppm, typical for the ArC*H*$_3$ protons of kite-kite quinoxaline dimers, maintained their original position, confirming the simultaneous presence of **2a•2a** and upy•upy species in solution.

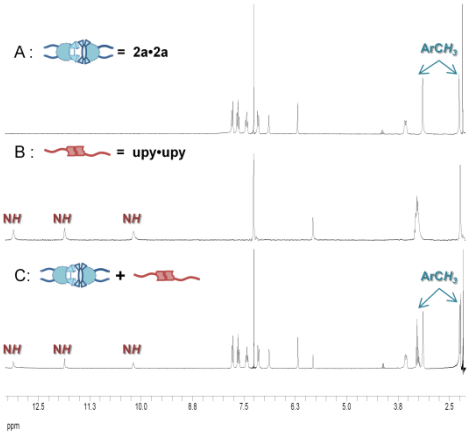

Figure 1: Partial ^{1}H NMR spectra (300 MHz) in $CDCl_3$ of (A) **2a•2a**, (B) **upy•upy**, (C) **2a•2a** + **upy•upy** (1:1).

The next step was to track the self-assembly of ditopic monomer **3** in solution. Also in this case, diagnostic signals for kite-to-kite dimerization (3.10 and 2.13 ppm) and for H-bonding formation (region between 13.14 and 9.75 ppm) were observed, demonstrating that both the binding motifs were operational in chloroform solution (Figure 2, spectrum A).

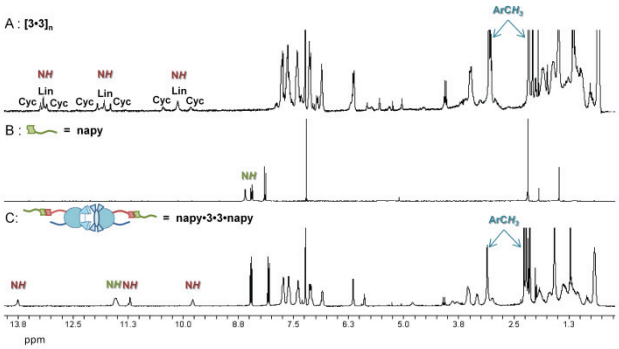

Figure 2: Partial ^{1}H NMR spectra (300 MHz) in $CDCl_3$ of (A) [**3•3**]$_n$, (B) **napy•napy**, (C) **napy•3•3•napy**. Lin and Cyc indicate respectively the resonances belonging to the linear and the cyclic structures.

Interestingly, H-bonded N*H* protons displayed three sets of signals instead of one, as usually expected for upy•upy dimerization. The source of this splitting lies in the concomitant of formation of linear and cyclic oligomers (Fig. 3). The smaller lateral peaks flanking the major ones are attributed to the cyclic structures, as already shown for a related upy•napy system.[13] The different connectivity between the dissymmetric cavitand monomers accounts for the NMR multiplicity observed both in the quinoxaline region (7.73-6.86 ppm, in $CDCl_3$) and in the NH resonances for the cyclic structures.

To support this hypothesis, an equimolar amount of 2,7-acetamido-1,8-naphthyridine[14] (napy) was added to the solution of 3. The use of naphthyridine motifs to dissociate **upy•upy** homodimers by turning them in robust **upy•napy** heterodimers, is well known in the literature.[15] In our case, after the napy addition, the multiple sets of signals related to the H-bonded N*H* protons, merged into a single signal, with diagnostic chemical shifts for **upy•napy** heterodimers (Figure 2, spectrum C). The napy addition did not affect kite-to-kite dimerization, as proved by the unchanged chemical shifts for the ArC*H*$_3$ protons. Thus, the simplification in the NMR spectrum was determined by the quantitative formation of geometrically equivalent **napy•3•3•napy** tetrameric species, which destroyed the cyclic structures.

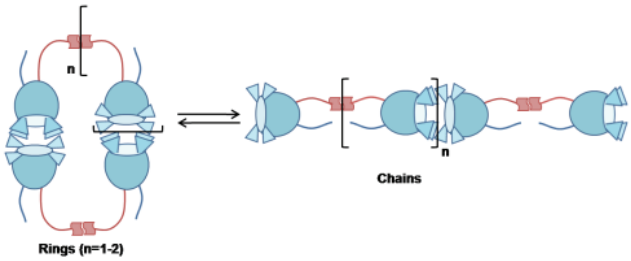

Figure 3: The proposed equilibrium between cyclic and linear structures.

Further support to the cyclic-linear equilibrium came from variable temperature ^{1}H NMR experiments. Upon heating to 343 K in a $CCl_4/C_2D_4Cl_2$ solution, the resonances belonging to the cyclic structures almost disappeared, leaving unchanged the resonances belonging to the linear species. This temperature-driven ring-opening polymerization of upy•upy cyclic structures has been already described by Sijbesma and Meijer.[16] Under the same conditions, no significant shifts were observed for the ArC*H*$_3$ protons, demonstrating the high

stability of kite-kite solvophobic interactions. This despite the fact that carbon tetrachloride is one of the best solvents for the dissociation of velcrands.[11c]

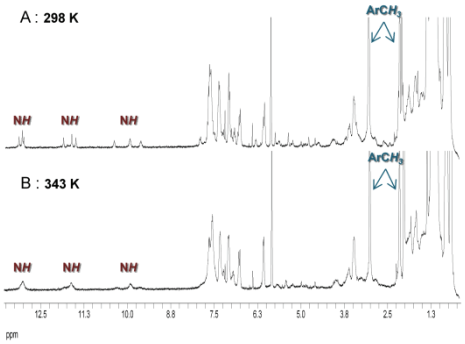

Figure 4: Partial ^{1}H NMR spectra in $CDCl_3$ of (A) [**3•3**]$_n$ at 298 K, (B) [**3•3**]$_n$ at 343 K.

The strength of the two binding interactions was apparent from a simple ^{1}H NMR dilution experiment. When a solution of **3** in chloroform was diluted to 50 μM, no new peaks appeared nor did any shift occur, putting a lower limit on the dimerization constants $K_{ass} > 10^5$ M^{-1}. Moreover, no signals due to monomeric species appeared when solution was frozen to 233 K. Thus, the performed ^{1}H NMR experiments suggested a high stability for the complex formation, in line with the association constants reported in literature (in chlorinated solvents, $K_{ass} > 10^6$ M^{-1} for the H-bonding interaction,[17] and $K_{ass} > 10^5$ M^{-1} for the solvophobic one[11c]).

The reversible disassembly/reassembly of both cyclic and linear species **3** was proved by addition/removal of methanol to a chloroform solution of **3**.

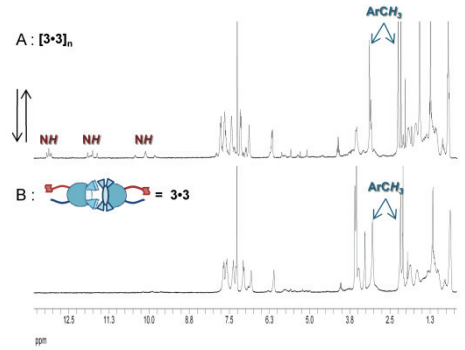

Figure 5: Partial ^{1}H NMR spectra of (A) [**3•3**]$_n$, (B) **3•3** in $CDCl_3$/MeOD (8:2).

As pictured in Figure 5, the additions destroyed the H-bonding network, which formed again when methanol was removed. On the contrary, all the attempts to break reversibly the kite-kite dimeric units failed. Change in solvents, as well as increase in temperature, resulted inefficient.

The average molecular weight M_W of the cyclic-linear oligomer mixture **3** was experimentally determined at different concentrations by static light scattering (SLS) measurements in chloroform. The M_W of the polymer increased linearly with the concentration in the range of 20–45 gL^{-1} and reached an upper value of 7700 Da, corresponding to an average degree of polymerization of 5 units (Table 1). Above this concentration threshold, saturation of the light scattering signal occurred. The low number of connected monomer units N_w obtained represents a further evidence of the formation of cyclic structures, which are favored at low concentration regimes.[18]

conc (mg/ml)	M_W (Da)	$\langle N_w \rangle$
19	2700±300	2
23	4900±100	3
31	5800±300	4
45	7700±400	5

Table 1: SLS measurements of M_W for the polymer **3**, in chloroform (dn/dc = 0.146 ml/g).

Dynamic Light Scattering (DLS) measurements were made to validate the SLS data. A clear growing trend was observed as function of monomer **3** concentration, as shown in Figure 6. The size of the observed objects in solution is in line with the dimensions expected for cyclic structures (see inset of Figure 6). This implies that the equilibrium at these concentrations is shifted toward the formation of cyclic oligomers, as shown by SLS measurements.

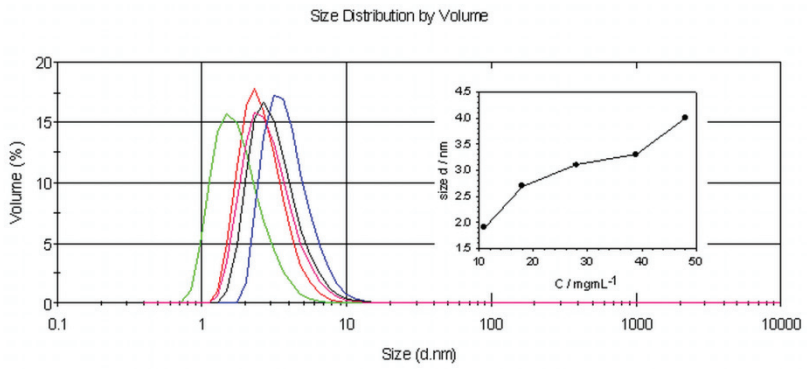

Figure 6: Size distribution by volume of compound **3** aggregates in chloroform solutions at different concentrations (PdI=0.2) and average hydrodynamic diameter vs. concentration of **3**.

In order to shift the ring-chain equilibrium towards the formation of linear structures we moved to higher concentrations regimes.[19] Figure 7 shows the ^{1}H NMR spectrum for a 104 mM solution of **3** in $CDCl_3$. Under this regime, the signals belonging to the cyclic structures disappeared, thus demonstrating that (i) at low concentrations the macrocycles are present in large amount and (ii) the equilibrium can be turned toward the formation of linear polymers increasing the concentration. Unfortunately, at these concentrations, the SLS and DLS measurements are not accessible, due to the saturation of the signal.

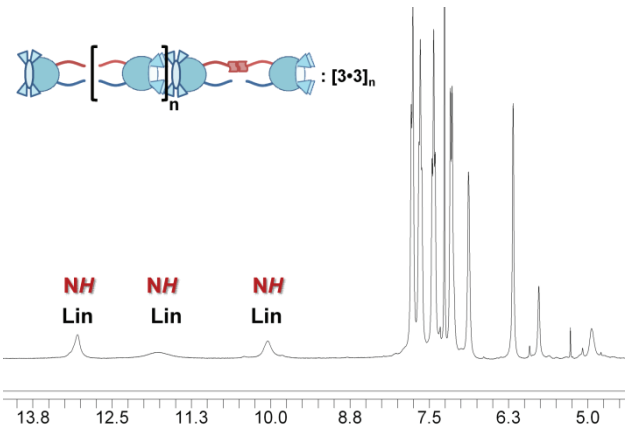

Figure 7: Partial ^{1}H NMR spectra of $[\mathbf{3{\bullet}3}]_n$, in $CDCl_3$ at 104 mM concentration.

3.3 Conclusions.

In this work we have introduced a new ditopic cavitand monomer **3**, capable of solvophobic interactions at the upper rim and multiple H-bonding at the lower rim. The two interaction modes are fully orthogonal and strong, both featuring dimerization K_{ass} above 10^5 M^{-1}. The polymerization potential of the cavitand monomer is hampered by the formation of cyclic structures at low concentrations, as shown by NMR experiments and supported by SLS and DLS measurements. The ring-chain equilibrium can be shifted toward the predominant formation of linear oligomers by heating the solution and by increasing the concentration. Reversible assembly/disassembly of **3** was achieved by selective intervention on the H-bond motif, via addition of a competing solvent. Instead, the solvophobic kite-to-kite dimerization is resilient, being effective even in low polarity solvents. Therefore the introduction of a single connection unit at the lower rim does not affect the solvophobic interaction mode. Further work is in progress to determine the aggregation behavior of **3** in higher concentrations regime.

3.4 Experimental Section.

Tetraalkyl-footed quinoxaline-bridged cavitand 2a.
To a solution of resorcinarene **1a** (0.50 g, $7.01 \cdot 10^{-4}$ mol) in dry DMF (15 mL), K_2CO_3 (0.80 g, $5.78 \cdot 10^{-3}$ mol) and 2,3-dichloroquinoxaline (0.67 g, $3.35 \cdot 10^{-3}$ mol) were added. The resulting mixture was stirred overnight at 80 °C. After cooling to r.t. the suspension was poured into H_2O (50 mL) and stirred for 10 minutes in an ice bath. The precipitate was filtered, washed with water and dried. The crude product was purified by column chromatography (SiO_2, CH_2Cl_2/EtOH 98:2) giving the quinoxaline-bridged cavitand **2a** (0.53 g, $4.35 \cdot 10^{-4}$ mol, 62%).
^{1}H NMR ($CDCl_3$, 300 MHz): δ (ppm) 7.79 (d, 4H, Qx, J= 8.1Hz); 7.64 (t, 4H, Qx, J= 8.1Hz); 7.42 (t, 4H, Qx J = 8.1Hz); 7.15 (d, 4H, Qx, J= 8.1Hz); 6.89 (s, 2H, Ar**H**); 6.19 (s, 2H, Ar**H**); 3.56 (m, 4H, ArC**H**); 3.16 (s, 6H, ArC**H$_3$**); 2.26 (s, 6H, ArC**H$_3$**); 1.94 (m, 4H, ArCHC**H$_2$**); 1.72 (m, 4H, ArCHC**H$_2$**); 1.28-1.03 (m, 8H, CH_2C**H$_2$**CH_3); 0.70 (t, 12H, CH_2CH_2C**H$_3$**, J= 7.2Hz). **HR-ESI-MS:** m/z calcd. for $C_{76}H_{64}N_8O_8$ (1217.4 Da), $[M+H]^+$: 1217.49199; found: 1217.49199; $[2M+H]^+$ (dimer): 2433.98062; found: 2433.98595.

Monohydroxy-footed quinoxaline-bridged cavitand 2b.
To a solution of monohydroxy-footed resorcinarene **1b** (0.90 g, $1.23 \cdot 10^{-3}$ mol) in dry DMF (25 mL), K_2CO_3 (1.41 g, $1.02 \cdot 10^{-2}$ mol) and 2,3-dichloroquinoxaline (1.17 g, $5.89 \cdot 10^{-3}$ mol) were added. The resulting mixture was stirred overnight at 80 °C. After cooling to r.t. the suspension was poured into H_2O (150 mL) and stirred for 30 minutes in an ice bath. The precipitate was filtered, washed with water and dried. The crude product was purified by column chromatography (SiO_2, CH_2Cl_2/EtOAc 8:2, then CH_2Cl_2/EtOH 95:5) giving the quinoxaline-bridged cavitand **2b** (1.00 g, $8.11 \cdot 10^{-4}$ mol, 66%).
^{1}H NMR (DMSO-d_6, 300 MHz): δ (ppm) 7.71 (t, 4H, Qx, J= 7.8Hz); 7.62 (d, 4H, Qx, J= 8.1Hz); 7.50 (t, 4H, Qx, J= 7.8Hz); 7.06 (d, , 4H, Qx, J= 8.1Hz); 6.99 (s, 2H, Ar**H**); 6.53 (s, 2 H, Ar**H**); 4.20 (t, 1H, CH_2CH_2O**H**, J= 5.1Hz); 3.41 (m, 4H, ArC**H**); 3.19 (m, 2H, CH_2C**H$_2$**OH); 2.98 (s, 6H, ArC**H$_3$**); 2.25 (m, 4H, ArCHC**H$_2$**); 2.09 (s, 6H, ArC**H$_3$**); 1.80-1.70 (m, 4H, ArCHC**H$_2$**); 1.20-0.91 (m, 8H, $ArCHCH_2C$**H$_2$**); 0.64 (t, 9H, CH_2CH_2C**H$_3$**, J= 7.2Hz). **ESI-MS:** m/z calcd. for $C_{76}H_{64}N_8O_9$ (1233.4 Da), [M+Na]+: 1255.5; found: 1255.4.

Monoureidopyrimidone-footed quinoxaline-bridged cavitand 3.
To a suspension of quinoxaline-bridged cavitand **2b** (0.95 g, $7.66 \cdot 10^{-4}$ mol) in toluene (35 mL), 2(6-isocyanatohexylaminocarbonylamino)-6-methyl-4[1H]pyrimidinone[12] (0.25 g, $8.43 \cdot 10^{-4}$ mol) and dibutyltindilaurate (3.0 mol%) were added. The mixture was stirred under reflux overnight. Reaction was quenched by solvent removal in vacuo. The crude was then dissolved in CH_2Cl_2, and the solution recovered after filtration was concentrated to dryness. The resulting product was purified by column chromatography (SiO_2, CH_2Cl_2/EtOAc 8:2, then CH_2Cl_2/EtOH 95:5) giving cavitand **3** (0.35 g, $2.29 \cdot 10^{-4}$ mol, 30%).
^{1}H NMR (DMSO-d_6, 300 MHz): δ (ppm) 11.55 (bs, 1H, Upy); 9.67 (bs, 1H, Upy); 7.71 (bt, 4H, Qx, J= 7.0Hz); 7.61 (d, 4H, Qx, J= 8.1Hz); 7.50 (t, 4H, Qx, J= 8.1Hz); 7.25 (bs, 1H, Upy); 7.07 (d, 4H, Qx, J= 7.0Hz); 6.97 (s, 2H, Ar**H**); 6.81 (bt, 1H, OC(O)N**H**, J= 4.9Hz); 6.52 (bs, 2H, Ar**H**); 5.74 (s, 1H, C**H**CCH_3); 3.74 (m, 2H, C**H$_2$**OC(O)); 3.42 (m, 4H, ArC**H**); 3.05 (m, 2H, NHC(O)NHC**H$_2$**); 2.98 (s, 6H, ArC**H$_3$**); 2.75 (m, 2H, OC(O)NHC**H$_2$**); 2.26 (m, 4H, ArCHC**H$_2$**); 2.08 (s, 6H, ArC**H$_3$**); 2.06 (s, 3H, ArC**H$_{3upy}$**); 1.70 (m, 4H, ArCHC**H$_2$**); 1.34-0.92 (m, 8H + 8H, $ArCHCH_2C$**H$_2$** + $OC(O)NHCH_2(C$**H$_2$**$)_4NH(O)CO$); 0.65 (t, 9H, CH_2CH_2C**H$_3$**,

J= 7.1Hz). **HR-ESI-MS:** m/z calcd. for $C_{89}H_{83}N_{13}O_{12}$ (1525.6 Da), $[M+H]^+$: 1526.63569; found: 1526.63542; $[2M+H]^+$ (dimer): 3052.26802; found: 3052.25702.

3.5 References and Notes.

[1] (a) J.-M. Lehn in *Supramolecular Science: Where It Is and Where It Is Going* (Eds. R. Ungaro, E. Dalcanale), **1999**, pp. 287-304, (Kluwer AcademicPublishers: Dordrecht); (b) J.-M. Lehn, *Chem. Eur. J.* **1999**, *5*, 2455-2463; (c) J.-M. Lehn, *Proc. Natl. Acad. Sci.U.S.A.* **2002**, *99*, 4763-4768; (d) *Supramolecular Polymers, Second Edition* (Ed. A. Ciferri), **2005**, (Francis & Taylor: New York,. NY), 2563.

[2] H-bonding: (a) R. P. Sijbesma, F. H. Beijer, L. Brunsveld, B. J. B. Folmer, J. H. K. K. Hirschberg, R. F. M. Lange, J. K. L. Lowe, E.W. Meijer, *Science* **1997**, *278*, 1601-1604; (b) R. K. Castellano, D. M. Rudkevich, J. Rebek, *Proc. Natl. Acad. Sci. U.S.A.* **1997**, *94*, 7132-7137; (c) H. Xu, D. M. Rudkevich, *Chem. Eur. J.* **2004**, *10*, 5432-5442; (d) G. B. W. L. Ligthart, H. Ohkawa, R. P. Sijbesma, E. W. Meijer, *J. Am. Chem. Soc.* **2005**, *127*, 810-811; (e) T. Park, S. C. Zimmerman, *J. Am. Chem. Soc.* **2006**, *128*, 11582-11590; (f) E. M. Todd, S. C. Zimmerman, *J. Am.Chem. Soc.* **2007**, *129*, 14534-14535.

[3] Metal-ligand coordination: (a) J.-P. Sauvage, *Chem. Rev.* **1994**, *94*, 993-1019; (b) I. Manners, *Angew. Chem. Int. Ed.* **1996**, *35*, 1602-1621; (c) U. Michelsen, C. A. Hunter, *Angew. Chem. Int. Ed.* **2000**, *39*, 764-767; (d) U. S. Schubert, C. Eschbaumer, *Angew. Chem. Int. Ed.* **2002**, *41*, 2892-2926; (e) D. G. Kurth, N. Severin, J. P. Rabe, *Angew. Chem. Int. Ed.* **2002**, *41*, 3681-3683.

[4] Host-guest: (a) M. Miyauchi, Y. Takashima, H. Yamaguchi, A. Harada, *J. Am. Chem. Soc.* **2005**, *127*, 2984-2989; (b) H. Takahashi, Y. Takashima, H. Yamaguchi, A. Harada, *J. Org. Chem.* **2006**, *71*, 4878-4883; (c) V. H. Soto Tellini, A. Jover, J. C. Garcia, L. Galatini, F. Meijide, J. V. Tato, *J. Am. Chem. Soc.* **2006**, *128*, 5728-5734; (d) R. M.

Yebeutchou, F. Tancini, N. Demitri, S. Geremia, R. Mendichi, E. Dalcanale, *Angew. Chem. Int. Ed.* **2008**, *47*, 4504-4508.

[5] D. Philp, J. F. Stoddart, *Angew. Chem. Int. Ed.* **1996**, *35*, 1154-1196.

[6] H. Hofmeier, U. S. Schubert, *Chem. Commun.* **2005**, 2423-2432.

[7] (a) W. Gerhardt, M. Crne, M. Weck, *Chem. Eur. J.* **2004**, *10*, 6212-6221; (b) K. P. Nair, J. M. Pollino, M. Weck, *Macromolecules* **2006**, *39*, 931-940; (c) C. R. South, C. Burd, M. Weck, *Acc. Chem. Res.* **2007**, *40*, 63-74; (d) J. R. Carlisle, M. Weck, *Functional Organic Materials* **2007**, 261-292; (e) A. V. Ambade, S. K. Yang, M. Weck, *Angew. Chem., Int. Ed.* **2009**, *48*, 2894-2898.

[8] (a) L. Brunsveld, B. J. B. Folmer, E. W. Meijer, R. P. Sijbesma, *Chem. Rev.* **2001**, *101*, 4071-4098; (b) G. B. W. L. Ligthart, O. A. Scherman, R. P. Sijbesma, E. W. Meijer, in *Macromulecular Engeneering. Precise Synthesis, Materials Properties, Application* (Eds. K. Matijaszewski, Y. Gnanou, L. Liebler), **2007**, pp. 351-398, (Whiley-VCH, Weinhaim).

[9] (a) L. Pirondini, A. G. Stendardo, S. Geremia, M. Campagnolo, P. Samorì, J. P. Rabe, R. Fokkens, E. Dalcanale, *Angew. Chem., Int. Ed.* **2003**, *42*, 1384-1387.

[10] For a related approach see: (a) H. Ihm, J.-S. Ahn, M. S. Lah, Y. H. Ko, K. Paek, *Org. Lett.* **2004**, *6*, 3893-3896; (b) M.-J. Kwak, K. Paek, *Bull. Korean Chem. Soc.* **2007**, *28*, 1440-1442.

[11] (a) J. A. Bryant, C. B. Knobler, D. J. Cram, *J. Am. Chem. Soc.* **1990**, *112*, 1254-1255; (b) J. A. Bryant, J. L. Ericson, D. J. Cram, *J. Am. Chem. Soc.* **1990**, *112*, 1255-1256; (c) D. J. Cram, H.-J. Choi, J. A. Brayant, C. B. Knobler, *J. Am. Chem. Soc.* **1992**, *114*, 7748-7765.

[12] H. M. Keizer, R. Van Kessel, R. P. Sijbesma, E. W. Meijer, *Polymer* **2003**, *44*, 5505-5511.

[13] T. F. A. de Greef, G. Ercolani, G. B. W. L. Ligthart, E. W. Meijer, R. P. Sijbesma, *J. Am. Chem. Soc.* **2008**, *130*, 13755-13764.

[14] C. Alvarez-Rua, S. Garcia-Granda, S. Goswami, R. Mukherjee, S. Dey, R. M. Claramunt, M. D. S. Maria, I. Rozas, N. Jagerivic, I. Alkorta, J. Elguero, *New J. Chem.* **2004**, *28*, 700-707.

[15] (a) X. Zhao, X.-Z. Wang, X.-K. Jiang, Y.-Q. Chen, Z.-T. Li, G.-J Chen, *J. Am. Chem. Soc.* **2003**, *125*, 15128-15139; (b) X.-Q. Li, D.-J. Feng, X.-K Jiang,Z.-T. Li, *Tetrahedron* **2004**, *60*, 8275-8284.

[16] B. J. B. Folmer, R. P. Sijbesma, E. W. Meijer, *J. Am. Chem. Soc.* **2001**, *123*, 2093-2094.

[17] S. H. M. Söntjens, R. P. Sijbesma, M. H. P. Van Genderen, E. W. Meijer, *J. Am. Chem. Soc.* **2000**, *122*, 7487-7493.

[18] T. F. A. de Greef, M. M. J. Smulders, M. Wolffs, A. P. H. J. Schenning, R. P. Sijbesma, E. W Meijer, *Chem. Rev.* **2009**, *109*, 5687-5754.

[19] S. H. M. Söntjens, R. P. Sijbesma, M. H. P. van Genderen, E. W. Meijer, *Macromolecules* **2001**, *34*, 3815-3818.

Cavitand-Based Ion-Pair Receptors

4

4.1 Introduction.

The development of synthetic receptors able to mimic non-covalent interactions in nature and to bind charged species efficiently and selectively is a topic of growing interest in supramolecular chemistry.
While in the past years many efforts have been devoted to the realization of specific cation[1] or anion[2] receptors, recently the attention has been focused on the design of heterotopic ion-pair receptors,[3] featuring simultaneous complexation of both cationic and anionic species. These systems are particular intriguing because of their potential applications in biological processes, in the environmental protection, as well as in the industrial field, acting, for example, as salt extraction, solubilization or membrane transfer agents.[4]
So far the research in ion-pair receptors has been mainly focused on calipyrroles,[5] calixarenes[6] and crown ethers coupled with azamacrocycles.[7]
In this work we introduce cavitands as a new class of ion-pair receptors where, multiple weak non-covalent interactions lead to a contact ion-pair complexation. Herein we report the optimization of the cavitand lower rim functionalization and geometry, which allowed us to move from a limited anion host to an efficient ion-pair receptor.

4.2 Results and Discussion.

4.2.1 General Receptor Design.

When a new ion-pair receptor is designed, special attention has to be paid at its geometry optimization. In the specific case of contact ion-pair complexation, the anion and cation binding sites must be positioned in close proximity to avoid the energetically unfavorable separation of two opposite charged species.[8]

Our starting point was the observation of several crystal structures of resorcinarene[9] and cavitand[10] complexes with charged species where the anion is included within the alkyl feet pocket at the lower rim due to multiple CH-anion interactions with the H_{down} aromatic hydrogens[11] and the ArCHCH_2 α-methylene units of the chains.[12]

Moving from this consideration, we chose to design and prepare resorcinarene-based cavitands as ion-pair receptors according the following guidelines: i) maximize the CH-anion interactions by blocking the resorcinarene in the cone conformation, in which the four H_{down} converge to the lower rim pocket; ii) introduce four additional bridging groups for the cationic counterion in close proximity of the anionic site (Figure 1).

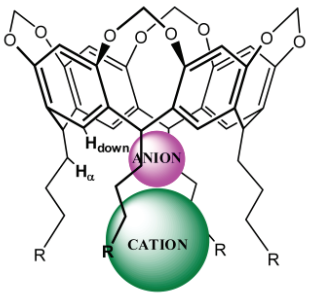

Figure 1: Schematic representation of the target receptor and of the complexation strategy.

To avoid any intramolecular competition in the ion-pair binding, a complexation inefficient upper rim cavity was required. Methylene groups were therefore selected as binding units, since they freeze the macrocycle in the desired cone conformation, without attributing any specific binding property to the resulting shallow cavity. Even if Schalley and coworkers demonstrated that methylene-bridged cavitands

are able to bind anionic species in gas phase,[13] no evidences have ever been shown of such affinity between anions and methylene-bridged cavitands in solution, where the solvent effect cannot be neglected.

4.2.2 Hydrocarbon-footed cavitands.

To evaluate a suitable functionalization for the cavitand lower rim, theoretical calculations based on PM3 semiempirical methods, using SPARTAN,[14] were performed. These studies suggested that the target receptor **1**, with four phenyl-ended feet, provided an optimal spatial arrangement for the complexation of tetrabutylammonium chloride (TBAC) at the bottom of the cavitand bowl. The phenyl groups should bind the cation by additional cation-π interactions,[15] favoring the ion-pair complexation.
Receptor **1** was indeed prepared according the synthetic pathway shown in Scheme 1. At first, an acid catalyzed condensation between resorcinol and 5-phenylpentanal was exploited to obtain resorcinarene **7**, which was subsequently functionalized at the upper rim with methylene bridges, by reacting with chlorobromomethane, in presence of K_2CO_3.

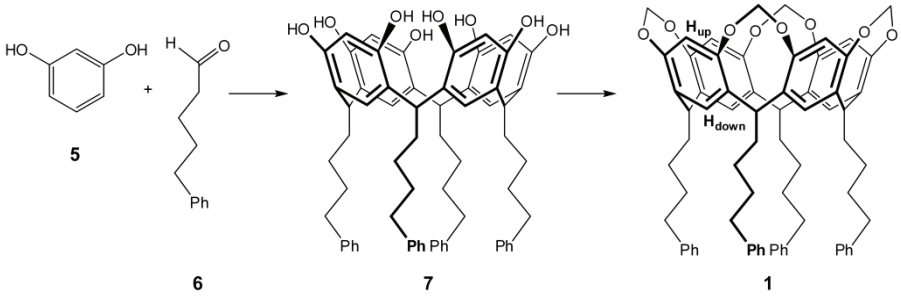

Scheme 1: Synthesis of target receptor **1**: a) EtOH/HCl, 24 h, r.t; 72 h, 80 °C; b) $BrCH_2Cl$, dry DMF, overnight, 80 °C.

In order to evaluate the effect induced by the selected lower rim functionalization on the cavitand binding ability, receptors **2** and **3** were also prepared, according to known literature procedures.[13,16] Cavitand **2** features four hexyl feet at the lower rim, while cavitand **3** presents four phenyl-ended ethyl chains. In both cases, the binding affinity for TBAC is expected to be lower than in the case of target receptor **1**, because,

respectively, the stabilizing cation-π interaction was removed (cavitand **2**), or the volume provided for the guest allocation was reduced (cavitand **3**).[17]

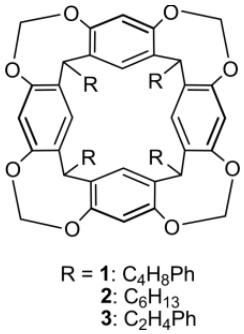

Figure 2: Target receptors **1**, **2**, **3**.

Cavitand **1** molecular structure has been solved. The crystal packing (Figure 3) revealed that, in the solid state, the cavitand feet define a rather wide cavity (5.2 Å wide and 8.7 Å deep), large enough to engulf TBAC as a whole. Partial interdigitation of the cavitand legs is observed, and a methanol molecule is nested in the shallow cavity at the upper rim.

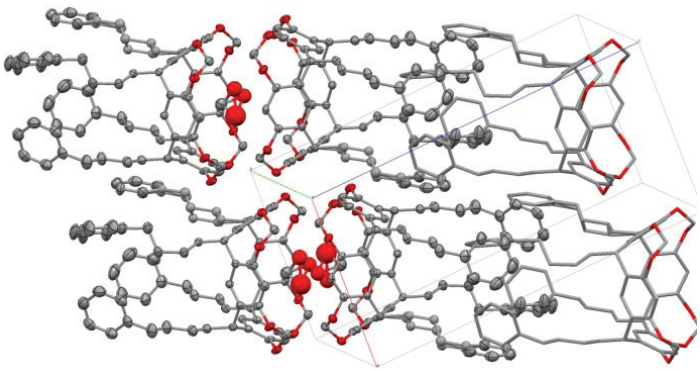

Figure 3: Receptor **1** crystal packing view.

Cavitand **1** binding properties were initially examined, in acetone-d_6 solution, by ^{1}H NMR titration.

The largest change in the cavitand chemical shifts (Figure 4) is the downfield movement of 0.78 ppm for the aromatic H_{down} protons, which

is indicative of their interaction with a bound chloride anion.[11a] Consistent with this hypothesis is also the smaller downfield shift featured by the nearby ArCHC*H*$_2$ protons of the receptor alkyl chains ($\Delta\delta$ = 0.45 ppm).

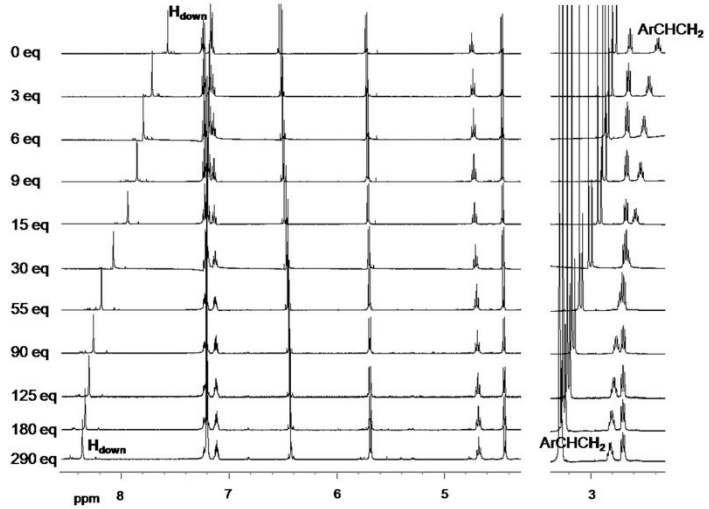

Figure 4: Partial ^{1}H NMR spectra in acetone-d_6 for titration of receptor **1** with TBAC.

In contrast to what would be expected, assuming simultaneous cation and anion complexation, no shifts were observed for the protons of the phenyl groups in the receptor, or for the signals related to the guest cationic moiety. Since no changes were recorded for the receptor *H*$_{up}$ or OC*H*$_2$O protons, we can also exclude the cation complexation at the upper rim.

Having verified a 1:1 stoichiometry for the complexation, by means of continuous variation method, the association constant (K_{ass}), based on monitoring of *H*$_{down}$ signal shifts, was calculated using a non-linear curve fitting in MATLAB fitting tools[18] (see Appendix C for details about the used fitting equations). The K_{ass} value resulted smaller than expected (25 ± 2 M^{-1}), but justified by considering that only the anion was bound, and that energy was thus required to separate the anionic and cationic species.

Removal of the phenyl units resulted in a reduced association constant between **2** and TBAC (K_{ass} = 9 ± 2 M^{-1}) under the same conditions. Also

in this case, the major downfield shift was observed for the H_{down} protons ($\Delta\delta$ = 0.39 ppm, Appendix C, Figure 4).
In the case of cavitand **3**, no binding of TBAC was observed (Appendix 3, Figure 3). The reduction of the alkyl spacer length between the cavitand and the phenyl moieties totally suppressed complexation.
To evaluate the solvent effect on TBAC complexation, the same set of experiments were conducted with cavitand **1** in $CDCl_3$ and DMSO-d_6. Both solvents completely suppressed anion binding (Appendix C, Figures 5 and 6), indicating that both tightly associated[19] (chloroform) and fully solvated (DMSO)[20] ion-pairs are unsuitable for cavitand **1**.
Overall, cavitand **1** acts as a pure anion receptor, with no affinity for the tetrabutylammonium cation, despite of the presence of the phenyl substituents. The complexation event is strongly solvent mediated.

4.2.3 Phosphate-footed cavitand 4.

The next step was the replacement of the phenyl groups in **1** with four phosphate derivatives, which are well known for their ability to bind positive charged species like ammonium cations, through cation-dipole and H-bonding interactions.[10,21]
The phosphates were installed according to the synthetic sequence shown in Scheme 2. First, the hydroxyl-footed resorcinarene **8**[8b] was reacted with chlorobromomethane, in presence of K_2CO_3, affording methylene-bridged cavitand **9**. **9** was then converted into **4** by treatment with trimethyl phosphite and tetrabromo methane.

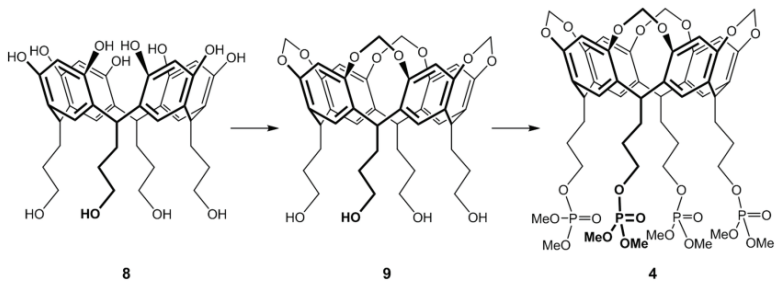

Scheme 2: Synthesis of target receptor **4:** a) $BrCH_2Cl$, dry DMF, overnight, 80 °C; b) CBr_4, $P(OMe)_3$, 2.5 h, r.t; H_2O/CH_2Cl_2, 40 min.

To test the influence of pure cation-dipole interactions, cavitand **4** was exposed to three different tetrabutylammonium salts, namely chloride (TBAC), bromide (TBAB) and iodide (TBAI). The chemical shift changes of the diagnostic H_{down} and ArCHCH_2 protons and the K_{ass} value obtained by ^{1}H NMR titration in acetone-d_6 are reported in Table 1.

GUEST	Δδ H_{down} (ppm)	Δδ ArCHCH_2 (ppm)	K_{ass} (M^{-1})
TBAC	+ 0.88	+ 0.51	150 ± 30
TBAB	+ 0.67	+ 0.48	140 ± 10
TBAI	+ 0.41	+ 0.42	73 ± 3

Table 1: Observed chemical shift changes and K_{ass} values for titration of **4** with TBA halides. ($\Delta\delta = \delta_{saturation} - \delta_{free}$).

In all cases a 1:1 stoichiometry for the complexation was determined via the continuous variation method.

No significant counterion effect was revealed by comparing the K_{ass} value. Even more compelling is the limited improvement in K_{ass} determined in moving from **1** to **4**. A supplementary ^{31}P NMR titration in acetone-d_6 was carried out (Appendix C, Figure 8) in order to assess the effective role of the phosphate units. The recorded change in ^{31}P chemical shift upon addition of 12 eq. of TBAC was negligible ($\Delta\delta$ = -0.005 ppm). Therefore, the foreseen cation-dipole interactions among the phosphates and tetrabutylammonium are negligible, limiting the role of cavitand **4** to that of a simple anion receptor.

Also in this case, shifting to $CDCl_3$ as solvent, led to the complete suppression of TBAC complexation, like in the case of **1**.

Since pure cation-dipole interactions did not suffice to bind ammonium cations, additional H-bonding was introduced in the system, by switching to a primary ammonium counterion.

Octylammonium was selected because of its solubility in chlorinated solvents, where H-bonding is enhanced. In this way the four P=O moieties of cavitand **4** can also act as H-bond acceptors.[22]

The complexation data in $CDCl_3$ between **4** and the Cl^-/Br^-/I^- octylammonium salt series are summarized in Table 2.

Illustrative ^{1}H and ^{31}P NMR chemical shift variations upon titration of cavitand **4** with octylammonium bromide are reported in Figures 5 and 6.

GUEST	Δδ H_{down} (ppm)	Δδ NH (ppm)	Δδ P(O) (ppm)	K_{ass} (M^{-1})
Octylam. Cl	+ 0.23	+ 0.19	- 0.20	$(1.5 \pm 0.2) \cdot 10^{3}$
Octylam. Br	+ 0.55	+ 0.49	- 0.57	$(2.1 \pm 0.4) \cdot 10^{4}$
Octylam. I	+ 0.56	+ 0.79	- 0.96	n.d.*

Table 2: Observed chemical shift changes and K_{ass} values for titration of **4** with octylammonium halides. ($\Delta\delta = \delta_{saturation} - \delta_{free}$). * data non-suitable for K_{ass} determination.

In these titration experiments, we monitored not only the usual downfield shift of the cavitand *H*$_{down}$ protons, diagnostic of anion binding, but also the downfield shift for the guest N*H* signals, indicative of the cation H-bonding with the P=O groups (Figure 5).

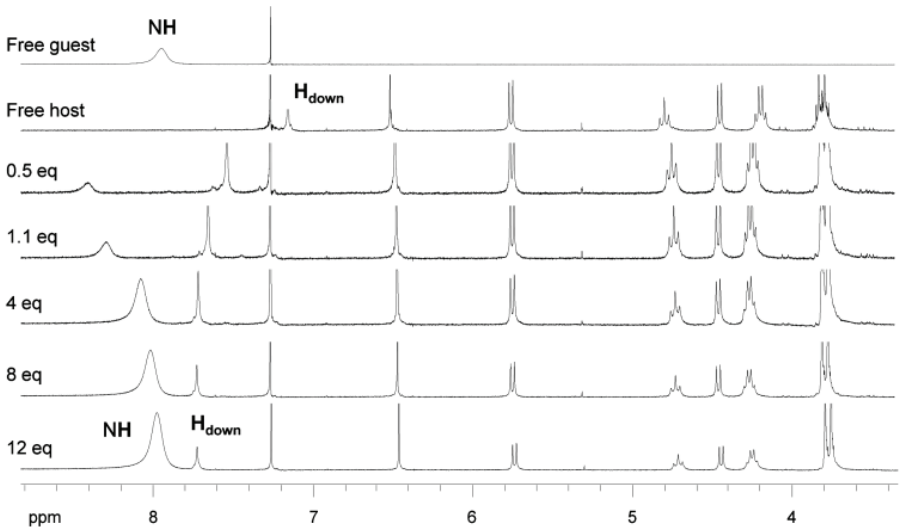

Figure 5: Partial ^{1}H NMR spectra in $CDCl_3$ for titration of receptor **4** with octylammonium bromide.

The presence of NH···O=P H-bonding is confirmed by the corresponding ^{31}P NMR titration, where the upfield shift of the phosphate signal is observed in the all three guests (Figure 6, Table 2).[23]
The presence of this upfield shift is a clear indication of the predominance of H-bonding over cation-π interactions in the cation binding mode.

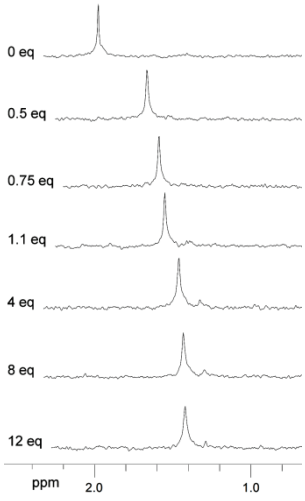

Figure 6: Partial ^{31}P NMR spectra in $CDCl_3$ for titration of receptor **4** with octylammonium bromide.

For octylammonium bromide a K_{ass} value one order of magnitude higher than for the corresponding chloride was determined (Table 2). As for the iodide salt, larger chemical shift variations for all diagnostic signals were recorded. For the iodide derivative, the corresponding K_{ass} value could not be exactly determined, because of a too high standard deviation in the curve fitting. This is due to the incomplete solubility of octylammonium iodide in $CDCl_3$ at room temperature, at the concentrations required for ^1H NMR studies.
As control experiments, the same titrations were repeated with cavitands **1** and **2** in $CDCl_3$. In both cases, the cavitands signals were unaffected by the presence of octylammonium chloride (Appendix C, Figures 10 and 11).
The binding of octylammonium salts by **4** was monitored also via isothermal titration calorimetry (ITC), to overcome the solubility problems,[24] as well as to dissect the enthalpic and entropic contributions to complexation (Table 3).

In the case of octylammonium chloride, the low K_{ass} value, close to the detection limit of the technique,[25] jeopardized a quantitative evaluation. The obtained qualitative estimation ($780 < K_{ass} < 1600\ M^{-1}$) is compatible with the value determined via NMR ($1300 < K_{ass} < 1700\ M^{-1}$ Table 2). In the other two cases, the data fitted well for a 1:1 binding profile, leading to association constants in the range of $10^4\ M^{-1}$, with a higher affinity for the iodide compound than for the bromide. In this latter case, in which the K_{ass} was precisely determined also via NMR, a perfect match of the experimental results was obtained (cfr. Tables 2 and 3).
The thermodynamic parameters revealed that the binding is both enthalpy and entropy driven. This is quite unusual for ion-pair recognition.

GUEST	ΔH (KJ mol^{-1})	TΔS (KJ mol^{-1})	ΔG (KJ mol^{-1})	K_{ass} (M^{-1})
Octylam. Cl	n.d.*	n.d.*	n.d.*	$(1.6 \pm 0.4) \cdot 10^3$ **
Octylam. Br	-7.1± 0.3	17.1± 0.4	-24.2± 0.2	$(1.8 \pm 0.2) \cdot 10^4$
Octylam. I	-18.3± 0.3	8.3 ± 0.2	-26.6± 0.8	$(4.7 \pm 0.4) \cdot 10^4$

Table 3: Thermodynamic parameters and K_{ass} values for ITC titration of **4** with octylammonium halides. * data non-suitable for thermodynamic disquisitions; ** qualitative average value.

The observed trend in enthalpic contribution can be rationalize recalling that, in apolar solvents, the recognition of ion-pairs increases with the reduction of electrostatic interactions between anion and cation.[26]
The opposite entropic trend can be attributed to the different degree of solvation in the ion-pair series, which decreases with the decreasing charge density of anion ($Cl^- > Br^- > I^-$).[27] Since extensive guest desolvation is required for ion-pair binding by **4**, the release of more structured solvent molecules leads to an higher desolvation gain.
The two terms partially balance each other in the composition of the resulting ΔG values. The positive TΔS contribution to the complexation implies that the entropy losses due to conformational freezing of the host upon binding, and to the reduction in translational freedom in the newly formed complexes, are more than compensated by the desolvation of both components.

4.3 Conclusions.

CH-anion interactions coupled to H-bonding to P=O groups have been exploited to realize the efficient ion-pair cavitand receptor **4**. The key feature characterizing the host is the presence of a preorganized pocket for anion binding in close proximity to four H-bond acceptors P=O groups.
The search for optimal cation binding units has shown that H-bonding are more effective than cation-π and cation-dipole interactions in apolar media.
The NMR experimental K_{ass} values have been validated by complementary ITC titrations.
The unexpected finding that the complexation is also entropy driven can be attributed in part to the preorganization of the anion pocket, which does not undergo major conformation changes upon complexation.

4.4 Experimental Section.

5-phenylpentan-1-ol.
$LiAlH_4$ (3.42 g, $8.98 \bullet 10^{-2}$ mol) was suspended in dry diethyl ether (220 mL). The mixture was cooled at 0 °C and a solution of 5-phenylvaleric acid (4.00 g, $2.24 \bullet 10^{-2}$ mol) in dry diethyl ether (22 mL) was added dropwise. The mixture was stirred at room temperature for 4 h.
The system was then cooled at 0 °C and H_2O (3.4 mL) was slowly added, followed by an aqueous 3 M solution of KOH (3.4 mL) and by further 11.4 mL of H_2O. The mixture was stirred at 0 °C for 1 h.
The crude was filtered and the organic phase was dried over $MgSO_4$. The resulting solution was concentrated to dryness, to afford 5-phenylpentan-1-ol (3.14 g, $1.92 \bullet 10^{-2}$ mol, 86%).Colorless oil.
TLC: (SiO_2, cyclohexane: ethyl acetate7:3): R_f = 0.38. **^{1}H NMR ($CDCl_3$, 300 MHz):** δ = 7.29 (t, 2H, $\mathbf{H_{orto}}$, J=6.0 Hz); 7.21-7.18 (m, 3H, $\mathbf{H_{meta}}$ + $\mathbf{H_{para}}$); 3.64 (t, 2H, C$\mathbf{H_2}$OH, J=6.3 Hz); 2.64 (t, 2H, C$\mathbf{H_2}$Ph, J=7.2 Hz); 1.72-1.62 (m, 4H, C$\mathbf{H_2}$$CH_2$OH + C$\mathbf{H_2}$$CH_2$Ph); 1.47-1.40 (m, 2H, C$\mathbf{H_2}$$CH_2CH_2$OH). **^{13}C NMR ($CDCl_3$, 75 MHz):** δ = 142.60; 128.43; 128.31; 125.70; 62.92; 35.94; 32.67; 31.31; 25.44. **HR-EI-MS:** *m/z* calcd. for $[C_{11}H_{13}]^-$ ($[M\text{-}H_2O]^+$) requires 146.1095; found: 146.1090.

5-phenylpentanal 6.

To a suspension of PCC (6.19 g, $2.87 \bullet 10^{-2}$ mol) in dry CH_2Cl_2 (60 mL), a solution of 5-phenylpentanol (3.14 g, $1.92 \bullet 10^{-2}$ mol) in dry CH_2Cl_2 (50 mL) was rapidly added, at room temperature. The mixture turned black becoming homogeneous; then a black solid was deposited on the walls of the flask. The reaction was stirred at room temperature for 3 h.

After 3 h, the solution was decanted and the black residue was washed several time with CH_2Cl_2. The collected organic phases were partially concentrated and finally filtered on a silica plug (eluent CH_2Cl_2), to afford **6** (2.59 g, $1.60 \bullet 10^{-2}$ mol, 83%). Pale yellow oil.

TLC: (SiO_2, cyclohexane: ethyl acetate 8:2): R_f = 0.51. **^{1}H NMR ($CDCl_3$, 300 MHz):** δ = 9.76 (t, 1H, C**H**O, J=1.8 Hz); 7.30 (tt, 2H, $\mathbf{H_{orto}}$, J^1=7.2 Hz, J^3=1.2 Hz); 7.22-7.12 (m, 3H, $\mathbf{H_{meta}}$ + $\mathbf{H_{para}}$); 2.65 (t, 2H, C$\mathbf{H_2}$Ph, J=7.0 Hz); 2.46 (m, 2H, C$\mathbf{H_2}$CHO); 1.68 (m, 4H, C$\mathbf{H_2}$$CH_2$CHO + C$\mathbf{H_2}$$CH_2$Ph). **^{13}C NMR ($CDCl_3$, 75 MHz):** δ = 202.57; 141.97; 128.41; 128.12; 125.87; 43.77; 35.66; 30.89; 21.71. **HR-EI-MS:** *m/z* calcd. for $[C_{11}H_{13}O]^+$ ($[M\text{-}H_2]^+$) requires 160.0888; found: 160.0880.

Phenylbutyl-footed resorcinarene 7.

A solution of resorcinol (1.76 g, $1.60 \bullet 10^{-2}$ mol) in absolute ethanol (16 mL) was cooled at 0 °C and an aqueous 37% HCl solution (3.3 mL) was added. A solution of **6** (2.59 g, $1.60 \bullet 10^{-2}$ mol) in absolute ethanol (15 mL) was slowly added over a 20-min period. The solution was allowed to warm at room temperature and stirred for a day.

After 24 h, the reaction was slowly heated at 80 °C, and stirred under reflux for 3 days. No precipitate formed during this period. The red solution was cooled at 0 °C and added to H_2O (150 mL). The voluminous precipitate was stirred for 20 min and finally collected by filtration, affording the desired resorcinarene **7** (2.88 g, $2.84 \bullet 10^{-3}$ mol, 71%). Orange solid.

m.p. > 300 °C (slow decomposition). **TLC:** (SiO_2, CH_2Cl_2/MeOH 9:1): R_f = 0.33. **^{1}H NMR (acetone-d_6, 300 MHz):** δ = 8.50 (s, 8H, ArO**H**); 7.56 (s, 4H, Ar$\mathbf{H_{down}}$); 7.26-7.13 (m, 20H, $\mathbf{H_{orto}}$ + $\mathbf{H_{meta}}$ + $\mathbf{H_{para}}$); 6.27 (s, 4H, Ar$\mathbf{H_{up}}$); 4.34 (t, 4H, ArC**H**, J=8.1 Hz); 2.59 (t, 8H, C$\mathbf{H_2}$Ph, J=5.7 Hz); 2.32 (m, 8H, ArCHC$\mathbf{H_2}$); 1.68 (m, 8H, $ArCHCH_2C\mathbf{H_2}$); 1.43 (m, 8H, C$\mathbf{H_2}$$CH_2$Ph). **^{13}C NMR (acetone-d_6, 75 MHz):** δ = 152.77; 143.53; 129.13; 129.03; 126.45; 125.49; 125,20; 103.80; 36.66; 34.18; 34.04;

32.22; 28.66. **HR-ESI-MS:** *m/z* calcd. for $C_{68}H_{72}O_8$ (1016.2 Da), $[M+H]^+$ 1017.5300; found: 1017.5321.

Methylene-bridged phenylbutyl-footed cavitand 1.
In a dried Schlenk tube, resorcinarene **7** (2.00 g, $1.97 \bullet 10^{-3}$ mol) was dissolved in dry DMF (40 mL). Oven-dried K_2CO_3 (2.56 g, $1.97 \bullet 10^{-2}$ mol) was added, followed by bromochloromethane (5.11 mL, $7.87 \bullet 10^{-2}$ mol). The mixture was stirred at 80 °C overnight. Reaction was quenched in HCl 1M (150 mL). An orange solid deposited on the walls of the flask. Solution was decanted and the solid was dissolved in CH_2Cl_2. The resulting organic solution was at first dried over $MgSO_4$, then concentrated to dryness. The crude was finally purified by column chromatography (eluent CH_2Cl_2), affording cavitand **1** (1.57 g, $1.48 \bullet 10^{-2}$ mol, 75%). White solid.
m.p. > 310 °C (slow decomposition). **TLC:** (SiO_2, CH_2Cl_2): R_f = 0.56. **^{1}H NMR (acetone-d_6, 300 MHz,):** δ = 7.58 (s, 4H, Ar**H$_{down}$**); 7.26-7.15 (m, 20H, **H$_{orto}$** + **H$_{meta}$** + **H$_{para}$**); 6.54 (s, 4H, Ar**H$_{up}$**); 5.74 (d, 4H, C**H$_{in}$**, J=7.5 Hz); 4.75 (t, 4H, ArC**H**, J=8.1 Hz); 4.47 (d, 4H, C**H$_{out}$**, J=7.5 Hz); 2.63 (t, 8H, C**H$_2$**Ph, J=7.5 Hz); 2.37 (m, 8H, ArCHC**H$_2$**),1.74 (m, 8H, ArCHCH$_2$C**H$_2$**); 1.45 (m, 8H, C**H$_2$**CH$_2$Ph). **^{13}C NMR (acetone-d_6, 75 MHz):** δ = 155.91; 143.35; 139.46; 129.16; 129.13; 126.53; 122.89; 117,48; 100.39; 37.31; 36.56; 32.30; 29.88; 28.35. **HR-ESI-MS:** *m/z* calcd. for $C_{72}H_{72}O_8$ (1064.1 Da), $[M+Na]^+$ 1087.5119; found: 1087.5121.

Methylene-bridged propanol-footed cavitand 9.
In a dried Schlenk tube, propanol-footed resorcinarene (3.00 g, $4.17 \bullet 10^{-3}$ mol) was dissolved in dry DMF (40 mL). Oven-dried K_2CO_3 (7.00 g, $4.17 \bullet 10^{-2}$ mol) was added, followed by bromochloromethane (10 mL, $1.67 \bullet 10^{-1}$ mol). The mixture was stirred at 80 °C overnight. Reaction was quenched by solvent removal in vacuo. The crude was suspended in HCl 1M (150 mL), filtered and purified by flash silica cromatography (eluent CH_2Cl_2:MeOH 9:1), affording cavitand **9** (2.02 g, $2.63 \bullet 10^{-3}$ mol, 63%). White solid.
m.p. > 300 °C (slow decomposition). **TLC:** (SiO_2, CH_2Cl_2:MeOH 9:1): R_f = 0.33. **^{1}H NMR (acetone-d_6, 300 MHz):** δ = 7.61 (s, 4H, Ar**H$_{down}$**); 6.51 (s, 4H, Ar**H$_{up}$**); 5.71 (d, 4H, C**H$_{in}$**, J=7.8 Hz); 4.56 (t, 4H, ArC**H**, J=7.8 Hz); 4.47 (t, 4H, CH$_2$O**H**, J=5.1 Hz); 4.39 (d, 4H, C**H$_{out}$**, J=7.8 Hz); 3.51 (m, 8H, C**H$_2$**OH); 2.40 (m, 8H, ArCHC**H$_2$**); 1.46 (m, 8H, ArCHCH$_2$CH$_2$). **^{13}C**

NMR (acetone-d_6, 75 MHz): δ = 155.91; 139.55; 123.43; 117,26; 100.37; 62.33; 37.55; 32.33; 26.93. **HR-ESI-MS** : *m/z* calcd. for $C_{44}H_{48}O_{12}$ (768.3 Da), $[M+Na]^+$ 791.3038; found: 791.3060.

Methylene-bridged propyldimethoxyphosphate-footed cavitand 4.
To a suspension of cavitand **9** (0.30 g, $3.90 \cdot 10^{-4}$ mol) in dry pyridine (6 mL), CBr_4 (0.79 g, $2.39 \cdot 10^{-3}$ mol) was added, and the mixture was stirred at r.t. for 10 minutes. The suspension was then cooled at 0 °C, and trimetylphosphite (0.23 mL, $1.95 \cdot 10^{-3}$ mol) was added. The solution was stirred at r.t. for 2.5 h, then a mixture 1:1 H_2O:CH_2Cl_2 (10 mL) was added and stirring was continued for 40 minutes. Solvents were removed *in vacuo*, and the crude was purified by flash chromatography on basic alumina (eluent CH_2Cl_2:EtOH 96:4). The obtained product was suspended in H_2O and recovered by filtration (0.17 g, $1.42 \cdot 10^{-3}$ mol, 36%). Pale pink solid.
m.p. > 290 °C (slow decomposition). **TLC:** (SiO_2, CH_2Cl_2:MeOH 9:1): R_f = 0.69. **^{1}H NMR (DMSO-d_6, 300 MHz):** δ = 7.57 (s, 4H, Ar**H$_{down}$**); 6.56 (s, 4H, Ar**H$_{up}$**); 5.73 (d, 4H, C**H$_{in}$**, J=7.5 Hz); 4.61 (t, 4H, ArC**H**, J=7.6 Hz); 4.40 (d, 4H, C**H$_{out}$**, J=7.5 Hz); 4.07 (m, 8H, C**H$_2$**OP(O)); 3.66 (d, 24H, OC**H$_3$**, J=11.1 Hz); 2.46 (m, 8H, ArCHC**H$_2$**); 1.66 (m, 8H, ArCHCH$_2$C**H$_2$**). **^{13}C NMR (DMSO-d_6, 75 MHz):** δ = 157.01; 140.59; 124.82; 119.57; 101.68; 69.57; 56.76; 38.49; 30.98; 27.59. **^{31}P NMR (DMSO-d_6, 121 MHz):** δ = 2.17 (s, **P**(O)). **HR-ESI-MS:** *m/z* calcd. for $C_{52}H_{68}O_{24}P_4$ (1200.4 Da), $[M+Na]^+$ 1223.2943; found: 1223.2950.

Octylammonium chloride 10.
To a solution of octylamine (2.00 mL, $1.21 \cdot 10^{-2}$ mol) in Et_2O (20 mL), an excess of aqueous 36% HCl (3 mL) was added. The resulting mixture was stirred at r.t. for 20 minutes. Solvent was removed under reduced pressure, and the product was recrystallized from Et_2O (1.98 g, $1.21 \cdot 10^{-2}$ mol, quantitative yield). White solid.
m.p. 204-205 °C. **^{1}H NMR ($CDCl_3$, 300 MHz):** δ = 8.28 (bs, 3H, N**H$_3$**); 2.98 (m, 2H, C**H$_2$**NH$_3$); 1.77 (m, 2H, C**H$_2$**CH$_2$NH$_3$); 1.37-1.27 (m, 10H, (C**H$_2$**)$_5$CH$_2$CH$_2$NH$_3$); 0.87 (t, 3H, CH$_2$C**H$_3$**, J=6.6 Hz). **^{13}C NMR ($CDCl_3$, 75 MHz):** δ = 40.06; 31.72; 29.05; 28.97; 27.68; 26.54; 22.59; 14.06. **HR-ESI-MS:** *m/z* calcd. for $C_8H_{20}NCl$ (165.3 Da) , $[M-Cl]^+$ 130.1590; found: 130.1584. **Elemental analysis:** requires C: 57.99%; H: 12.16%:

N: 8.45%; Cl: 21.40%; found: C: 58.28%; H: 12.14%: N: 8.38%; Cl: 21.25%.

Octylammonium bromide 11.
To a solution of octylamine (2.00 mL, $1.21 \bullet 10^{-2}$ mol) in Et_2O (20 mL), an excess of aqueous 47% HBr (3 mL) was added. The resulting mixture was stirred at r.t. for 1 h. Solvent was removed *in vacuo*, and the product was recrystallized from acetone at 0 °C (2.52 g, $1.20 \bullet 10^{-2}$ mol, quantitative yield). White crystals.
m.p. 207-208 °C. **^{1}H NMR ($CDCl_3$, 300 MHz):** δ = 7.93 (bs, 3H, N**H$_3$**); 3.04 (m, 2H, C**H$_2$**NH_3); 1.81 (m, 2H, C**H$_2$**CH_2NH_3); 1.40-1.27 (m, 10H, (C**H$_2$**)$_5CH_2CH_2NH_3$); 0.88 (t, 3H, CH_2C**H$_3$**, J=6.6 Hz). **^{13}C NMR ($CDCl_3$, 75 MHz):** δ = 40.32; 31.86; 29.19; 29.07; 27.65; 26.71; 22.78; 14.30. **HR-ESI-MS:** *m/z* calcd. for $C_8H_{20}NBr$ (210.0 Da) , $[M\text{-}Br]^+$ 130.1590; found: 130.1589. **Elemental analysis:** requires C: 45.72%; H: 9.59%: N: 6.66%; Br: 38.02%; found: C: 45.68%; H: 9.34%: N: 6.67%; Br: 37.82%.

Octylammonium iodide 12.
To a solution of octylamine (2.00 mL, $1.21 \bullet 10^{-2}$ moL) in Et_2O (20 mL), an excess of aqueous 57% HBr (3 mL) was added. The resulting mixture was stirred at r.t. for 1 h. Solvent was removed *in vacuo*, and the product was recrystallized from hexane (3.05 g, $1.19 \bullet 10^{-2}$ mol, quantitative yield). Pale yellow solid.
m.p. 205-206 °C. **^{1}H NMR ($CDCl_3$, 300 MHz):** δ = 7.52 (bs, 3H, N**H$_3$**); 3.14 (m, 2H, C**H$_2$**NH_3); 1.86 (m, 2H, C**H$_2$**CH_2NH_3); 1.42-1.27 (m, 10H, (C**H$_2$**)$_5CH_2CH_2NH_3$); 0.88 (t, 3H, CH_2C**H$_3$**, J=6.6 Hz). **^{13}C NMR ($CDCl_3$, 75 MHz):** δ = 40.67; 31.86; 29.20; 29.06; 27.45; 26.82; 22.80; 14.31. **HR-ESI-MS:** *m/z* calcd. for $C_8H_{20}NI$ (257.2 Da) , $[M\text{-}I]^+$ 130.1590; found: 130.1584. **Elemental analysis:** requires C: 37.37%; H: 7.84%: N: 5.45%; I: 49.35%; found: C: 37.09%; H: 7.72%: N: 5.39%; I: 49.54%.

4.5 References and Notes.

[1] (a) J. M. Lehn, *Pure and Appl. Chem.* **1979**, *51*, 979-997; (b) R. Ungaro, A. Pochini, *Topics in Inclusion Science* **1991**, 3, 127-147; (c) G.

W. Gokel, A. Nakano, *Crown Compd.* **1992**, 1-26; (d) E. Grell, R. Warmuth, *Pure and Appl. Chem.* **1993**, *65*, 373-379; (e) H. Huang, L. Mu, J. He, J.-P. Cheng, *J. of Org. Chem.* **2003**, *68*, 7605-7611.

[2] (a) S. E. Matthews, P. D. Beer, *Supramolecular Chemistry* **2005**, *17*, 411-435; (b) J. L. Sessler, P. A. Gale, W.-S. Cho, in *Monographs in Supramolecular Chemistry*, (Ed. J. F. Stoddart), **2006**, RSC Publishing, Cambridge U.K.; (c) V. Amendola, L. Fabbrizzi, *Chem. Commun.* **2009**, 513-531; (d) C. Caltagirone, P. A. Gale, *Chem. Soc. Rev.* **2009**, *38*, 520-563.

[3] P. A. Gale, *Coordination Chemistry Reviews* **2003**, *240*, 191-221.

[4] (a) D. M. Rudkevich, J. D. Mercer-Chalmers, W. Verboom, R. Ungaro, F. de Jong, D. N. Reinhouldt, *J. Am. Chem. Soc.* **1995**, *117*, 6124-6125; (b) N. Pelizzi, A. Casnati, A. Friggeri, R. Ungaro, *J. Chem. Soc. Perkin Trans. 2* **1998**, 1307-1312; (c) D. J. White, N. Laing, H. Miller, S.Parson, S. Coles, P. A. Tasker, *Chem. Commun.* **1999**, 2077-2078.

[5] (a) R. Custelcean, L. H. Delmau, B. A. Moyer, J. L. Sessler, W.-S. Cho, D. Gross, G. W. Bates, S. J. Brooks, M. E. Light, P. A. Gale, *Angew. Chem. Int. Ed* **2005**, *44*, 2537-2542; (b) J. L. Sessler, S. K. Kim, D. E. Gross, C.-H. Lee, J. S. Kim, V. M. Lynch, *J. Am. Chem. Soc.* **2008**, *130*, 13162-13166; (c) M. P. Wintergerst, T. G. Levitskaia, B. A. Moyer, J. L. Sessler, L. H. Delmau, *J. Am. Chem. Soc.*, **2008**, *130*, 4129–4139.

[6] (a) A. Arduini, G. Giorgi, A. Pochini, A. Secchi, F. Ugozzoli, *J. Org. Chem.* **2001**, *66*, 8302-8308; (b) A. Arduini, E. Brindani, G. Giorgi, A. Pochini, A. Secchi, *J. Org. Chem.* **2002**, *67*, 6188-6194; (c) M. D. Lankshear, A. R. Cowley, P. D. Beer, *Chem. Commun.* **2006**, 612-614; (d) A. Senthilvelan, I.-T. Ho, K.-C. Chang, G.-H. Lee, Y.-H. Liu, W.-S. Chung, *Chem. Eur. J.* **2009**, *15*, 6152-6160.

[7] (a) M. J. Deetz, M. Shang, B. D. Smith, *J. Am. Chem. Soc.* **2000**, *122*, 6201-6207; (b) T. Tozawa, Y. Misawa, S. Tokita, Y. Kubo, *Tetrahedron Lett.* **2000**, *41*, 5219-5223; (c) M. K. Chac, J.-I. Lee, N.-K. Kim, K.-S. Jeong, *Tetrahedron Lett.* **2007**, *48*, 6624-6627.

[8] (a) J. M. Mahoney, A. M. Beatty, B. D. Smith, *Inorg. Chem.* **2004**, *43*, 7617-7621; (b) M. Cametti, N. Nissinen A. Dalla Cort, L. Mandolini, K. Rissanen, *J. Am. Chem. Soc.* **2005**, *127*, 3831-3837.

[9] (a) A. Shivanyuk, K. Rissanen, E. Kolehmainen, *Chem. Commun.* **2000**, 1107-1108; (b) H. Mansikkamäki, M. Nissinen, K. Rissanen, *Chem. Commun.* **2002**, 1902-1903; (c) H. Mansikkamäki, M. Nissinen, C. Schalley, K. Rissanen, *New J. Chem.* **2003**, *27*, 88-97.

[10] E. Biavardi, M. Favazza, A. Motta, I. L. Fragala, C. Massera, L. Prodi, M. Montalti, M. Melegari, G. Condorelli, E. Dalcanale, *J. Am. Chem. Soc.* **2009**, *131*, 7447-7455.

[11] Example of aromatic CH-anion interactions: (a) D.-W. Yoon, H. Hwang, C.-H. Lee, *Angew. Chem. Int. Ed.* **2002**, *41*, 1757-1759; (b) K. Chellappan, N. J. Singh, I.-C. Hwang, J. W. Lee, K. S. Kim, *Angew. Chem. Int. Ed.* **2005**, *44*, 2899-2903; (c) W. J. Belcher, M. Fabre, T. Farhan, J. W. Steeed, *Org. Biomol. Chem.* **2006**, *4*, 781-786.

[12] Example of non aromatic CH-anion interactions: (a) C. A. Ilioudis, D. A. Tocher, J. W. Steed, *J. Am. Chem. Soc.* **2004**, *126*, 12395-12402; (b) H. Maeda, Y. Kusunose, *Chem. Eur. J.* **2005**, *11*, 5661-5666.

[13] S. S. Zhu, H. Staats, K. Brandhorst, J. Grunenberg, F. Gruppi, E. Dalcanale, A. Lützen, K. Rissanen, C. A. Schalley, *Angew. Chem. In. Ed.* **2008**, *47*, 788-792.

[14] SPARTAN'08, Wavefuntion, Inc., USA.

[15] E. A. Meyer, R. K. Castellano, F. Diederich, *Angew. Chem. Int. Ed.* **2003**, *42*, 1211-1250.

[16] (a) L. M. Tunstad, J. A. Tucker, E. Dalcanale, J. Weiser, J. A. Bryant, J. C. Sherman, R. C. Helgeson, C. B. Knobler, D. J. Cram, *J. Org. Chem.* **1989**, *54*, 1305-13012; (b) B. C. Gibb, R. G. Chapman, J. C. Sherman *J. Org. Chem.* **1996**, *61*, 1505-1509.

[17] For the corresponding resorcinarene behavior see: H. Mansikkamäki, C. Schalley, M. Nissinen, K. Rissanen, *New J. Chem.* **2005**, *29*, 116-127.

[18] *Matlab, version 7.0*, Schrödinger LLc, New York, NY (USA), **2007**.

[19] (a) H. Mo, A. Wang, P. Stone Wilkinson, T. C. Pochapsky, *J. Am. Chem. Soc.* **1997**, *119*, 11666-11673; (b) C. Hasselgren, K. Fisher, S. Jagner, I. Dance, *Chem. Eur. J.* **2000**, *6*, 3671-3678.

[20] (a) R. H. Erlich, E. Roach, A. I. Popov, *J. Am. Chem. Soc.* **1970**, *92*, 4989-4990; (b) J. H. Exner, E. C. Steiner, *J. Am. Chem. Soc.* **1974**, *96*, 1782-1787; (c) M. R. Crampton, I. A. Robotham, *Journal of Chemical Research, Synopses* **1997**, 22-23; (d) J. R. Pliego, J. M. Riveros, *Physical Chemistry Chemical Physics* **2002**, *4*, 622-1627; (e) O. N. Kalugin, A. K. Adya, M. N. Volobuev,Y. V. Kolesnik, *Physical Chemistry Chemical Physics* **2003**, *5*, 1536-1546.

[21] (a) R. M. Yebeutchou, F. Tancini, N. Demitri, S. Geremia, R. Mendichi, E. Dalcanale, *Angew. Chem. In. Ed.* **2008**, *47*, 4504-4508; (b) E. Biavardi, G. Battistini, M. Montalti, R. M. Yebeutchou, L. Prodi, E. Dalcanale, *Chem. Commun.* **2008**, 1638-1640; (c) B. Gadenne, M. Semeraro, R. M. Yebeutchou, F. Tancini, L. Pirondini, E. Dalcanale, A. Credi, *Chemistry--A European Journal* **2008**, *14*, 8964-8971.

[22] J. L. Cook, C. A. Hunter, C. M. R. Low, A. Perez-Velasco, J. G. Vinter, *Angew. Chem. Int. Ed.* **2007**, *46*, 3706-3709.

[23] F. E. Evans, N. O. Kaplan, *FEBS Letters* **1979**, *105*, 11-14.

[24] The guest concentration required by ITC is much lower with respect to NMR, thus allowing complete octylammonium iodide solubilization in $CDCl_3$ at room temperature.

[25] J. L. Sessler, D. E. Gross,W.-S. Cho, V. M. Lynch,F. P. Schmidtchen, G. W. Bates, M. E. Light, P. A. Gale, *J. Am. Chem. Soc.* **2006**, *128*, 12281-12288.

[26] (a) S. Roelens, R. Torriti, *J. Am. Chem. Soc.* **1998**, *120*, 12443-12452; (b) V. Böhmer, A. Dalla Cort, L. Mandolini, *J. Org. Chem.* **2001**, *66*, 1900-1902.

[27] F. P. Schmidtchen, in *Encyclopedia of Supramolecular Chemistry* (Eds. J. E. Atwood, J. W. Steed), **2007**, Taylor & Francis, Chap. Isothermal Titration Calorimetry.

Calix-Pyrrole-based Receptors

5

5.1 Introduction.

Calix[4]pyrroles[1] are a well known class of supramolecular receptors.[2] The ease of synthesis and the versatility featured by these compounds, made them particularly useful in recognition and transport applications, such as biological analyte sensing or antiviral drug delivery.[3]

Hydrogen bonding, the dominating mode of interaction of neutral calixpyrroles, allows these compounds to be used as anion sensors. Their ability to act also as ion-pair receptors has only recently been discovered.

In particular, Gale and co-workers[4] have shown that, in the solid state, large diffuse cations, such as cesium and imidazolium ions, occupy the electron rich cone-like cavity, which is formed upon anion binding to the NH portions of the calix[4]pyrrole core.

This discovery has prompted various structural modifications aiming at fine-tuning the affinity and selectivity for a variety of guests.

One of the most attractive strategies currently being explored involves expansion of the central calix[4]pyrrole binding cavity, leading to the formation of larger calixpyrrole-type macrocycles.[5]

Alternatively, Sessler and co-workers[6] proposed more complex systems to implement the molecular recognition. In particular, they reported the synthesis of a crown-6-calix[4]arene capped calix[4]pyrrole, that combines the cation complexing properties of calixarenes, with the

affinity for anions of calixpyrroles. The final outcome is an effective host for solvent separated ion-pairs.
In this chapter we present a new family of calix-pyrroles, with multiple binding sites distributed into an enlarged cavity, for targeting both anionic and cationic guests. As building *meso*-tetramethyltetrakis(3-hydroxyphenyl)calix[4]pyrrole which features free hydroxyl moieties was employed, especially suitable for further functionalization. In particular, we have introduced two phosphonate bridges, in order to exploit the affinity of P=O groups towards positively charged species, thus implementing the global receptor efficiency, by promoting cation recognition.

5.2 Results and Discussion.

5.2.1 Synthesis of the Building-Blocks.

The *meso*-tetramethyltetrakis(3-hydroxyphenyl)calix[4]pyrrole **1** was prepared by Ballester's group at the Institut Català d'Investigació Química (ICIQ) of Tarragona (Spain), following a published procedure.[7]

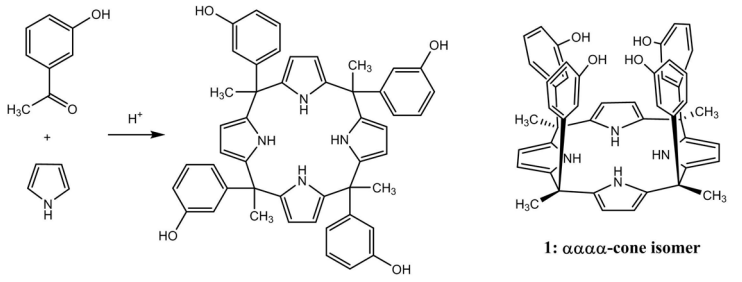

Scheme 1: Synthesis of *meso*-tetramethyltetrakis(3-hydroxyphenyl)calix[4]pyrrole.

The acid-catalyzed condensation of pyrrole with *meta*-hydroxyacetophenone led to the formation of different isomeric forms (αααα, ααaβ, ααββ and αβαβ). The major isomer **1**, in cone conformation, was isolated by crystallization from chlorobenzene, and subsequently functionalized by reaction with dichlorophenylphosphine. The resulting phosphonite intermediate, was oxidized in situ by addition of H_2O_2, affording the phosphonate species **2**. Because of the

lack of stereospecificity of this latter reaction, all the three possible isomers were obtained. Namely, the **2ii** isomer features the two P=O groups facing inward the cavity; the **2oo** isomer presents the phosphonate moieties pointing outward the cavity; the **2io** isomer bears one of the P=O outward the cavity, and the other one inward.

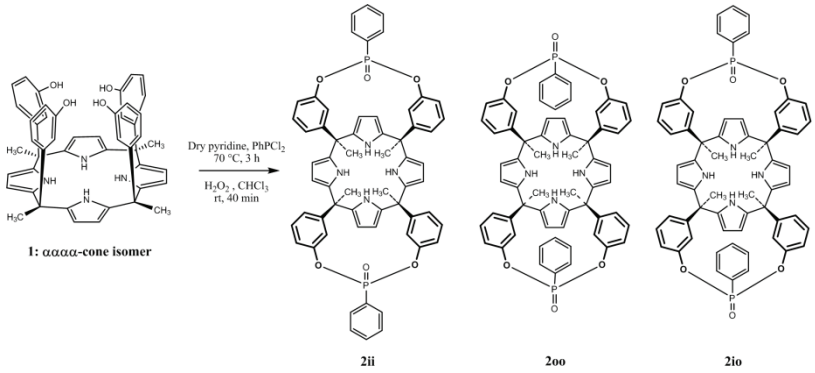

Scheme 2: Introduction of the phosphonate bridges on the *meso*-tetramethyltetrakis(3-hydroxyphenyl)calix[4]pyrrole.

The separation of the three species was performed either by crystallization or chromatography. The identification of the isomers was conveniently made by ^{1}H and ^{31}P NMR spectroscopy, and exploiting X-ray analysis.

Suitable crystals were obtained by crystallization from CH_3CN/CH_2Cl_2 (ratio 1:1) and the solved structures are reported below.

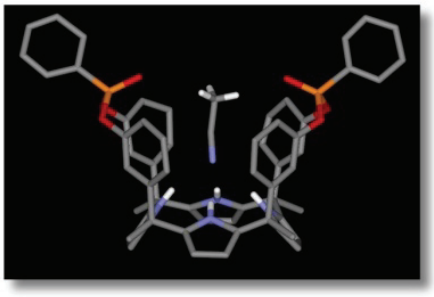

Figure 1: X-ray crystal structure for the **2ii** isomer: CH_3CN included in the cavity.

Figure 2: X-ray crystal structure for the **2oo** isomer: CH_3CN included in the cavity.

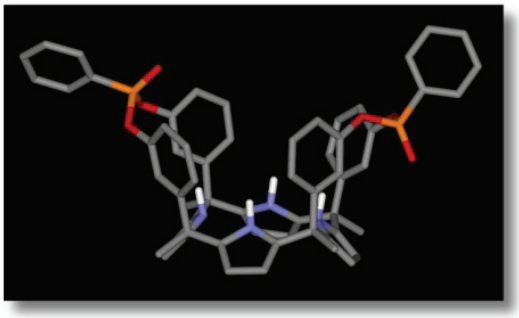

Figure 3: X-ray crystal structure for the **2io** isomer; solvents omitted for clarity.

In the three cases the pyrrolic NH point in the cavity direction.
Comparison with the phosphonate cavitandscrystal structures shows that in this case the phenyl group does not fill the cavity in the PO out configuration.

5.2.2 Complexation Studies in Solution: isomer 2ii.

The solution behaviour of the synthesized receptors was initially investigated by ^1H NMR spectroscopy, starting from the isomer **2ii**. Due to the low solubility of this compound in acetonitrile, the experiments were carried out in $CDCl_3$.
Preliminary molecular modelling calculations, performed using Maestro Macromodel Software, showed that the generated calixpyrrole binding cavity does not feature the optimal spacial arrangement for alkali metal ion guesting (Na^+, K^+, Cs^+). However, it appeared suitable for the binding of large diffuse cations, such as tetraalkylammonium ions.

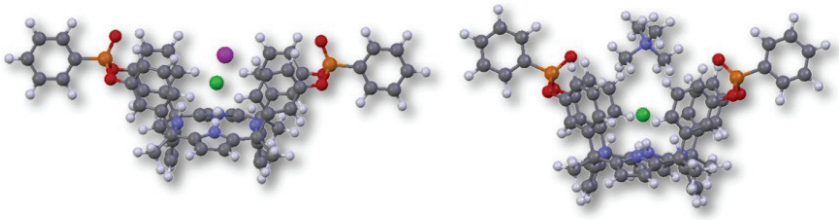

Figure 4: Molecular modelling structures showing **2ii** complexes with: Left) KCl; Right) TMACl.

At first, we chose tetrabutylammonium chloride (TBACl) as target guest. The addition of 4 equivalents of TBACl to a 1 mM solution of **2ii** did not produce any appreciable changes in the proton signals corresponding neither to the **2ii** host nor to the guest (Figure 5).

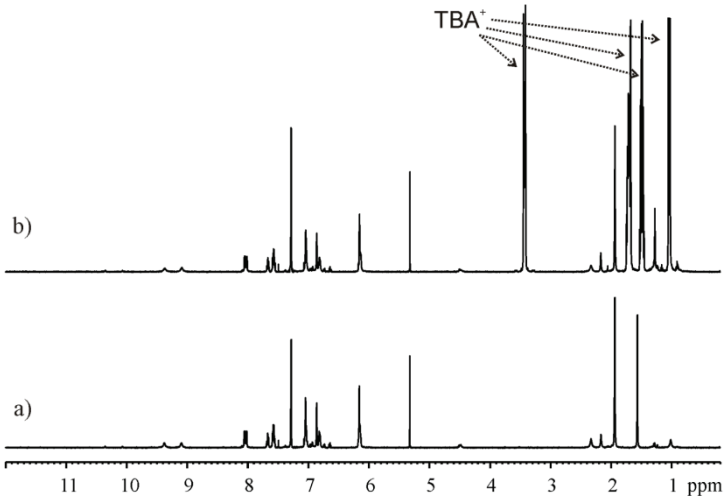

Figure 5: ^{1}H NMR spectra in $CDCl_3$ of: a) **2ii**; b) **2ii** + 4 eq. TBACl. [**2ii**] = 1 mM.

Taking into account the well known affinity of calix[4]pyrroles for halides, we can assume that the complete lack of binding observed in the studied case, is related to the inefficiency as ion-pair receptor of the isomer **2ii**. Since chloroform is unable to break ion-pairs, in this solvent only receptors capable of simultaneous anion and cation recognition are effective. Due to the large size of TBACl cation, its inclusion in the calixpyrrole cavity cannot occur.

To support this hypothesis, we repeated the previous titration in $CDCl_3$, using the smaller tetramethylammonium chloride (TMACl) as guest. In this case, significant changes in the ^1H NMR spectrum were observed.
For instance, in the free calixpyrrole spectrum two singlets were observed for the pyrrolic N*H*s, namely one at 9.11 ppm and another at 9.38 ppm.[8] However, upon the salt addition, two singlets appeared at 10.89 and 11.36 ppm, featuring a downfield shift consistent with the formation of hydrogen bonds between the cavity's N*H*s and the chloride anion. Also the splitting into multiple signals for the aromatic protons of the *meso*-phenyl ring, and the upfield shift of the β-pyrrolic resonances are in line with the anion inclusion into the calixpyrrole cavity.
On the contrary, no diagnostic changes are observed for the methyl protons belonging to the guest. A possible explanation invokes the cation positioning on the top of the calixpyrrole cavity, held by the electrostatic interactions with the anion, and far enough from the phosphonate moieties to interact with them, because of the relatively small size of TMA.

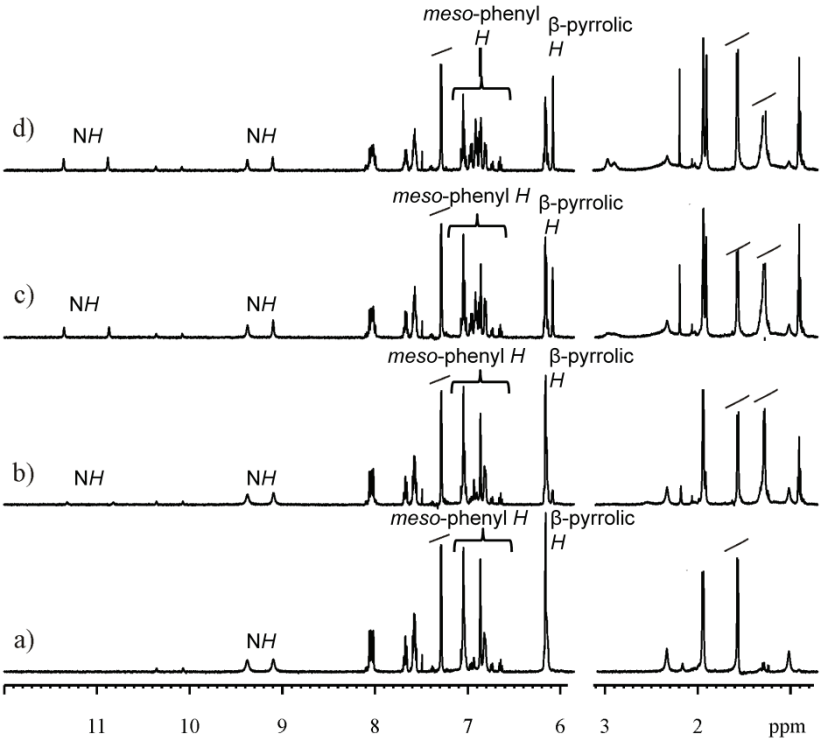

Figure 6: ^1H NMR spectra in $CDCl_3$ of: a) **2ii**; b) **2ii** + ~0.5 eq. TMACl; c) **2ii** + ~3 eq. TMACl; d) **2ii** + ~5 eq. TMACl. [**2ii**] = 1 mM.

Unfortunatly, due to the low solubility of this salt in chloroform, it was not possible to control the concentration of the tetramethylammonium chloride. In order to overcome the solubility problem, we moved to tetramethylphosphonium chloride (TMPCl), expecting a moderate solubility increase, thanks to the bigger size of the chosen cation.
The stepwise addition of a TMPCl into a 1 mM solution of **2ii** produced similar changes to the ones observed upon the addition of TMACl.

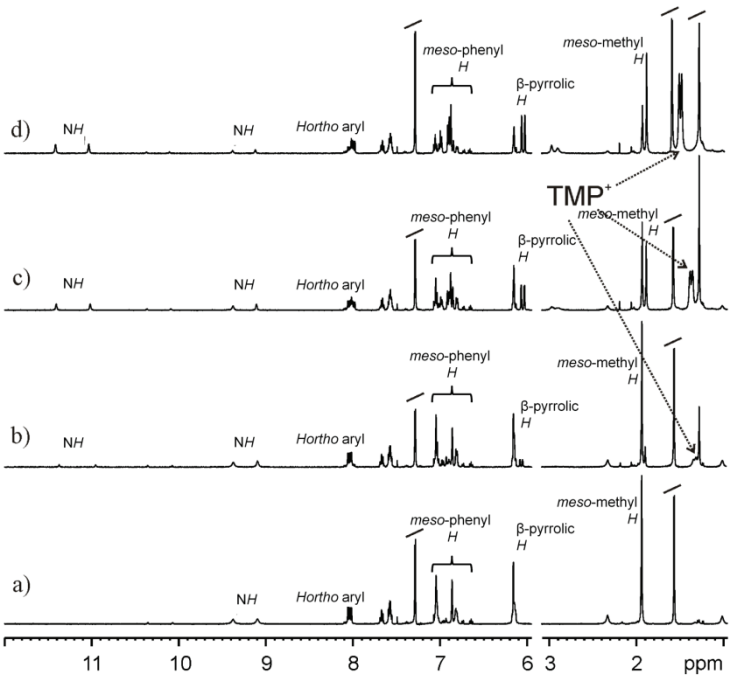

Figure 7: ^{1}H NMR spectra in $CDCl_3$ of: a) **2ii**; b) **2ii** + ~0.3 eq. TMPCl; c) **2ii** + ~1.1 eq. TMPCl; d) **2ii** + ~2 eq. TMPCl. [**2ii**] = 1 mM.

The cavity's N*H*s signals shift downfield to 11.41 and 11.02 ppm; the splitting of the aromatic protons belonging to the *meso*-phenyl ring is evident; the signals for the β-pyrrolic protons shift upfield giving rise to two doublets at 6.07 and 6.03 ppm, and the same upfield shift is observed for the singlet corresponding to the *meso*-methyl groups that moves from 1.94 to 1.89 ppm.
Particularly interesting are the signals corresponding to the methyl protons of the guest and to the *ortho*-aryl protons belonging to the PhP(O) of the host. The first one initially appears at 1.33 ppm and shift

to 1.50 ppm when 2 equivalents of TMPCl are added. The second one slightly moves in the opposite direction. These observations are consistent with the occurrence of ion-dipole interactions between the P=O moieties and the TMP cation. The integration of the signals corresponding to the bound and the free N*H*s, assuming a 1:1 stoichiometry, allowed the estimation of the binding constant (K_a = 2200 M^{-1}).
Work is in progress to evaluate the complexation properties of the **2oo** and **2io** isomers.

5.2.3 Solid State Studies: isomer 2ii.

Additional investigations performed by X-ray analysis provided clear information about the binding way of isomer **2ii** toward TMPCl.
Suitable crystals were obtained by slow evaporation of the solution used to perform the NMR titration. In figure 8 is depicted the solved structure of the TMPCl•**2ii** complex. The distances between the chloride anion and the calixpyrrole nitrogens are ranging between 3.23 Å and 3.30 Å, in agreement with the formation of hydrogen bonding. On the other hand, the two oxygens belonging to the P=O moieties are respectively 4.42 Å and 4.65 Å far away from the phosphorous atom of the phosphonium cation, and the distances from the oxygen atoms to the closest carbon atom of the methyl groups are 3.12 Å and 3.15 Å. These observations indicate that the cation is held by electrostatic interactions with the P=O groups. Thus, the X-ray crystal structure clearly demonstrate that, in the solid state, the **2ii** isomer acts as ditopic cation-anion receptor.

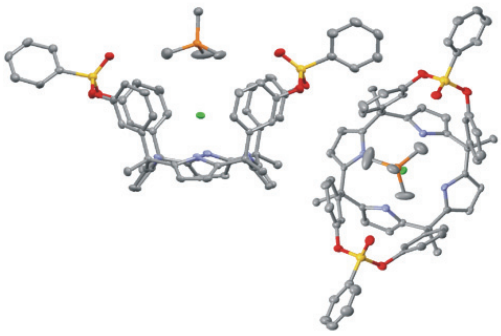

Figure 8: X-ray crystal structure of TMPCl•**2ii** complex. Thermal ellipsoids at 50% level. Solvents omitted for clarity.

Finally, it is interesting to notice the columnar arrangement adopted by the calix[4]pyrrole units in the crystal packing (Figure 9). The cation serves to bridge two **2ii** units, leading to the formation of a columnar network. One of the methyl groups is included in the middle of the electron-rich cup formed by the four pyrrole rings, while the other three N-CH_3 moieties are located on the top of the encapsulated chloride anion. The distance between the chloride and the phosphorous atom of the phosphonium cation is 4.02 Å.

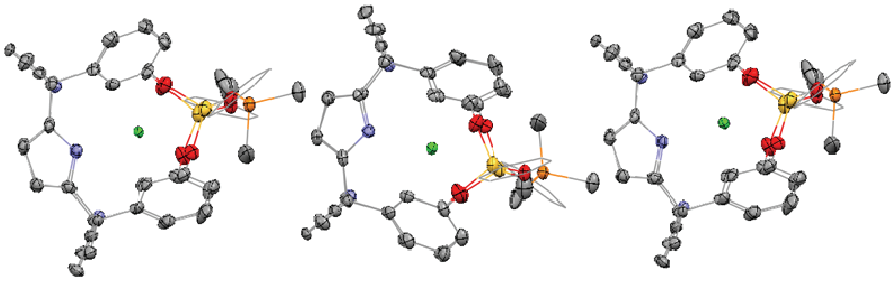

Figure 9: Partial packing showing the columnar arrangement of the TMPCl•**2ii** structure. Thermal ellipsoids at 50% level. Solvents omitted for clarity.

5.3 Conclusions.

A new family of calix[4]pyrrole-based receptors has been designed and synthesized, by expanding the central calix[4]pyrrole binding cavity via *meso*-modification. In particular, the free hydroxyl moieties featured by a *meso*-tetramethyltetrakis(3-hydroxyphenyl)calix[4]pyrrole have been functionalized with phosphonate bridges, thus introducing additional motifs with remarkable affinity for positively charged species. All the isomers resulting from the performed non-stereospecific bridging reaction have been isolated and fully characterized. The binding behaviour for the **2ii** isomer, bearing all the P=O groups facing inward the calixpyrrole cavity, has been investigated in solution by ^{1}H NMR spectroscopy, and in the solid state, by X-ray analysis. The capability of this compound to act as ion-pair receptor has been demonstrated by the performed studies.

5.4 Experimental Section.

***Meso*-tetramethyldiphenylphosphonatecalix[4]pyrrole 2.**
To a solution of *meso*-tetramethyltetrakis(3-hydroxyphenyl)calix[4]pyrrole **1** (0.10 g, $1.35 \cdot 10^{-4}$ mol) in freshly distilled pyridine (7 mL), dichlorophenylphosphine (0.04 mL, $2.72 \cdot 10^{-4}$ mol) was added at room temperature, under argon atmosphere. After 3 hours of stirring at 70 °C, the solution was allowed to cool at room temperature and 1.4 mL of a 1:1 mixture of aqueous 35% H_2O_2 and $CHCl_3$ were added. The resulting mixture was stirred for 30 minutes at room temperature, then the solvent was removed *in vacuo*. Addition of water resulted in the precipitation of a white powder, which was purified by silica column chromatography (CH_2Cl_2/MeOH 100:0.6). While the first fraction afforded pure **2io** isomer, the second one returned a mixture of **2ii** and **2oo** isomers. The two compounds were isolated exploiting their different solubility in acetonitrile. While in this solvent the **2oo** isomer resulted completely soluble, the **2ii** isomer crystallized. The pure **2oo** isomer was thus obtained by filtration of the acetonitrile suspension toward a cotton plug, followed by concentration to dryness of the organic phase. The remaining **2ii** isomer was then dissolved by washing with CH_2Cl_2 and recovered by evaporation of the collected organic solution.
2ii isomer (0.078 g, $7.92 \cdot 10^{-5}$ mol, 59%).
^{1}H NMR ($CDCl_3$, 300 MHz): δ = 9.36 (s, 2H, N**H**); 9.07 (s, 2H, N**H**); 8.02 (m, 8H, P(O)Ar**H$_o$**); 7.83 (m, 4H, P(O)Ar**H$_p$**); 7.55 (m, 8H, P(O)Ar**H$_m$**); 7.02 (m, 8H, Ar**H**); 6.84 (s, 4H, Ar**H**); 6.79 (d, 4H, Ar**H**, J= 6.6 Hz); 6.13 (m, 8H, C_2**H$_4$**N); 1.92 (s, 12H, C**H$_3$**). **^{31}P NMR ($CDCl_3$/D_2O, 172 MHz)** δ = 9.07 (s, **P**(O)). **ESI-MS:** *m/z* calcd. for $C_{60}H_{50}N_4O_6P_2$ (985.0 Da), $[M+Na]^+$: 1007.3; found: 1007.4 $[M+Na]^+$.
2oo isomer (0.015 g, $1.52 \cdot 10^{-5}$ mol, 11%).
^{1}H NMR ($CDCl_3$, 300 MHz): δ = 8.93 (s, 2H, N**H**); 8.78 (s, 2H, N**H**); 8.06 (m, 8H, P(O)Ar**H$_o$**); 7.63 (m, 4H, P(O)Ar**H$_p$**); 7.53 (m, 8H, P(O)Ar**H$_m$**); 7.45 (s, 4H, Ar**H**); 7.12 (m, 4H, Ar**H**); 6.83 (d, 4H, Ar**H**, J= 7.0Hz); 6.66 (d, 4H, Ar**H**, J= 6.8Hz); 6.18 (bs, 4H, C_2**H$_4$**N); 6.06 (bs, 4H, C_2**H$_4$**N); 1.93 (s, 12H, C**H$_3$**). **^{31}P NMR ($CDCl_3$/D_2O, 172 MHz)** δ = 8.38 (s, **P**(O)). **ESI-MS:** *m/z* calcd. for $C_{60}H_{50}N_4O_6P_2$ (985.0 Da), $[M+Na]^+$: 1007.3; found: 1007.4 $[M+Na]^+$.
2io isomer (0.040 g, $4.06 \cdot 10^{-5}$ mol, 30%).

^{1}H NMR ($CDCl_3$, 300 MHz): δ = 10.15 (s, 2H, N**H**); 9.97 (s, 1H, N**H**); 9.86 (s, 1H, N**H**); 7.99 (m, 8H, P(O)Ar**H$_o$**); 7.58 (m, 4H + 8H, P(O)Ar**H$_p$** + P(O)Ar**H$_m$**); 7.33 (s, 2H, Ar**H**); 7.09 (m, 6H, Ar**H**); 6.93 (m, 8H, Ar**H**); 6.75 (m, 4H, Ar**H**); 6.16 (m, 4H, C_2**H$_4$**N); 5.96 (bs, 4H, C_2**H$_4$**N); 1.95 (bs, 12H, C**H$_3$**). **^{31}P NMR ($CDCl_3$/D_2O, 172 MHz)** δ = 10.58 (s, ½ **P**(O)); 9.07 (s, ½ **P**(O)); 8.38 (s, 1 **P**(O)). **ESI-MS:** *m/z* calcd. for $C_{60}H_{50}N_4O_6P_2$ (985.0 Da), $[M+Na]^+$: 1007.3; found: 1007.5 $[M+Na]^+$.

5.5 References and Notes.

[1] W. Sliwa, *Chemistry of Heterocyclic Compounds* **2004**, *40*, 683-700.

[2] (a) P. A. Gale, J. L. Sessler, V. Král, V. Lynch, *J. Am. Chem. Soc.* **1996**, *118*, 5140-5141; (b) P. A. Gale, J. L. Sessler, V. Král, *Chem. Commun.* **1998**, 1-8.

[3] J. L. Sessler, P. Jr. Anzenbacher, K. Jursikova, H. Miyaji, J. W. Genge, N. A. Tvermoes, W. Allen, J. A. Shiver, *Pure & Appl. Chem.* **1998**, *70*, 2401-2408.

[4] R. Custelcean, L. H. Delmau, B. A. Moyer, J. L. Sessler, W.-S. Cho, D. Gross, G. W. Bates, S. J. Brooks, M. E. Light, P. A. Gale, *Angew. Chem. Int. Ed.* **2005**, *44*, 2537–2542.

[5] (a) P. A. Gale, J. Genge, V. Král, M. A. McKervey, J. L. Sessler, *Tetrahedron Lett.* **1997**, *38*, 8443-8444; (b) B. Turner, M. Botoshansky, Y. Eichen, *Angew. Chem. Int. Ed.* **1998**, *37*, 2475-2478; (c) G. Cafeo, F. H. Kohnke, G. L. La Torre, A. J. P. White, D. J. Williams, *Angew. Chem. Int. Ed.* **2000**, *39*, 1496-1498; (d) J. L. Sessler, P. Jr. Anzenbacher, J. A. Shriver, K. Jurisıkova, H. Miyaji, V. M. Lynch, M. Marquez, *J. Am. Chem. Soc.* **2000**, *122*, 12061-12062; (e) P. Piaütek, V. M. Lynch, J. L. Sessler, *J. Am. Chem. Soc.* **2004**, *126*, 16073-16076.

[6] J. L. Sessler, S. K. Kim, D. E. Gross, C.-H. Lee, J. S. Kim, V. M. Lynch, *J. Am. Chem. Soc.* **2008**, *130*, 13162–13166.

[7] L. Bonomo, E. Solari, G. Toraman, R. Scopelliti, M. Latronico, C. Floriani, *Chem. Commun.* **1999**, 2413-2414.

[8] Signals at 10.08 ppm and 10.38 ppm are probably related to pyrrolic NH's involved in H-bonding with residual molecules of water present in the sample (δ_{water} = 1.56 ppm).

Hierarchical Self-Assembly on Silicon 6

6.1 Introduction.

The development of self-assembly protocols generating functional surfaces with well-defined structures and tunable properties is one of the main goals of modern materials chemistry.[1] The perspective of hybrid materials, held together by different kinds of noncovalent interactions, presenting distinct and unrelated association dynamics, is particularly intriguing because they lead to adaptive materials,[2] characterized by switchable functions. The resulting complexity of these hybrid materials requires implementing combinations of two or more different interaction modes, among which hydrogen bonding, host-guest complexation and metal-ligand coordination are pivotal. They have in common an high level of structural definition and tunable strength, which allow to design functional materials at the molecular level. Although these weak interactions were employed individually to build supramolecular architectures on surfaces,[3,4,5,6] few efforts have been made on the route of their concurrent employment for the generation of hybrid materials and stimuli responsive surfaces.[7,8,9]

Starting from this premise, we designed a set of molecules featuring one or two binding motifs, to use as "switching modules" to control the self-assembly process in the multistep growth of supramolecular structures on silicon. As binding motifs, we chose hydrogen bonding and host-guest interactions, because of their tunable strength, selectivity and directionality. For H-bonding, we exploited the self-assembly of ureidopyrimidone (UPY) derivatives and 2,7-diamino-1,6-naphthyridine diamides (NAPY) to generate robust H-bonded heterodimers.[10] For the host-guest binding mode, our longstanding interest in phosphonate

cavitand chemistry,[11] led us to employ these molecules as efficient hosts for N-methylpyridinium and N-methylammonium salts.[12] The two have in common the following features: (i) remarkable stability of their respective complexes with K_{ass} above 10^7 M^{-1} in chlorinated solvents, (ii) high fidelity in recognition. The first characteristic is crucial for generating robust self-assembly protocols, while the second is essential for the orthogonality of the two interaction modes. An additional feature pertaining to the host-guest motif is the presence of specific decomplexation modes, operating either electrochemically[13] or via protonation/deprotonation.[12a]

In this chapter we report a precise and reversible hierarchical assembly on silicon using a sequence of host-guest and H-bonding interactions. The entire process has been fully tested and characterized in solution, and then successfully transferred to the solid state. The complete orthogonality of the two interactions allows the molecular level control of each step of the solid state assembly and the predictable response to precise external stimuli.

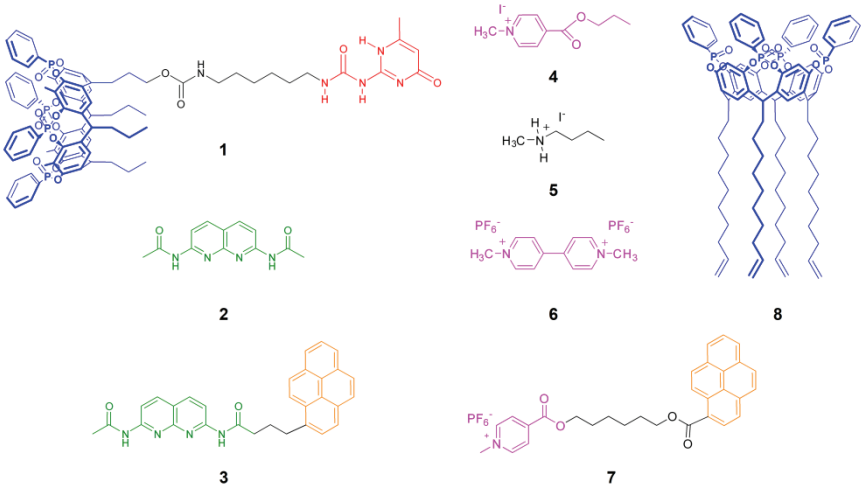

Chart 1

6.2 Results and Discussion.

6.2.1 Synthesis of the Molecular Components.

The compounds used in the present work are shown in Chart 1 and their preparation is reported in the experimental section. The target molecule **1** was synthesized in five steps starting from the known monohydroxy footed silylcavitand **I** (Scheme 1).[12b]

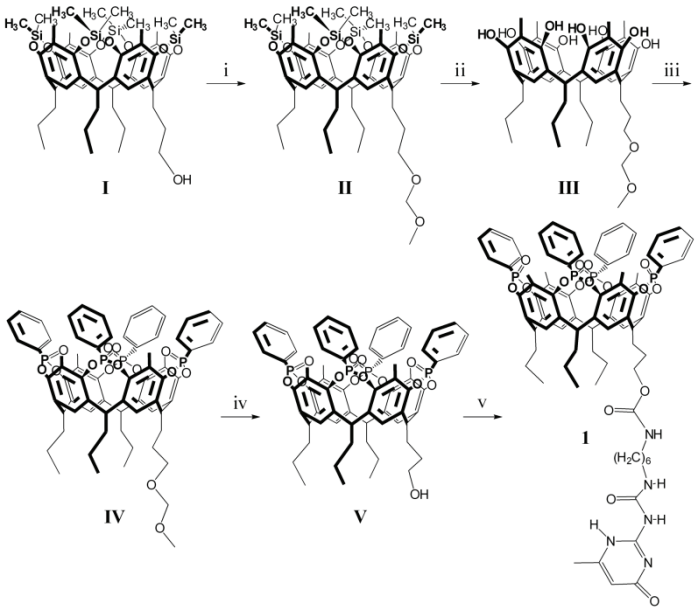

Scheme 1: i) DIPA, $CHCl_3$/DMF, 40 °C, 48 h, 75%; ii) HF, DMF, 45 °C, overnight, qt. yield; iii) $PhPCl_2$, pyridine, 70 °C, 3 h; H_2O_2/$CHCl_3$, r.t., 30 min, qt. yield; iv) HCl, $CHCl_3$/MeOH, 60 °C, overnight, 93%; 2(6-isocyanatohexylaminocarbonylamino)-6-methyl-4[1]pyrimidinone, DABCO, $CHCl_3$, reflux, 48 h, 49%.

The hydroxyl group at the lower rim was initially protected by reaction with chloromethyl methyl ether. The subsequent treatment of the resulting product **II** with an aqueous 36% HF solution caused the selective removal of the dimethylsilyl bridges, affording the free resorcinarene **III**, ready for the functionalization with dichlorophenylphosphine. This latter reaction gave rise to a tetraphosphonite intermediate,[14] which was *in situ* oxidized by addition of H_2O_2,[12b] to give tetraphosphonate cavitand **IV**. Only the isomer

featuring all the P=O groups pointing inwards the cavity was formed, thanks to the stereospecificity of this bridging reaction. Then, the methylmethoxy protection was removed by an HCl catalyzed hydrolysis to give **V**. Addition of 2(6-isocyanatohexylaminocarbonylamino)-6-methyl-4[1]pyrimidinone[15] at the free hydroxyl function, in the presence of 1,4-diazobicyclo[2.2.2]octane (DABCO) as catalyst, afforded cavitand **1** in 34% overall yield.

The symmetric 2,7-acetamido-1,8-naphthyridine **2** was prepared following a known literature protocol,[16] while the asymmetric 2(1-pyrenebutyricamido)-7-acetamido-1,8-naphthyridine **3** was synthesized by the Pd-catalyzed amidation of 2-chloro-7-acetamido-1,8-naphthyridine,[17] according to a procedure reported by Meijer and coworkers.[18]

Preparation of monotopic guests **4**, **5** and **7** was previously reported,[12a] as well as that of cavitand **8**.[19]

6.2.2 Properties of the Modular Components 1 and 3.

Cavitand **1** is functionalized at the upper rim with four phosphonate bridges in their all-inward configuration, and, at the lower rim, with a single ureidopyrimidone (UPY) unit. While the P=O groups impart molecular recognition properties toward methylpyridinium guests and methylammonium salts, the UPY motif enables the molecule to dimerize according to a DDAA-AADD quadruple H-bonding network (A, D: hydrogen bond acceptor and donor respectively). The association constant between a tetraphosphonate cavitand and a methylpyridinium guest was determined by ITC and fluorescence to be in the 10^7 M^{-1} regime (CH_2Cl_2, 298 K),[12a] while complexation of methylalkylammonium salts is much stronger, occurring with constants exceeding 10^9 M^{-1} (CH_2Cl_2, 298 K).[12b] As far as the UPY unit is concerned, Meijer and coworkers showed that DDAA-AADD sequences have a dimerization constant of $6 \cdot 10^7$ M^{-1} ($CHCl_3$, 298 K).[20]

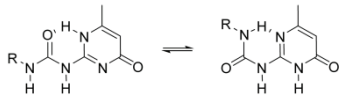

Figure 1: Pyrimidinone isomerization between 4[1H] and 4[3H] forms.

The asymmetric 2,7-diamino-1,6-naphthyridine diamide (NAPY) **3**, was equipped with a pyrenic unit to allow fluorescence monitoring of its complexation/decomplexation both in solution and on surfaces. Moreover, in addition to its homodimerization capability, which is quite weak (K_{ass}= 10^1-10^2 M^{-1}, $CHCl_3$, 298 K), **3** is complementary to an ADDA H-bonding array. This is the typical array shown by UPY systems, once the self-complementary 4[1H]-pyrimidinone conformer isomerizes to the non-complementary 4[3H]-pyrimidinone conformer (Figure 1). For this reason NAPY motifs like that of molecule **3**, are used to dissociate stable UPY-UPY homodimers and to turn them in robust UPY-NAPY heterodimers,[21] introducing switchability in H-bonded networks.
Molecules **4** and **6** are efficiently complexed by tetraphosphonate cavitands, thanks to a synergistic combination of multiple cation-dipole and CH_3-π interactions.[12c] While guest **4** presents just one binding site, leading to the formation of 1:1 complexes, methylviologen **6** has a ditopic character, allowing formation of 2:1 complexes.[22] For this reason monotopic guest **4** was chosen for the complexation studies in solution, while ditopic guest **6** was employed to build supramolecular structures on silicon surface. Finally, tetraphosphonate cavitands bind very efficiently methylalkylammonium salts such as N-methylbutylammonium iodide **5**. The additional, synergistic H-bonding interactions between the adjacent inward facing P(O) groups and the two NH of the guest, enhance the complexation. This results in a higher association constant for this guest family, that justify the use of methylalkylammonium salts as effective competitive guests to replace methylpyridinium species.

6.2.3 Complexation Studies in Solution.

In order to test the orthogonality and reversibility of H-bonding and host-guest interactions, we performed complexation studies in solution monitored by ^{1}H NMR spectroscopy.
The following sequential set of experiments was devised: i) formation of **1•3** UPY•NAPY heterodimer; ii) complexation of the monotopic methylpyridinium guest **4** by **1•3** to give the ternary complex **1•3•4**; iii) selective disassembly/reassembly of the H-bond motif in **1•3•4**; iv) guest exchange in **1•3•4** to give **1•3•5** using methylbutylammonium iodide **5**. The entire sequence is sketched in Scheme 2.

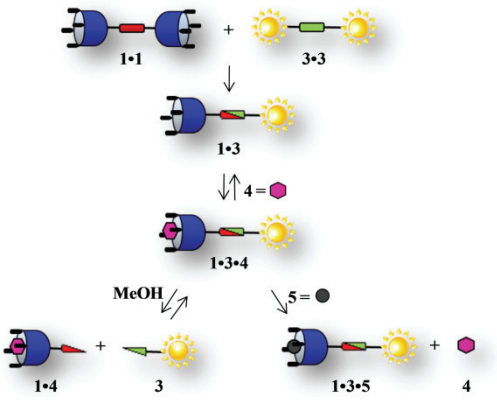

Scheme 2: Assembly/disassembly sequence in solution

i) UPY•NAPY heterodimer formation. In chloroform solution, monomers **1** and **3** exist exclusively as **1•1** and **3•3** homodimers, as confirmed by the presence, in the ^{1}H NMR spectrum, of signals typical for the hydrogen bonded NH protons (red triangles in Figure 2a and green triangles in Figure 2b).

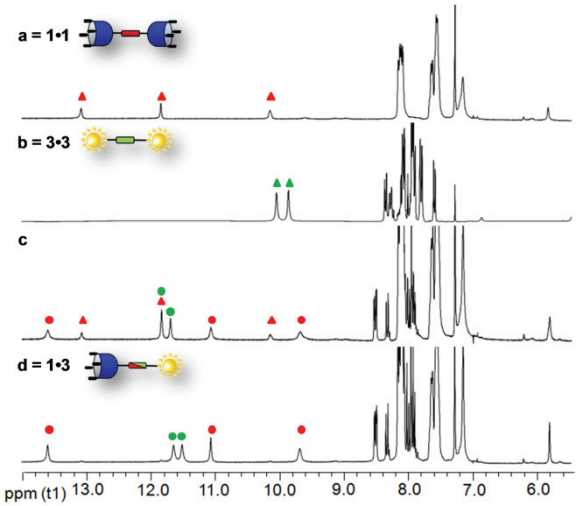

Figure 2: Section of ^{1}H NMR spectra (10 mM, $CDCl_3$) monitoring of UPY-NAPY **1•3** formation: diagnostic NH signals of (a) **1•1** (red triangles), (b) **3•3**, (green triangles), (c) **1•1** + **1•3 (**1:0.5), (d) **1•3** (red + green dots).

Addition of increasing amounts of **3•3** to a **1•1** solution resulted in the complete dissociation of **3•3** and in the concurrent exclusive formation of **1•3** heterodimer. This process was proved by the disappearance of the NH signals related to the **3•3** H-bonded complex, and by the appearance of two sets of NH signals due to the UPY NH protons. The first set, relative to the **1•1** homodimer, vanished when the 1:1 ratio was reached, meanwhile the second set increased in magnitude to become the only one present (red and green dots in Figures 2c and 2d). Moreover, a shift for the NAPY NH peaks was observed, consistent with a slow equilibration of dimers on the NMR experiment time scale.

ii) Host-Guest Complexation. Addition of **4** gave rise to the hybrid H-bonded/host-guest system **1•3•4**. Formation of the host-guest complex was proved by the upfield shift of H_{ORTHO} and H_{META} pyridine protons, due to the shielding effect of the receptor cavity (spectra a and c in Figure 3). On the other hand, the unchanged position of H-bonded NH protons demonstrated that host-guest complex formation did not interfere with the previously assembled UPY-NAPY dimer (spectra b and c in Figure 3).

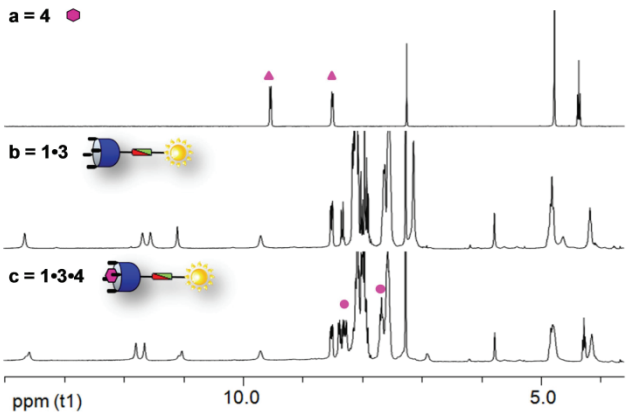

Figure 3: Section of ^{1}H NMR spectra (10 mM, $CDCl_3$) monitoring of host-guest complexation: signals relative to N-Me pyridinium aromatic protons of (a) **4** (pink triangles), (b) **1•3** (1:1), (c) **1•3•4** (1:1:1, pink dots).

iii) H-bonding motif disassembly/reassembly. Addition of MeOD to the **1•3•4** solution ($CDCl_3$/MeOD 8:2) produced the selective disassembly of the H-bonded heterodimer, while the host-guest system

persisted (spectrum b in Figure 4). When the added MeOD was removed by vacuum evaporation, and the sample was redissolved in $CDCl_3$, the initial **1•3•4** ternary complex was fully restored, demonstrating the solvent dependent reversibility of the H-bond motif (Cfr spectra a and c in Figure 4).

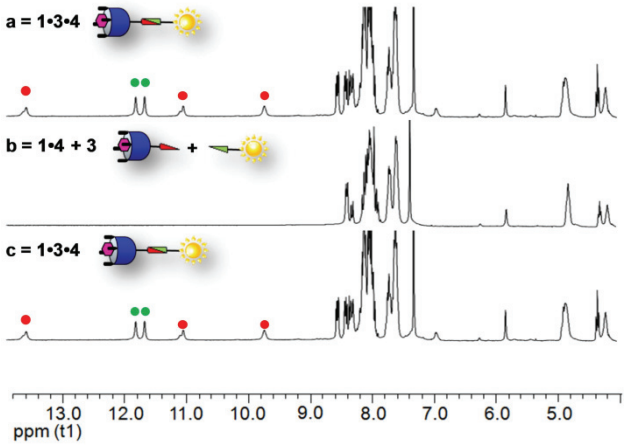

Figure 4: Solvent-driven UPY-NAPY disassembly monitored by ^{1}H NMR (10 mM) following the NH diagnostic peaks (red and green dots): (a) **1•3•4** (1:1:1) in $CDCl_3$, (b) **1•3•4** (1:1:1) in $CDCl_3$:MeOD (8:2), (c) **1•3•4** (1:1:1) redissolved in $CDCl_3$.

iv) Guest Exchange. Addition of 1 equivalent of **5** to the **1•3•4** complex led to the formation of the new **1•3•5** ternary complex.

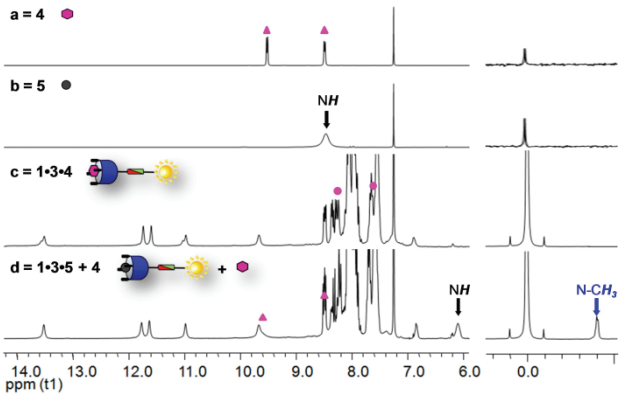

Figure 5: ^{1}H NMR spectra (10 mM, $CDCl_3$) monitoring of guest exchange: (a) free **4** (aromatic protons, pink triangles), (b) **5**, (c) **1•3•4** (1:1:1) (pink dots), (d) **1•3•5** (1:1:1) + free **4**.

The position of the aromatic pyridine protons and the upfield shifts undergone by the NH and N-CH_3 of the ammonium salt, proved that the competitive guest replaced completely the methylpyridinium moiety inside the cavity (spectrum d in Figure 5). This process again, did not interfere with the **1•3** heterodimer, as demonstrated by the unchanged position of the H-bonded NH signals.

6.2.4 Fluorescence Complexation Studies in Solution.

The above-said findings were also supported by photophysical investigations. In this case, the three components assembly was proved by starting from an equimolar solution ($2x10^{-6}$ M) of **2** and **7**, which presents a methylpyridinium unit as recognition moiety connected to a pyrene unit. This latter system was used in this case since the formation of its complex with tetraphosphonate cavitands can be monitored through the increase of the luminescence intensity of the pyrene, due to the decrease of exoergonicity of the photo-induced electron transfer process from the pyrene to the methylpyridiniun induced by the formation of the host-guest complex, as previously reported.[12a] As a consequence, to avoid the presence of overlapping signals coming from chromophores of the same nature, we used **2** instead of **3**.

The absorption spectrum of this solution (Figure 6) was the sum of the spectra of the two components, proving that no interaction occurred at this stage among NAPY and **7**. In particular in the 270-300 nm range, the spectrum is dominated by a band typical of the pyrene unit (not shown for clarity), while in the region between 300 and 400 nm both NAPY (prevalently in the 300-345 nm region) and pyrene (prevalently at lower energies) absorb with similar efficiency (violet line in Figure 6). Accordingly, also the fluorescence spectrum (black line in Figure 7a), where both the contributions of NAPY and **7** are present, is the one expected assuming no association and the lack of any energy transfer process among the two species in solution.

The following step in this experiment was the addition of **1** that, on the contrary, led to noticeable changes in both the absorption and emission spectra. In particular, a slight decrease of the absorbance was observed at 330 and 346 nm, together with an absorbance increase around 355 nm. These changes are those expected from the association of UPY and

NAPY, since they were already observed in an analogous experiment performed in absence of **7** in solution, and particularly the band rising at 355 nm is distinctive for the **1•2** complex.
The absorption spectroscopy did not provide however any information about the eventual association between the cavitand unit in **1** and the methylpyridinium in **7**, since the absorption spectrum of this host-guest complex is simply the sum of the components spectra.

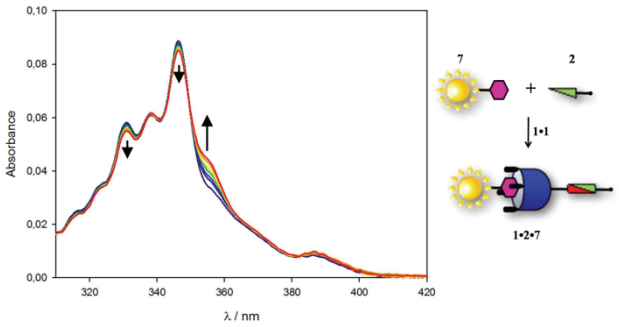

Figure 6: Absorption spectra of a 2x10^{-6} M solution of **2** and **7** and upon addition of increasing amount of **1** (0-1 equiv).

On the contrary, fluorescence spectroscopy revealed that interesting changes in the luminescence properties of the system occur during the host-guest complex formation. On one hand, after a careful correction of the spectra, it was possible to evidence an increase of the signal in the 380-460 nm region, where the emission of the pyrene unit of **7** rises upon the tail of the emission band of NAPY; this emission increase can be explained by the formation of the host-guest complex between **1** and **7**, as previously explained.[12a] On the other hand, the fluorescence measurements gave further support to the formation of the **1•2** complex: Figure 7a displays the characteristic decrease of emission intensity in the 340-380 nm region, that NAPY features when complexed to an UPY unit; the same quenching efficiency was observed in the analogous experiment carried out in absence of **7**. It is noteworthy that in this case the efficiency of an eventual energy transfer process from NAPY to the pyrene derivative in **7** in the **1•2•7** ensemble is negligible, most probably because of the large separation between this two units; the same energy transfer process is instead quite efficient in **3**, where the same units are connected by a short spacer.

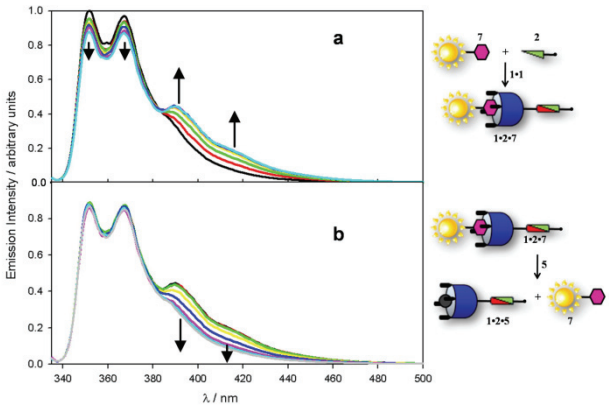

Figure 7: Emission spectra (λ_{exc} = 325 nm) of a 2x10^{-6} M solution of **2** and **7** and upon addition of increasing amount of **1** (0-1 eq.) (a), and upon subsequent addition of **5** (0-1 eq.) (b).

The evidences from both the absorption and the fluorescence spectra are thus in agreement with the formation of the ternary **1•2•7** adduct. To further support this conclusion, we added an equivalent of **5** as hexafluorophosphate salt. A decrease of the fluorescence intensity in the 380-460 nm region were observed (Figure 7b), as expected, because the more competitive ammonium salt can expel the methylpyridinium moiety from the cavity, thus restoring the original, low fluorescence intensity of the pyrene group in **7**.
It is worth noticing that, as evidenced by NMR spectroscopy for **1•3•5**, the attempt to break the newly formed **1•2•5** host-guest complex by addition of a base able to deprotonate the ammonium salt reducing its affinity for the cavitand, failed. In this case, in fact, DBU interacted before with the H-bonded network than with the host-guest system, leading to the dissociation of UPY-NAPY units. Therefore, this approach resulted unfit for closing the assembly-disassembly cycle. Moving the entire protocol on silicon surface will overcome this problem.

6.2.5 Complexation Studies on Silicon Surface.

To perform complexation studies on surface, cavitand **8** was grafted on a silicon wafer, via photochemical hydrosilylation on an H-terminated Si(100) surface.

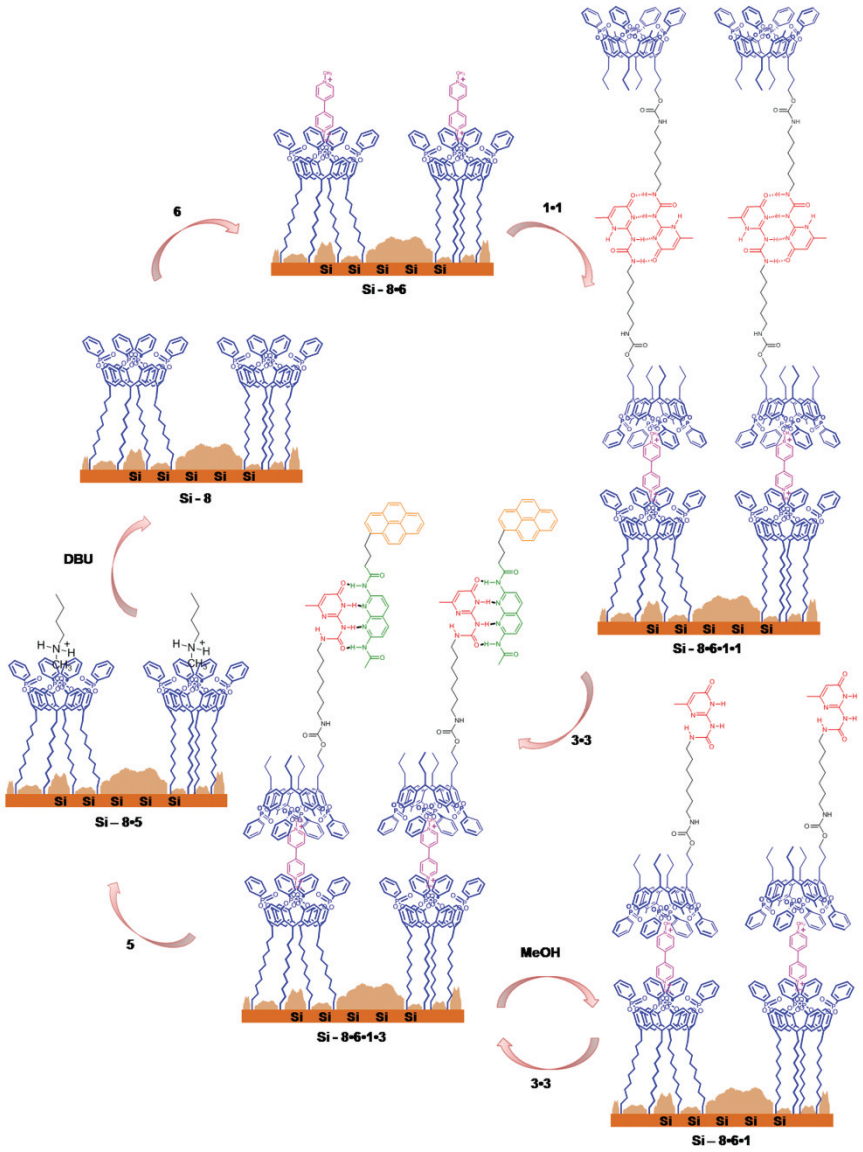

Figure 8: Self-assembly cycle on the Si-surface. The lumps on the Si wafer indicate SiO_2 growth on the surface after cavitand grafting.

The procedure, described in details in reference 12c, consists in a first etching with a 2.5% HF solution to remove the native oxide, followed by surface decoration with cavitand **8** via photochemical hydrosilylation.

The hydrogenated Si-wafer was soaked in a degassed 50 mM solution of **8** in mesitylene, and irradiated with a 254 nm UV-radiation, inducing the hydrosilylation of the cavitand terminal double bonds. In this way robust Si-C bonds between the substrate and the organic molecule formed, affording a cavitand-decorated surface, as proved by X-ray photoelectron spectroscopy (XPS) measurements (Table 1), which confirmed the presence of phosphorus on the wafer. In this case, we chose to prepare a pure cavitand monolayer in order to maximize the amount of receptors on the silicon surface. Under these conditions, the wafer coverage is not complete, leading to partial oxidation of the residual bare Si-surface.[23]

	Si 2p	O 1s	C 1s	P 2p
HF etched	77.0	7.8	15.2	-
Pure Si-8	15.0	17.3	65.0	2.7

Table 1: XPS Atomic composition analysis of (a) HF freshly etched surface, (b) pure **Si-8** monolayers.

Additional characterization of the **Si-8** monolayer was performed by X-Ray Reflectivity (XRR) analysis.

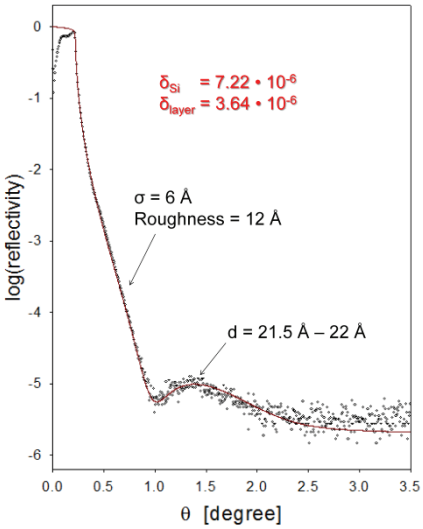

Figure 9: Reflectivity data (points) and theoretical fit (solid line) for **Si-8** layer.

Model A: *3 layers*			
Layer	$q_c = 4\pi\sin(\theta_c)/\lambda$	*σ [Å]*	*t [Å]*
Buffer	0.003	0.03	0.52
Layer 1	0.026	5.68	21.75
Layer 2	0.0009	> 10	0.20
Model B: *2 layers*			
Layer	$q_c = 4\pi\sin(\theta_c)/\lambda$	*σ [Å]*	*t [Å]*
Layer 1	0.023	6.6	21.85
Layer 2	0.0003	6.8	0.15
Model C: *single monolayer*			
Layer	$q_c = 4\pi\sin(\theta_c)/\lambda$	*σ [Å]*	*t [Å]*
Layer 1	0.022	6.14	21.90

Table 2: XRR fit-determined parameters for Layer **Si-8**.

The reflectivity data and theoretical fits based on the Parrat formalism[24] are shown in Figure 9, with the fit-determined parameters listed in Table 2, where q_c is the scattering vector corresponding to the critical angle of total external reflection and σ is the standard deviation of a Gaussian distribution of the roughness at each layer interface. Applying a three layers model, or a bilayer model, or a monolayer model, we obtained always coherent results, probing the presence of a single layer with a thickness *(t)* of 21.5-22 Å. This value agrees with the expected one by molecular modeling (Figure 10).

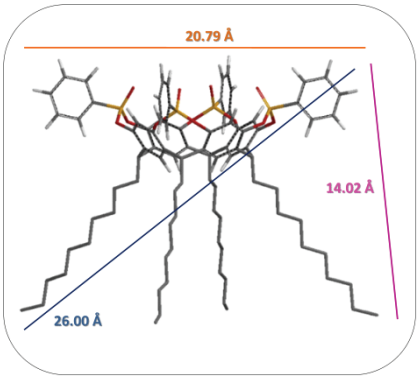

Figure 10: Molecular modeling for cavitand **8**.

In fact, even if the extended cavitand is 14 Å high, the partial anchoring of the terminal double bonds, afforded by the photochemical grafting, has to be taken into account. It follows that also the molecular lateral extension of 26 Å contributes to the layer thickness due to the oblique position of many cavitands, giving a sense at the obtained 21.5 Å average value. From the determined q_c values, we clarified the layer density. The obtained refractive index coefficient in the X-ray regime $\delta_{layer} = 3.64 \bullet 10^{-6}$, is significantly lower than that one of Si ($7.22 \bullet 10^{-6}$), but it is too high for a completely organic layer. This result was explained by the presence of silicon oxide islands among the anchored cavitands, formed because of the layer aging. The found roughness value (12 Å) agrees with this hypothesis and it is consistent with the picture of cavitand heads emerging from a silicon oxide network.

Atomic force microscopy (AFM) was also employed to interrogate the topology of the formed layers. The AFM topography image and the surface profile of the starting Si-monolayer are shown in Figure 11a. As expected, under consideration of the vertical resolution limit of AFM technique, a relatively flat surface was observed, which agrees with the previously proposed scenario.

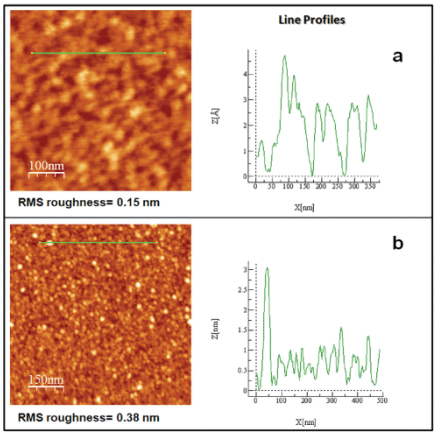

Figure 11: AFM topography image and surface profile for **Si–8** layer (a) and **Si–8•6•1•1** layer (b).

We then proceeded with a hierarchical construction of a supramolecular structure, exploiting the self-assembly driven growth. The cavitand-decorated Si surface was dipped into a 1 mM solution of methyl viologen **6** in acetonitrile, in order to obtain the guest complexation. After

removal of the physisorbed guest by extensive rinsing with CH_3CN and $CHCl_3$, the Si-wafer was exposed to a 1 mM solution of **1•1** homodimer in chloroform. The surface was rinsed again to remove the physisorbed species, then the AFM image of the grown **Si-8•6•1•1** structure was collected.
As shown in Figure 11b, a well defined profile was traced, featuring peaks of different height, in a range between 1.5 nm and 3 nm. These data demonstrated the growth of nanometric structures on the surface.

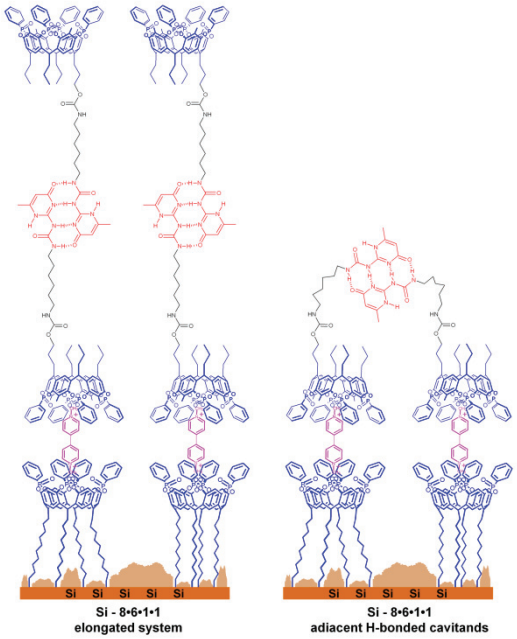

Figure 12: Possible arrangements of **1•1** homodimers once self-assembled on Si-surface.

In particular, the bigger peaks correspond to the length of the elongated **1•1** dimer linked at the surface thanks to host-guest interactions between the cavity of **1** and the still free pyridinium moiety of the previously anchored dimethyl viologen. As far as the smaller peaks are concerned, they can be attributed to a looped structure where the **1•1** dimer is anchored to two adjacent **Si–8•6** units (Figure 12).
In order to follow precisely the next steps and the successive assembly-disassembly processes, we turned to fluorescence measurements on surfaces.

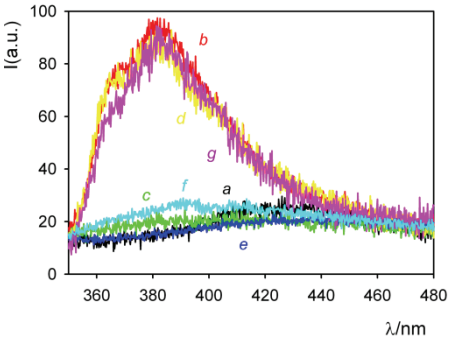

Figure 13: Fluorescent emission spectra of disassembled-reassembled modular components on Si-surface.

The starting point was the fluorescence silent structure **Si-8•6•1•1** (Figure 8 and Figure 13, trace a, black). Upon exposure to a 1 mM solution of **3•3** homodimer in chloroform, **Si-8•6•1•3** structure formed, according the exchange mechanism previously reported in solution (Figure 2). As result, a pyrenic unit was anchored on the surface, affording an emission band typical for the monomeric form of pyrene in the recorded surface fluorescence spectrum (Figure 13, trace b, red).
Dipping the **Si-8•6•1•3** wafer in a 8:2 $CHCl_3$/MeOH mixture resulted in the disassembly of unit **3**, as proved by the disappearance of the pyrenic band (Figure 13, trace c, green and Figure 8). The subsequent treatment with a 1 mM solution of **3•3** homodimer, restored the destroyed H-bonded network, as confirmed by the reappearance of the pyrenic peak in the fluorescence spectrum (Figure 13, trace d, yellow and Figure 8).
Selective host-guest exchange was obtained by simply dipping **Si-8•6•1•3** into a 1 mM solution of butylmethylammonium iodide **5** in chloroform, with the consequent disappearance of the pyrene emission band in the collected spectrum (Figure 13, trace e, blue).
Immersion of **Si-8•5** in a DBU solution restored the initial **Si-8** surface by removing guest **5** (Figure 13, trace f, cyan), ready to repeat the cycle again. The whole assembly cycle is highly reproducible as shown by the fluorescence spectrum of the **Si-8•6•1•3** reassembled system (Figure 13, trace g, magenta).

6.3 Conclusions.

In this chapter we have introduced a robust and reliable methodology for the self-assembly of complex architectures on silicon. The multistep growth of such supramolecular structures on the surface resulted from the combined use of orthogonal host-guest and H-bonding interactions, embedded in selected modular components. The two interactions are fully compatible in the assembly mode and individually addressable in the disassembly mode, enabling the molecular level control of each step on the surface and their complete reversibility under precise external stimuli. The entire process has been fully tested and characterized in solution, and then successfully transferred to the solid state. The transfer of the protocol to the silicon surface requires: (i) the covalent grafting of cavitand **8** on a silicon wafer as reactive layer to initiate the building process; (ii) the ditopic methyl viologen **6** for the multistep growth.
The design of the building blocks and of the entire protocol sequence was finalized to allow univocal surface characterization and to achieve complete reversibility. The **Si-8•6•1•1** to **Si-8•6•1•3** conversion allowed the introduction of the pyrene moiety for fluorescence detection, while the **Si-8•6•1•3** to **Si-8•5** guest exchange, followed by basic treatment, reset the starting surface. The problem related to the only non orthogonal disassembly process in solution, namely the DBU treatment of **1•3•5**, has been overcome on silicon, where a full cycle has been realized (Figure 8).
This work demonstrated that H-bonding and host-guest interactions can be concurrently employed to realize stimuli responsive surfaces and complex hybrid organic-inorganic materials.

6.4 Experimental Section.

MOM-protected silylcavitand II.
To a solution of monohydroxy footed silylcavitand[12b] (2.00 g, 2.1 mmol) in $CHCl_3$ (15 mL) and DMF (15 mL), diisopropylamine (3.4 mL, 20 mmol) and chloromethyl methyl ether (1 mL, 13 mmol) were added. The resulting mixture was heated at 40 °C for 48 h. After solvent removal by vacuum evaporation, the crude was dissolved in CH_2Cl_2 and extracted

with CH_2Cl_2/H_2O. The organic phase was evaporated to dryness and the resulting product was purified by column chromatography (CH_2Cl_2/MeOH 99:1) to give pure **2** (1.57 g, 1.6 mmol, 75%).
^{1}H NMR ($CDCl_3$, 300 MHz) δ (ppm) 7.19 (s, 2H, Ar**H**); 7.17 (s, 2H, Ar**H**); 4.64 (s, 2H, OC**H$_2$**O); 4,60 (t, 4H, ArC**H**, J=8,1 Hz); 3.60 (t, 2H, CH_2CH_2C**H$_2$**O, J=6.6 Hz); 3.38 (s, 3H, OC**H$_3$**); 2.30 (m, 2H, C**H$_2$**CH_2CH_2O); 2.17 (m, 6H, C**H$_2$**CH_2CH_3); 1.91 (s, 12H, ArC**H$_3$**); 1.58 (m, 2H, CH_2C**H$_2$**CH_2O); 1.31 (m, CH_2C**H$_2$**CH_3); 0.97 (m, 9H, CH_2CH_2C**H$_3$**); 0.51 (s, 12H, SiC**H$_{3OUT}$**); -0.69 (s, 12H, SiC**H$_{3IN}$**). **ESI-MS:** *m/z* calcd. for $C_{54}H_{76}O_{10}Si_4$ (997.5 Da), $[M+Na]^+$: 1020.5; found: 1020.3.

MOM-protected resorcinarene III.
An aqueous 36% HF solution (3.1 mL) was added to **II** (1.57 g, 1.6 mmol) dissolved in DMF (40 mL). The mixture was heated at 45 °C overnight. The solvent was removed in vacuo and the product was washed with water. Vacuum filtration afforded pure **III** (1.29 g, 1.6 mmol, quantitative yield).
^{1}H NMR (Acetone-d$_6$, 300 MHz) δ (ppm) 7.96 (s, 8H, ArO**H**); 7.45 (s, 2H, Ar**H**); 7.44 (s, 2H, Ar**H**); 4.58 (s, 2H, OC**H$_2$**O); 4.40 (t, 4H, ArC**H**, J=7.5 Hz); 3.55 (bt, 2H, CH_2CH_2C**H$_2$**O); 3.30 (s, 3H, OC**H$_3$**); 2.36 (m, 2H, C**H$_2$**CH_2CH_2O); 2.28 (m, 6H, C**H$_2$**CH_2CH_3); 2.07 (s, 12H, ArC**H$_3$**); 1.55 (m, 2H, CH_2C**H$_2$**CH_2O); 1.30 (m, 6H, CH_2C**H$_2$**CH_3); 0.94 (bt, 9H, CH_2CH_2C**H$_3$**). **ESI-MS:** *m/z* calcd. for $C_{46}H_{60}O_{10}$ (772.9 Da), $[M-H]^-$: 771.9; found: 771.2.

MOM-protected tetraphosphonate cavitand IV.
To a solution of **III** (0.50 g, 0.6 mmol) in fresh distilled pyridine (15 mL), dichlorophenylphosphine (0.5 mL, 2.7 mmol) was added slowly, at room temperature. After 3 hours of stirring at 70 °C, the solution was allowed to cool at room temperature and 2 mL of a mixture of aqueous 35% H_2O_2 and $CHCl_3$ (1:1) was added. The resulting mixture was stirred for 30 minutes at room temperature, then the solvent was removed in vacuo. Addition of water resulted in the precipitation of a white powder, which is filtered to give pure **IV** (0.81 g, 0.6 mmol, quantitative yield).
^{1}H NMR ($CDCl_3$, 300 MHz): δ (ppm) 8.08 (m, 8H, P(O)Ar**H$_{ORTO}$**); 7.61 (m, 4H+8H, P(O)Ar**H$_{PARA}$** + P(O)Ar**H$_{META}$**); 7.34(s, 2H, Ar**H$_{DOWN}$**); 7.32 (s, 2H, Ar**H$_{DOWN}$**); 4.80 (bt, 4H, ArC**H**,); 4.69 (s, 2H, OC**H$_2$**O); 3.70 (bt, 2H, CH_2CH_2C**H$_2$**O); 3.46 (s, 3H, OC**H$_3$**); 2.44 (m, 2H, C**H$_2$**CH_2CH_2O); 2.14 (s,

12H, ArC**H$_3$**); 2.12 (m, 6H, C**H$_2$**CH$_2$CH$_3$); 1.70 (m, 2H, CH$_2$C**H$_2$**CH$_2$O); 1.33 (m, 6H, CH$_2$C**H$_2$**CH$_3$); 1.04 (m, 9H, CH$_2$CH$_2$C**H$_3$**). **^{31}P NMR (CDCl$_3$, 172 MHz):** δ (ppm) 6.28 (s, **P**(O)). **ESI-MS:** *m/z* calcd. for $C_{70}H_{72}O_{14}P_4$ (1261.2 Da), $[M+Na]^+$: 1284.2; found: 1284.4.

Monohydroxy footed tetraphosphonate cavitand V.

To a solution of **IV** (0.71 g, 0.56 mmol) in $CHCl_3$ (6 mL), methanol (10 mL) and an aqueous 36% HCl solution (1 mL) were added. The resulting suspension was heated at 60 °C overnight. The solvent was evaporated and the crude was extracted with CH_2Cl_2/H_2O. Concentration to dryness of the organic phase afforded pure **V** (0.64 g, 0.52 mmol, 93%). **^{1}H NMR (CDCl$_3$, 300 MHz):** δ (ppm) 8.09 (m, 8H, P(O)Ar**H$_{ORTO}$**); 7.61 (m, 4H + 8H, P(O)Ar**H$_{PARA}$**+ P(O)Ar**H$_{META}$**); 7.26 (s, 2H, + Ar**H$_{DOWN}$**); 7.23 (s, 2H, Ar**H$_{DOWN}$**); 4.79 (t, 4H, ArC**H**, J=6.6 Hz); 3.80 (t, 2H, C**H$_2$**OH, J=5.9 Hz); 2.50 (m, 2H, C**H$_2$**CH$_2$CH$_2$OH); 2.34 (m, 6H, C**H$_2$**CH$_2$CH$_3$); 2.14 (s, 12H, ArC**H$_3$**); 1.67 (m, 2H, CH$_2$C**H$_2$**CH$_2$OH); 1.43 (m, 6H, CH$_2$C**H$_2$**CH$_3$); 1.07 (bt, 9H, CH$_2$CH$_2$C**H$_3$**). **^{31}P NMR (CDCl$_3$, 172 MHz):** δ (ppm) 5.56 (s, **P**(O)). **ESI-MS:** *m/z* calcd. for $C_{68}H_{68}O_{13}P_4$ (1217.2 Da), $[M+Na]^+$: 1240.2; found: 1240.1.

Monoureidopyrimidone footed tetraphosphonate cavitand 1.

A suspension of 2(6-isocyanatohexylaminocarbonylamino)-6-methyl-4[1]pyrimidinone, cavitand **V** (0.91 g, 0.75 mmol) and 1,4-diazobicyclo[2.2.2]octane (DABCO) in $CHCl_3$ (40 mL), was heated under reflux for 48 h. The solvent was evaporated and the crude was purified by column cromatography (0-75% gradient of MeOH/CH_2Cl_2) to give pure cavitand **1** (0.56 g, 0.37 mmol, 49%).

^{1}H NMR (CDCl$_3$, 300 MHz): δ (ppm) 13.06 (s, 1H, CH$_3$CN**H**); 11.82 (s, 1H, CH$_2$NHC(O)N**H)**; 10.12 (s, 1H, CH$_2$N**H**C(O)NH); 8.09 (m, 8H, P(O)Ar**H$_{ORTO}$**); 7.57 (m, 4H+8H, P(O)Ar**H$_{PARA}$** + P(O)Ar**H$_{META}$**); 7.11 (s, 4H, Ar**H$_{DOWN}$**); 5.80 (s, 1H, C**H**CCH$_3$); 4.82 (bt, 4H, ArC**H**,); 4.19 (bt, 2H, C(O)OC**H$_2$**); 3.19 (m, 2H, NHC(O)NHC**H$_2$**); 3.05 (s, 2H, OC(O)NHC**H$_2$**); 2.56-2.43 (m, 2H + 2H +6H +3H, OC(O)NHCH$_2$C**H$_2$** + NHC(O)NHCH$_2$C**H$_2$** + ArCHC**H$_2$** + C**H$_3$**CCH); 2.02 (s, 12H, ArC**H$_3$**); 1.63 (m, 2H, C**H$_2$**CH$_2$OC(O)); 1.40-1.25 (m, 6H + 2H + 2H, CH$_2$C**H$_2$**CH**$_3$** + NHC(O)NHCH$_2$CH$_2$C**H$_2$** + OC(O)NHCH$_2$CH$_2$C**H$_2$**); 1.01 (m, 9H, CH$_2$CH$_2$C**H$_3$**). **^{31}P NMR (CDCl$_3$, 172 MHz):** δ (ppm) 5.57 (s, **P**(O)). **HR**

ESI-MS: *m/z* calcd. for $C_{81}H_{87}O_{16}N_5P_4$ (1509.2 Da), $[M+NH_4]^+$: 1527.5436; found: 1527.5433.

2(1-Pyrenebutyricamido)-7-acetamido-1,8-naphthyridine 3.
A Schlenck dried tube was charged with $Pd(OAc)_2$ (0.010 g, 0.046 mmol), 9,9-dimethyl-4,5-bis(diphenylphosphino) xanthene (0.053 g, 0.091 mmol), K_2CO_3 (0.140 g, 1.020 mmol), 7-acetamido-2-chloro-1,8-naphthyridine (0.160 g, 0.073 mmol), 1-pyrenebutyricamide[25] (0.250 g, 0.087 mmol) and 1,4-dioxane (33 mL). The Schlenck tube was capped, evacuated, and back-filled with Ar three times. While stirr under Ar, it was immersed into a 100 °C oil bath. After stirring for 24 h, the mixture was cooled, filtered over diatomaceous earth, and evaporated in vacuo. The crude was purified by column cromatography (CH_2Cl_2/MeOH 95:5) to give pure product **3** (0.220 g, 0.046 mmol, 64%).
^{1}H NMR ($CDCl_3$, 600 MHz): δ (ppm) 9.14 (bs, 2H, N**H**); 8.28 (d, 1H, J=9.0 Hz); 8,21 (d, 1H, J=9.0 Hz); 8.20 (d, 1H, J=7.2 Hz); 8.06-7.98 (m, 4H); 7.95-7.86 (m, 5H); 7.77 (d, 2H, J=7.2 Hz); 3.37 (t, 2H, C**H$_2$**Pyrene, J=7.2 Hz); 2.55 (t, 2H, C(O)C**H$_2$**, J=6.6 Hz); 2.27 (m, 2H, C(O)CH_2C**H$_2$**), 2.21 (s, 3H, C**H$_3$**C(O)). **HR ESI-MS:** *m/z* calcd. for $C_{30}H_{24}N_4O_2$ (472.3 Da), $[M+H]^+$: 473.1972; found: 473.1962.

6.5 References and Notes.

[1]A. B. Descalzo, R. Martìnez-Màñez, F. Sancenòn, K. Hoffmann, K. Rurack, *Angew. Chem. Int. Ed.* **2006**, *45*, 5924-5948.

[2] J. M. Lehn, *Chem. Eur. J.* **1999**, *5*, 2455-2463.

[3] H-bonding: (a) S. De Feyter, F. C. De Schryver, *Chem. Soc. Rev.* **2003**, *32*, 139-150; (b) J. A. Theobald, N. S. Oxtoby, M. A. Phillips, N. R. Champness, P. H. Beton, *Nature*, **2003**, *424*, 1029-1031; (c) M. Ruben, D. Payer, A. Landa, A. Comisso, C. Gattinoni, N. Lin, J. P. Collin, J.-P. Sauvage, A. De Vita, K. Kern, *J. Am. Chem. Soc.* **2006**, *128*, 15644-15651; (d) A. Llanes-Pallas, M. Matena, T. Jung, M. Prato, M. Stöhr, D. Bonifazi, *Angew. Chem Int. Ed.* **2008**, *47*, 7726-7730; (e) R. Madueno, M. T. Räisänen, C. Silien, M. Buck, *Nature* **2008**, *454*, 618-621.

[4] Host-guest: (a) M. J. W. Ludden, D. N. Reinhoudt, J. Huskens *Chem. Soc. Rev*. **2006**, *35*, 1122-1134; (b) M. J. W. Ludden, A. Mulder, R. Tampè, D. N. Reinhoudt, J. Huskens, *Angew. Chem. Int. Ed.* **2007**, *46*, 4104-4107.

[5] Metal-ligand coordination: (a) I. Weissbuch, P. N. W. Baxter, S. Cohen, H. Cohen, K. Kjaer, P. B. Howes, J. Als-Nielsen, G. S. Hanan, U. S. Schubert, J.-M. Lehn, L. Leiserowitz, M. Lahav, *J. Am. Chem. Soc.* **1998**, *120*, 4850-4860; (b) A. Hatzor, T. Moav, H. Cohen, S. Matlis, J. Libman, A. Vaskevich, A. Shanzer, I. Rubinstein, *J. Am. Chem. Soc.* **1998**, *120*, 13469-13477; (c) S. Levi, P. Guatteri, F. C. J. M. van Veggel, G. J. Vancso, E. Dalcanale, D. N. Reinhoudt, *Angew. Chem. Int. Ed.* **2001**, *40*, 1892-1896; (d) M. Busi, M. Laurenti, G. G. Condorelli, A. Motta, M. Favazza, I. L. Fragalà, M. Montalti, L. Prodi, E. Dalcanale, *Chem. Eur. J.* **2007**, *13*, 6891-6898; (e) S.-S. Li, B. H. Northrop, Q.-H. Yuan, L.-J. Wan, P. J. Stang, *Acc. Chem. Res.* **2009**, *42*, 249-259.

[6] π-stacking: (a) R. Bhosale, A. Perez-Velasco, V. Ravikumar, R. S. K. Kishore, O. Kel, A. Gomez-Casado, P. Jonkheijm, J. Huskens, P. Maroni, M. Borkovec, T. Sawada, E. Vauthey, N. Sakai, S. Matile, *Angew. Chem. Int. Ed.* **2009**, *48*, 6461-6464; (b) R. S. K. Kishore, O. Kel, N. Banerji, D. Emery, G. Bollot, J. Mareda, A. Gomez-Casado, P. Jonkheijm, J. Huskens, P. Maroni, M. Borkovec, E. Vauthey, N. Sakai, S. Matile, *J. Am. Chem. Soc.* **2009**, *131*, 11106-11116.

[7] A. Langner, S. L. Tait, N. Lin, R. Chandrasekar, M. Ruben, K. Kern, *Angew. Chem. Int. Ed.* **2008**, *47*, 8835-8838.

[8] For alternative combinations of orthogonal interaction modes on surfaces see: (a) F. Corbellino, A. Mulder, A. Sartori, M. J. W. Ludden, A. Casnati, R. Ungaro, J. Huskens, M. Crego-Calamata, D. N. Reinhoudt, *J. Am. Chem. Soc.* **2004**, *126*, 17050-17058; (b) M. J. W. Ludden, J. Huskens, D. N. Reinhoudt, *Small* **2006**, 1192-1202.

[9] For the combination of weak interactions in supramolecular polymers see: H. Hofmeier, U. S. Schubert, *Chem. Commun.* **2005**, 2423-2432.

[10] (a) F. H. Beijer, R. P. Sijbesma, H. Kooijman, A. L. Spek, E. W. Meijer, *J. Am. Chem. Soc.* **1998**, *120*, 6761-6769; (b) P S. Corbin, S. C. Zimmermann, *J. Am. Chem. Soc.* **1998**, *120*, 9710-9711; (c) X.-Z.

Wang, X.-Q. Li, X.-B. Shao, X. Zhao, P. Deng, X.-K. Jiang, Z.-T. Li, Y.-Q. Chen, *Chem. Eur. J.* **2003**, *9*, 2904-2913; (d) T. Park, E. M. Todd, S. Nakashima, S. C. Zimmermann, *J. Am. Chem. Soc.* **2005**, *127*, 18133-18142; (e) T. F. A. de Greef, G. B. W. L. Ligthart, M. Lutz, A. L. Spek, E. W. Meijer, R. P. Sijbesma, *J. Am. Chem. Soc.* **2008**, *130*, 5479-5486.

[11] (a) R. Pinalli, M. Suman, E. Dalcanale, *Eur. J. Org. Chem.* **2004**, 451-462; (b) L. Pirondini, E. Dalcanale, *Chem. Soc. Rev.* **2007**, *36*, 695-706.

[12] (a) E. Biavardi, G. Battistini, M. Montalti, R. M. Yebeutchou, L. Prodi, E. Dalcanale, *Chem. Commun.* **2008**, 1638-1640; (b) R. M. Yebeutchou, F. Tancini, N. Demitri, S. Geremia, R. Mendichi, E. Dalcanale, *Angew. Chem. Int. Ed.* **2008**, *47*, 4504-4507; (c) E. Biavardi, M. Favazza, A. Motta, I. L. Fragala, C. Massera, L. Prodi, M. Montalti, M. Melegari, G. Condorelli, E. Dalcanale, *J. Am. Chem. Soc.* **2009**, *131*, 7447-7455.

[13] B. Gadenne, M. Semeraro, R. M. Yebeutchou, F. Tancini, L. Pirondini, E. Dalcanale, A. Credi, *Chem. Eur. J.* **2008**, *14*, 8964-8971.

[14] W. Xu, J. P. Rourke, R. J. R. Puddephatt, *Chem. Commun.* **1993**, 145-147.

[15] H. M. Keizer, R. Van Kessel, R. P. Sijbesma, E. W. Meijer, *Polymer* **2003**, *44*, 5505-5511.

[16] C. Alvarez-Rua, S. Garcia-Granda, S. Goswami, R. Mukherjee, S. Dey, R. M. Claramunt, M. D. S. Maria, I. Rozas, N. Jagerivic, I. Alkorta, J. Elguero, *New J. Chem.* **2004**, *28*, 700-707.

[17] P. S. Corbin, S. C. Zimmerman, P. A. Thiessen, N. A. Hawriluk, T. J. Murray, *J. Am. Chem. Soc.* **2001**, *123*, 10475-10488.

[18] G. B. W. L. Lightart, H. Ohkawa, R. P. Sijbesma, E. W. Meijer, *J. Org. Chem.* **2006**, *71*, 375-378.

[19] B. Bibal, B. Tinant, J.-P. Declercq, J.-P. Dutasta, *Supramol. Chem.* **2003**, *15*, 25-32.

[20] S. H. M. Sontjens, R. P. Sijbesma, M. H. P. Van Genderen, E. W. Meijer, *J. Am. Chem. Soc.* **2000**, *122*, 7487-7493.

[21] (a) X. Zhao, X.-Z. Wang, X.-K. Jiang, Y.-Q. Chen, Z.-T. Li, G.-J. Chen, *J. Am. Chem. Soc.* **2003**, *125*, 15128-15139; (b) X.-Q. Li, D.-J. Feng, X.-K. Jiang, Z.-T. Li, *Tetrahedron* **2004**, *60*, 8275-8284.

[22] J.-P Dutasta, et al. *Phosphorus, Sulfur and Silicon* **2002**, *177*, 1485-1488.

[23] G. G. Condorelli, A. Motta, M. Favazza, I. L. Fragalà, M. Busi, E. Menozzi, E. Dalcanale, L. Cristofolini, *Langmuir* **2006**, *22*, 11126-11133.

[24] Parrat, L.G. *Phys. Rev. B.* **1954**, *95*, 359-369.

[25] T. J. Dale, J. Jr.Rebek, *J. Am. Chem. Soc.* **2006**, *128*, 4500-4501.

Appendix A
Materials and Methods.

A.1 Materials.

All reagents and chemicals were obtained from commercial sources and used without further purification. Dry pyridine was distilled from KOH before use or purchased from Aldrich and used as received (Pyridine absolute, over molecular sieves, $H_2O \leq 0.005\%$). CH_2Cl_2 was dried by distillation over CaH_2 according standard procedures. Dry DMF (DMF purissim. ≥ 99.5%(GC), over molecular sieves) was provided by Aldrich and used as received; dry diethyl ether (Diethyl ether purum ≥ 99.8%(GC), over molecular sieves) was purchased from Fluka and used as received.
Silica column chromatography was performed using silica gel 60 (Fluka 230-400 mesh ASTM), or silica gel 60 (MERCK 70-230 mesh). Alumina chromatography was performed using MP Alumina B, Akt. I (MP Biomedicals Germany GmbH).

A.2 Methods.

- **NMR Measurements.**

(Ch. 2-3-5-6): ^{1}H NMR spectra were obtained using a Bruker AC-300 (300 MHz) or a Bruker AVANCE 300 (300 MHz) spectrometer. All chemical shifts (δ) were reported in ppm relative to the proton resonances resulting from incomplete deuteration of the NMR solvents. ^{31}P NMR spectra were obtained using a Bruker AMX-400 (162 MHz)

spectrometer. All chemical shifts (δ) were recorded in ppm relative to external 85% H_3PO_4 at 0.00 ppm.
(Ch. 4): ^1H NMR spectra were obtained using a Varian Gemini 300 (300 MHz) or a Varian Mercury 300 (300 MHz) spectrometer. All chemical shifts (δ) were reported in ppm relative to the proton resonances resulting from incomplete deuteration of the NMR solvents. ^{31}P NMR spectra were obtained using a Varian Mercury 300 (121 MHz) spectrometer.

- **MS-Studies.**

(Ch. 2-3-5-6): Electrospray ionization ESI-MS experiments were performed on a Waters ZMD spectrometer equipped with an electrospray interface. Exact masses were determined using a LTQ ORBITRAP XL Thermo spectrometer equipped with an electrospray interface. GC-MS analysis were performed using a (Hewlett Packard) HP 6890/5973 GC/MSD system.
(Ch. 4): Electrospray ionization ESI-MS experiments were performed on a Bruker maXis ESI-Q-TOF, while MALDI characterizations were carried out on a Bruker Daltonics UltraFlex II instrument, using (3-hydroxypyridine-2-carboxylic acid)-2,5-Dihydroxybenzoic acid (3-HPA) as matrix.

- **Melting Point Determination.**

Melting points were determined by using a Büchi B-540 capillary melting point apparatus.

- **Fluorescence Measurements.**

Fluorescence spectra in solution were obtained with a modular UV/visible NIR spectrofluorimeter, Edinbourg, equipped with a 450 W Xe lamp. Corrections for instrumental response, inner filter effects and phototube sensitivity were performed. Fluorescence spectroscopy on Si surfaces were obtained with a spectrofluorimeter ISA FLUOROLOG 3 by using a He–Cd continuum laser at 325 nm with a 50 mW power. All solvents employed are CHROMASOLV, for HPLC grade. Chloroform is stabilized with amylene.

- **Atomic Force Microscopy Measurements.**

Atomic force microscopy (AFM) was carried out in tapping mode using a Veeco Dimension3100 instrument.

- **Light Scattering Measurements.**

(Ch. 2): Static light scattering (SLS) measurements were performed using a multi-angle laser light scattering (MALS) Dawn DSP-F photometer from Wyatt (Santa Barbara, CA, USA) in off-line (batch) mode in freshly distilled chloroform solvent at room temperature. All polymeric solutions were accurately filtered through 0.2 μm PTFE filters. The MALS photometer used a vertically polarized He-Ne laser (wavelength λ=632.8 nm) and simultaneously measured the intensity of the scattered light at 18 angular locations ranging from 19.2° to 149.2°. The MALS calibration constant was calculated using toluene as standard assuming a Rayleigh Factor of $1.406 \cdot 10^{-5}$ cm^{-1}. The normalization of the different photodiodes was performed by measuring the scattering intensity of a narrow molecular weight distribution (MWD) polystyrene standards (Mp=10.3 kg/mol, Mw/Mn=1.03, Rg=2.6 nm) in chloroform, assumed to act as isotropic scatterers.
The incremental refractive index, (dn/dc), for an equimolar 1:1 mixture of **1b** and **2c** in chloroform (n=1.446) at 25 °C was found 0.102 mL/g, and it was measured by a KMX-16 differential refractometer from LDC Milton Roy (Riviera Beach, FL, USA).
(Ch. 3): Static (SLS) and Dynamic (DLS) Light Scattering measurements: experiments were carried out using a Malvern Nano ZS instrument equipped with a 633 nm laser diode and working at a scattering angle of 173°. Samples were housed in fluorescence quartz cuvets of 1 cm optical path length. The solvents and the solutions used during light scattering measurements were thoroughly filtered through 0.2 μm PTFE syringe filters. Toluene was chosen as scattering standard.
Determination of the hydrodynamic diameter distributions was carried out through DLS: the width of DLS hydrodynamic diameter distribuition is indicated by PdI (Polydispersion Index). In case of a mono-modal distribuition (gaussian) calculated by means of cumulant analysis, PdI=(σ/Zavg)2, where σ is the width of the distribuition and Zavg is average diameter of the particles population respectively.

The incremental refractive index, (dn/dc), of **3** in dichloromethane (n=1.442) at 25 °C was found 0.146 mL/g, and it was measured by a KMX-16 differential refractometer from LDC Milton Roy (Riviera Beach, FL, USA).

- **ITC Measurements.**

ITC studies were performed using an isothermal titration microcalorimeter Microcal VP-ITC, thermostated at 298 K. Experimental titration curves were analyzed with the MicroCal Origin 5.0 program.
ΔH, ΔS and K values had been calculated as the average of a set of independent experiments; ΔG value is given by: ΔG = ΔH - TΔS.
Standard deviation for ΔH, ΔS and K was calculated according the function:

$$\sqrt{\frac{\sum_{i=1}^{n}(x_i - \bar{x})}{n-1}}$$

Where n is the number of independent experiments, x_i is the value recorded in the i-experiment, and $\bar{x}$ is the average value for x.
Standard deviation for ΔG was calculated according the function:

$$\boldsymbol{\delta_{\Delta G}} = \sqrt{\left(\frac{\partial \boldsymbol{G}}{\partial \boldsymbol{K}} * \boldsymbol{\delta_K}\right)^2} = \sqrt{\left(\frac{-\boldsymbol{R} * \boldsymbol{T} * \boldsymbol{\delta_K}}{\boldsymbol{K}}\right)^2} = \frac{\boldsymbol{R} * \boldsymbol{T} * \boldsymbol{\delta_K}}{\boldsymbol{K}}$$

- **Viscosity Measurements.**

Ubbelohde dilution viscometers were used for the intrinsic viscosity [η] measurements. Solutions of polymers were made in chloroform (HPLC grade) or in tetrachloroethane (98% GC grade). Temperature control was achieved using a thermostated water bath (for the experiments at 298 K), or exploiting an oil bath (for the measurement at variable temperature). Solvents and solutions were filtered through a 0.2 μm Teflon membrane filters directly into the viscometer.

- **XPS Analysis.**

The XPS spectra were run with a PHI ESCA/SAM 5600 Multy technique spectrometer equipped with a monochromated Al Kα X-ray source, a standard dual-anode Mg/Al source and a spherical capacitor analyser (SCA) with a mean diameter of 279.4 mm. The analyses were carried out at various photoelectron angles (relative to the sample surface) in the 10°-80° range with an acceptance angle of ±7° (the acceptance angle was fixed high to avoid photoelectron diffraction effects).
XPS B.E. scale was calibrated by centering the C 1s peak of the adventitious carbon at 285.0 eV.

- **X-Ray Reflectivity Measurements.**

X-ray reflectivity (XRR) measurements were performed by a Philips high resolution X-ray diffractometer equipped with a graded multi-layers mirror to increase the intensity of the incidence beam and with two channel-cut Ge-crystals as a monochromator for selecting the CuKα1 radiation. The fitting of the experimental profiles was performed by a calculation program based on Parrat formalism. This method allows to model any electron density profile, along the growth direction of the structure, by slicing the material in an arbitrary number of thin layers (step model). The roughness at each interface can be characterized assuming a Gaussian probability density of the broadening profile with a standard deviation σ accounting for the roughness extent.

- **X-Ray Analysis.**

For details about the performed X-Ray analysis see appendix B.

Appendix B
X-Ray Data Analysis.

B.1 X-Ray data for the linear polymer formed by self-assembly between methyl viologen $2PF_6^-$ and 1c *(Ch. 2).*

The molecular structure of the compound $C_{156}H_{153}N_3O_{28}P_8 + 2PF_6^- + 2.5CH_3CN$, was determined by single-crystal X-ray diffraction methods. Experimental details are summarized in Table 1. Intensity data were collected using Cu Kα radiation (λ= 1.54 Å) equipped with a CCD area detector at 100K. The structure was solved by direct method using DENZO-SMN, SCALEPACK, and AMoRe SHELXL program.[1] The data of 6 were performed and refined using suitable programs.[2]

Table 1: Crystal data and structure refinement information for the linear polymer.

Compound	**1c•methyl viologen 2 PF_6^-**
Formula	$C_{156}H_{153}N_3O_{28}P_8+2PF_6+C_2H_3N$
Formula weight	12626.12
Temperature	100 K
Wavelength	1.54 Å
Crystal System	Monoclinic
Space Group	$P2_1/c$
a / Å	13.7267±0.0007

b / Å	27.4467±0.0019
c / Å	42.02920±0.0025
α / °	90
β / °	108.2344±0.0707
γ / °	90
V/Å^3	15823.8
Z	4
D_c/g cm^{-3}	1.262
F(000)	6432
μ / mm^{-1}	2.569
$\theta_{min,\ max}$/ °	1.5
Resolution	1.5-200.0 Å
Reflections collected	4835
Indipendent reflections	2928
ObservedReflections[Fo>4σ(Fo)]	75147
I/σ(I) (all data)	11.9
I/σ(I) (max resolution)	2.3
Completeness(all data)	94.2%
Completeness(max resolution)	80.4%
Multiplicity(all data)	2.5
Multiplicity(max resolution)	1.5
Data/restraint/parameters	4646/494/540
R[I>2.0σ(I)]	0.2111
R(all data)	0.2603
Goodness of fit	2.352

B.2 X-Ray data for methylene-bridged phenylbutyl-footed cavitand 1 *(Ch. 4).*

Data were collected on a KappaCCD diffractometer . All diagrams and calculations were performed using maXus (Bruker Nonius, Delft & MacScience, Japan).[3]
Cell refinement: HKL Scalepack (Otwinowski & Minor 1997).
Data reduction: Denzo and Scalepak (Otwinowski & Minor, 1997).
Program(s) used to solve structure: *SIR*97(Altomare et al., J. *Appl. Cryst.*,1999).
Program(s) used to refine structure: *SHELXL*-97 (Sheldrick, 1997).

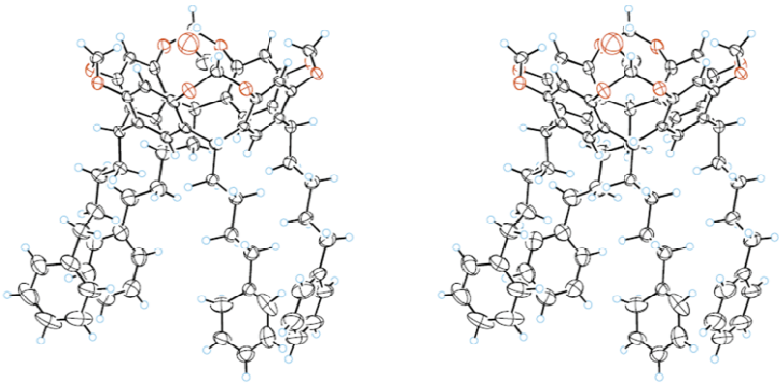

Figure 1: Single crystal view for target receptor **1**.

One heavily disordered residue refined over two positions. One disordered MeOH molecule in crystal structure. H-atoms of solvent not included.

Table 2: Crystal data and structure refinement information for the cavitand **1**.

Compound	**1**
Formula	$C_{73}H_{76}O_9$
Molecular weight	1097.40
Crystal system	Triclinic

Space group	$P\bar{1}$
a / Å	10.4857 (2)
b / Å	14.1656 (2)
c / Å	21.1231 (3)
α / °	108.5777 (7)
β / °	95.2911 (6)
γ / °	94.9210 (7)
V / Å^3	2939.26 (8)
Z	2
T / K	223
ρ / g cm^{-3}	not measured
D_x / mg m^{-3}	1.240
μ / mm^{-1}	0.080
θ / °	2.425-27.485
F(000)	1172
Cube	0.36 x 0.12 x 0.075 (mm)
fine-focus sealed tube	
Mo *Kα* radiation	λ = 0.71073
Cell parameters from	29683 refl.
Crystal color	Colorless

Data Collection

KappaCCD CCD diffractometer

Absorption correction:	none
Measured reflections	22999
Independent reflections	13472
Observed reflections	8691
Goodness–of–fit on F^2	0.999

Criterion:	> 2sigma(I)
θ_{max}/°	2.425-27.485
h	-13 →13
k	-18 →18
l	-27 →26
Refinement	
Refinement on F^2	fullmatrix least squares refinement
R(all)	0.1103
R(gt)	0.0677
wR(ref)	0.2033
wR(gt)	0.1789
S(ref)	1.177
Reflections	13472
Parameters	741
Restraints	11
H positions constr	
Calculated weights	$1/[\sigma^2(I_o)+(I_o+I_c)^2/900]$
Δ/σ_{max}	0.039
$\Delta\rho_{max}$	0.640eÅ^3
$\Delta\rho_{min}$	-0.518eÅ^3
Extinction correction:	none
Atomic scattering factors from:	International Tables Vol C Tables 4.2.6.8 and 6.1.1.4

B.3 X-Ray data for *meso*-metramethyldiphenylphosphonatecalix[4]pyrrole *(Ch.5).*

Crystal data and experimental details for data collection and structure refinement are reported in Table 3.

The crystal structures of isomers **2ii**, **2oo**, and **2io** were determined by X-ray diffraction methods. Intensity data and cell parameters were recorded at room temperature for **2ii** and for **2oo** and at 190 K for **2io**. The instruments used were a Bruker AXS Smart 1000 single-crystal diffractometer for **2ii** and **2io** and a Bruker Apex II single crystal diffractometer for **2oo** (employing a MoK_α radiation and a CCD area detector in all the three cases). The raw frame data were processed using SAINT and SADABS to yield the reflection data file.[4] For compound **2ii**, integration was carried out using the Apex II software suite, and the subsequent absorption correction was applied using the TWINABS[5] software package, leading to a twin4.hkl reflection file in which the Rint is equal to zero. The structures were solved by Direct Methods using the SIR97 program[3c] and refined on F_o^2 by full-matrix least-squares procedures, using the SHELXL-97 program.[3d,e]

The PLATON SQUEEZE procedure[6] was used for compound **2io** to treat regions of diffuse solvent which could not be sensibly modelled in terms of atomic sites. Their contribution to the diffraction pattern was removed and modified F_o^2 written to a new HKL file. The 90 electrons per unit cell thus locatedare included in the formula, formula weight, calculated density, μ and F(000). This residual electron density was assigned to four dichloromethane molecules per unit cell.

All non-hydrogen atoms were refined with anisotropic atomic displacements with the exception of two water molecules and one acetonitrile carbon atom in **2ii**, the acetonitrile molecules in **2oo** and the nitrogen atoms of the acetonitrile molecules in **2io**. The hydrogen atoms were included in the refinement at idealized geometry (C-H 0.95 Å) and refined "riding" on the corresponding parent atoms. The hydrogen atoms of the water molecules in **2ii** and of the OH group of the phenol in **2io** could neither be calculated nor located in the difference Fourier map.

The weighting schemes used in the last cycle of refinement were $w = 1/[\sigma^2F_o^2 + (0.1354P)^2]$, $w = 1/[\sigma^2F_o^2 + (0.1093P)^2]$ and $w = 1/[\sigma^2F_o^2 + (0.0140P)^2]$ where $P = (F_o^2 + 2F_c^2)/3$ for **2ii**, **2oo** and **2io** respectively.

Table 3: Crystal data and structure refinement information for isomers **2ii**, **2oo** and **2io**.

Compound	**2ii**	**2oo**	**2io**
Formula	$C_{62}H_{57}N_5O_8P_2$	$C_{64}H_{56}N_6O_6P_2$	$C_{74}H_{68}N_8O_7P_2$
Molecular weight	1062.07	1067.09	1243.3
Crystal system	Orthorhombic	Orthorhombic	Triclinic
Space group	*P*n2$_1$a	*P*2$_1$2$_1$2$_1$	*P*-1
a / Å	11.097(3)	16.273(2)	10.994(2)
b / Å	21.896(6)	17.889(2)	13.654(2)
c / Å	22.955(6)	19.236(2)	22.642(3)
α / °	-	-	88.100(3)
β / °	-	-	79.105(3)
γ / °	-	-	76.970(3)
V / Å^3	5577(3)	5599(1)	3251.4(8)
Z	4	4	2
T / K	293(2)	293(2)	173(2)
ρ / g cm^{-3}	1.265	1.266	1.270
μ / mm^{-1}	0.138	0.136	0.129
F(000)	2232	2240	1308
Data / parameters	7176 / 688	13752 / 681	14136 / 764
Total reflections	7176	36839	38933
Unique reflections (R_{int})	7176	13752 (0.0949)	14136 (0.1022)
Observed reflections [$I>2\sigma(I)$]	2802	5696	4340
Goodness–of–fit on F^{2a}	0.999	1.000	0.996

R indices [$I>2\sigma(I)$][b] R1, wR2	0.0916, 0.2269	0.0811, 0.1933	0.0657, 0.0978
Largest diff. peak and hole / eÅ^{-3}	1.528, -0.322	0.862, -0.330	0.494, -0.386

[a] Goodness-of-fit S = $[\Sigma w(F_o^2-F_c^2)^2/ (n-p)]^{1/2}$, where n is the number of reflections and p the number of parameters. [b]R1 = $\Sigma \| F_o | - | F_c \| / \Sigma | F_o |$, wR2 = $[\Sigma[w(F_o^2-F_c^2)^2]/\Sigma[w(F_o^2)^2]]^{1/2}$.

B.4 X-Ray data for 2ii•TMPCl complex *(Ch.5)*.

Crystal data and experimental details for data collection and structure refinement are reported in Table 4.

The crystal structures of complex **2ii•TMPCl** was determined by X-ray diffraction methods. Intensity data and cell parameters was recorded on a Bruker-Nonius diffractometer equipped with a APEX 2 4K CCD area detector, a FR591 rotating anode with MoKalpha radiation, Montel mirrors as monochromator and a Kryoflex low temperature device (T = 100 K).

The raw frame data were processed using SAINT and SADABS to yield the reflection data file.[4]

Crystal structure solution and refinement were carried out as implemented in SHELXTL Version 6.10[3d]. Refinement was also carried with the Multipol Refinement Programm XD 4.1.

All non-hydrogen atoms were refined with anisotropic atomic displacements. The hydrogen atoms were included in the refinement at idealized geometry (C-H 0.95 Å) and refined "riding" on the corresponding parent atoms.

The weighting schemes used in the last cycle of refinement was $\omega = 1/[\sigma^2F_o^2 + (0.105300P)^2 + 2.200900P]$, where $P = (F_o^2 + 2F_c^2)/3$.

Table 4: Crystal data and structure refinement information for complex **2ii•TMPCl**.

Compound	**2ii•TMPCl**
Formula	$C_{66}H_{64}N_4O_6P_3Cl_7$
Molecular weight	1349.8
Crystal system	Monoclinic
Space group	$P2_1/c$
a / Å	15.846(1)
b / Å	20.559(2)
c / Å	20.119(2)
β / °	102.535(2)
V / Å^3	6398.1(1)
Z	4
T / K	100(2)
ρ / g cm^{-3}	1.401
μ / mm^{-1}	0.124
F(000)	2800
Data / parameters	6363 / 813
Total reflections	8659
Unique reflections (R_{int})	6363
Observed reflections [$I>2\sigma(I)$]	5005
Goodness–of–fit on F^{2a}	0.998
R indices [$I>2\sigma(I)$][b] R1, wR2	0.0605, 0.0945
Largest diff. peak and hole / eÅ^{-3}	0.36, -0.312

[a] Goodness-of-fit S = $[\Sigma w(F_o^2-F_c^2)^2/ (n-p)]^{1/2}$, where n is the number of reflections and p the number of parameters. [b]R1 = $\Sigma \| F_o | - | F_c \| / \Sigma | F_o |$, wR2 = $[\Sigma[w(F_o^2-F_c^2)^2]/\Sigma[w(F_o^2)^2]]^{1/2}$.

References and Notes.

[1] (a) Z. Otwinowski, W. Minor, *Methods in Enzymology* (Eds. C. W. Carter, Jr. & R. M. Sweet) **1997**, New York:Academic Press, *276*, 307-326; (b) J. Navaza, *Acta Cryst. Sect. A,* **1994**, *50*, 157-163.

[2] DS viewerPro 5.0 *by* http://www.accelrys.com/com/about/msi.html.

[3] (a) S. Mackay, C. J. Gilmore, C. Edwards, N. Stewart, K. Shankland, *maXus Computer Program for the Solution and Refinement of Crystal Structures.* (Bruker Nonius), **1999**, MacScience, Japan & The University of Glasgow, The Netherlands; (b) C. K. Johnson, *ORTEP*-II. *A Fortran Thermal--Ellipsoid Plot Program. Report ORNL-5138.* **1976,**Oak Ridge National Laboratory, Oak Ridge, Tennessee, USA; (c) A. Altomare, M. C. Burla, M. Camalli, G. L. Cascarano, C. Giacovazzo, A. Guagliardi, A. G. Moliterni, R. Spagna, *J. Appl. Cryst.* **1999**, *32*, 115-119; (d) G. M. Sheldrick, *SHELXL*97. *Program for the Refinement of Crystal Structures*. **1997**, University of Göttingen, Germany; (e) G. M. Sheldrick, *Acta Cryst.*, **2008**, A64, 112.

[4] (a) *SADABS Bruker AXS*; **2004** Madison, Wisconsin, USA; (b) *SAINT, Software Users Guide, Version 6.0*; (c) Bruker AXS, *Software Users Guide, Version 6.0*; (d) *Bruker AXS* **1999**, Madison, WI, USA; (e) G. M. Sheldrick, *SADABS v2.03: Area-Detector Absorption Correction*. **1999**, University of Göttingen, Germany.

[5] *Bruker. TWINABS, Bruker AXS*, **2008**, Madison, WI, USA.

[6] SQUEEZE - P. v.d Sluis and A. L. Spek, *Acta Crystallogr., Sect A* **1990**, *46*, 194-201.

Appendix C
Additional Information for Ch.4.

NMR Experiments:

- **Titrations:**

Host was dissolved in acetone-d_6 (1.30 mL as received in ampoules from ARMAR Chemicals, 99.8 %D) or in $CDCl_3$ (1.30 mL as received in a 100 mL bottle from ARMAR Chemicals, 99.9 %D, stab. With Ag) or in DMSO-d_6 (1.30 mL as received in a 10 mL bottle from ARMAR Chemicals, 99.9 %D). Of these solutions, 0.50 mL were transferred into a new NMR tube, and $(CH_3)_4Si$ was added as an internal standard for chemical shift calibration. 0.60 mL of the remaining solution were used to dissolve the guest salts. Then, for each case, the solution containing the host only was titrated with the solution containing both host and guest. That way, the concentration of host remained constant during the course of the experiment. A ^1H NMR spectrum was recorded after each addition on a Varian Mercury 300 instrument. The temperature was held constant at 298 K. For ^{31}P NMR titration analogous procedure was followed. Association constants were obtained from a non-linear fitting of the experimental data. A series of 9-8 data points were recorded. The signal for cavitand H_{down} protons was monitored (δ).
The following equation was exploited to fit experimental data:[1]

$$\delta = \delta_H^0 + \frac{\delta_H^0 - \delta}{2[H_0]} * \left\{ [H_0] + [G_0] + \frac{1}{K_{ass}} - \sqrt{\left[\left([H_0] + [G_0] + \frac{1}{K_{ass}} \right)^2 - 4 * [H_0] * [G_0] \right]} \right\} \quad \textbf{eq. (1)}$$

In equation (1), δ is the chemical shift observed for H_{down} protons, δ_{H0} is the chemical shift for these protons in the free host, $[H_0]$ and $[G_0]$ are

the initial concentrations of host and guest, respectively. Since all these parameters are known, the association constant K_{ass} remains the only unknown, and hence it can be determined with high accuracy by this method.
Instead of using dedicated software (such as the package provided by Hunter),[2] the obtained data was directly evaluated with equation (1) using the curve fitting toolbox of Matlab.[3] This approach is more transparent, and, in fact, proved to be more time-efficient.
A fitting example was reported below (receptor **1**•TBAC in acetone-d_6 case).

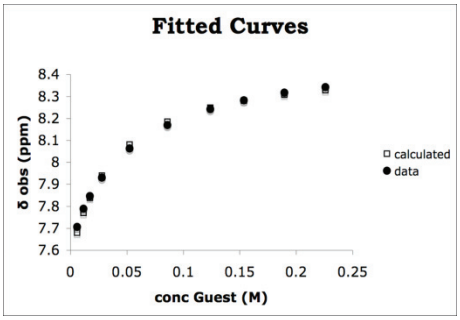

Figure 1: Calculated (□) and experimental (•) data points for titration of receptor **1** with TBAC.

Each reported K_{ass} value resulted from the average of two or three independent measurements. Standard deviation was calculated according equation (2):

$$\delta = \sqrt{\frac{\sum (\bar{x} - x_i)^2}{n-1}}$$

Eq. 2

In equation (2), δ is the standard deviation, $\bar{x}$ is the average value, x_i is the value recorded for each experiment, and n is the number of performed experiments.

- **Job Plot:**

Seven samples of different mole fractions of host and guest (c = 0.1 ... 0.9, [host] + [guest] = 3 mM) were prepared in acetone-d_6 or $CDCl_3$ and the chemical shift for the cavitand H_{down} protons was evaluated by ^1H

NMR (Varian Mercury 300 MHz, 298 K). Figure 2 reports an example of the obtained plot.

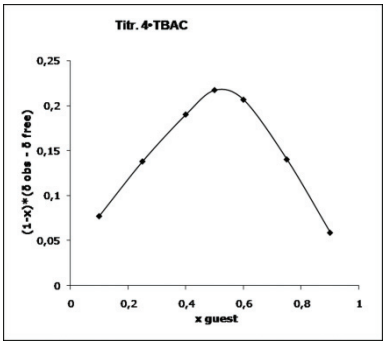

Figure 2: Example of obtained Job Plot for cavitand **4**•TBAC complex formation in acetone-d_6.

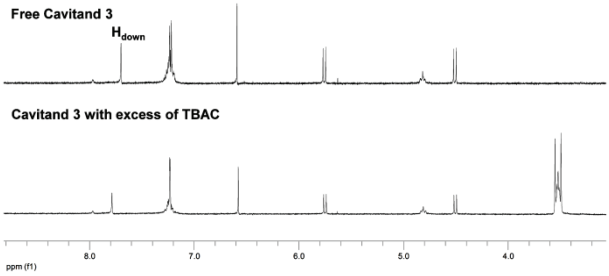

Figure 3: Partial ^{1}H NMR spectra in acetone-d_6 for titration of cavitand **3** with TBAC.

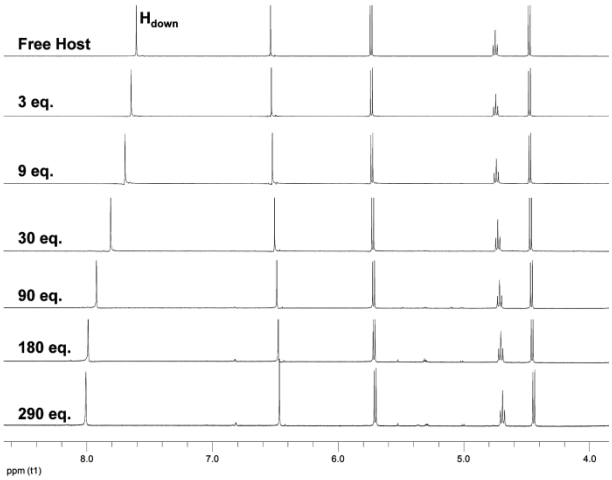

Figure 4: Partial ^{1}H NMR spectra in acetone-d_6 for titration of cavitand **2** with TBAC.

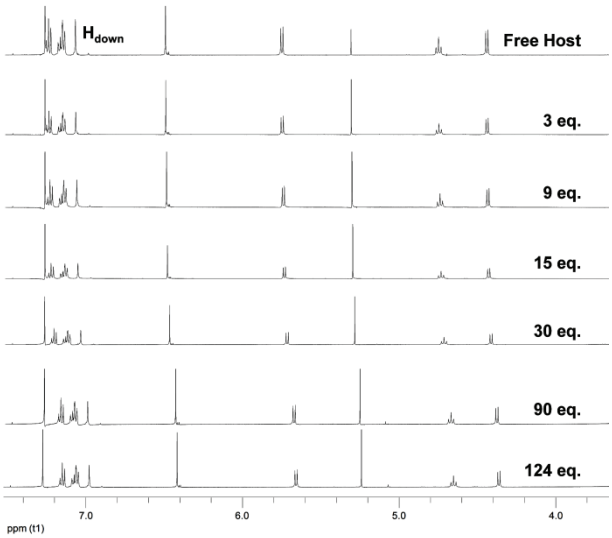

Figure 5: Partial ^{1}H NMR spectra in $CDCl_3$ for titration of cavitand **1** with TBAC.

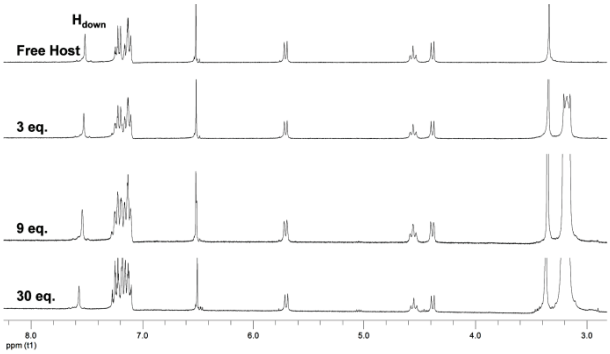

Figure 6: Partial ^{1}H NMR spectra in DMSO-d_6 for titration of cavitand **1** with TBAC.

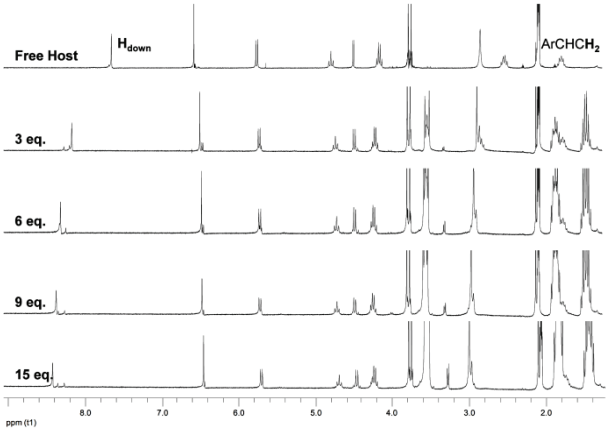

Figure 7: Partial ^{1}H NMR spectra in acetone-d_6 for titration of cavitand **4** with TBAC.

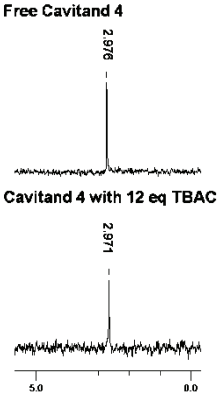

Figure 8: ^{31}P NMR spectra in acetone-d_6 for titration of cavitand **4** with TBAC.

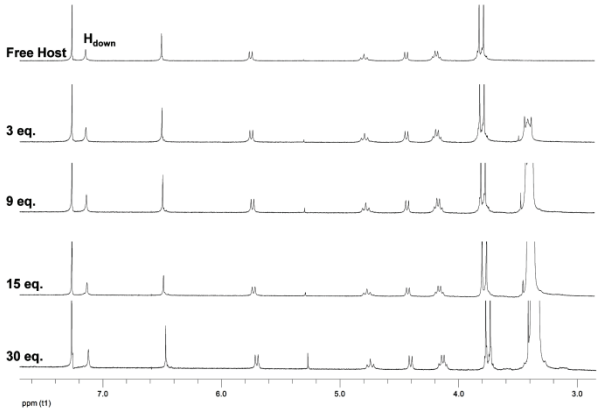

Figure 9: Partial ^{1}H NMR spectra in $CDCl_3$ for titration of cavitand **4** with TBAC.

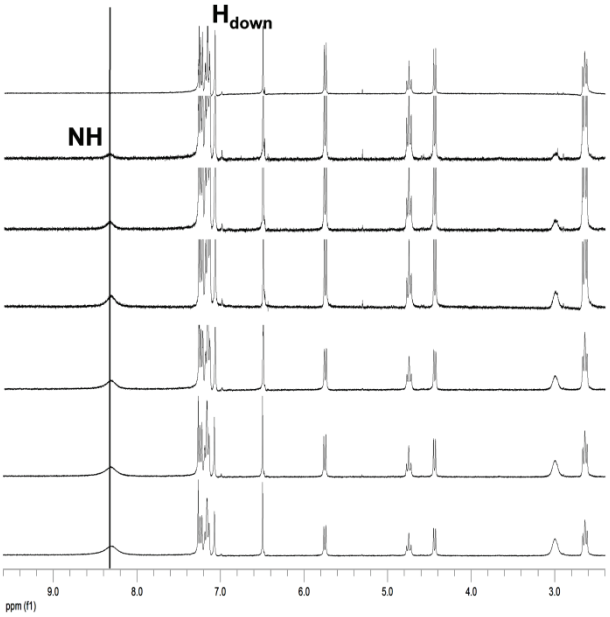

Figure 10: Partial ^{1}H NMR spectra in $CDCl_3$ for titration of cavitand **1** with octylammonium chloride.

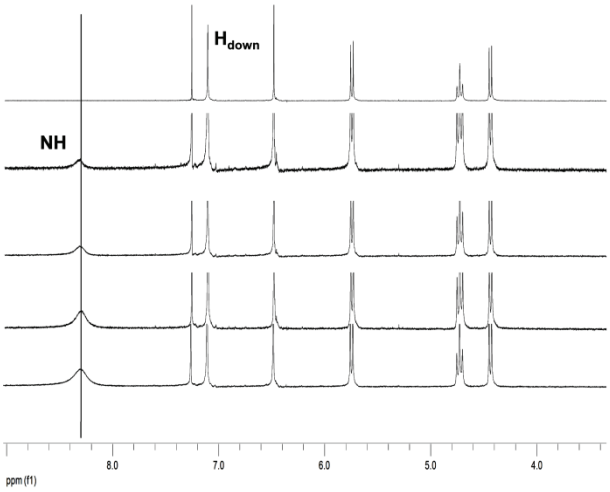

Figure 11: Partial ^{1}H NMR spectra in $CDCl_3$ for titration of cavitand **2** with octylammonium chloride.

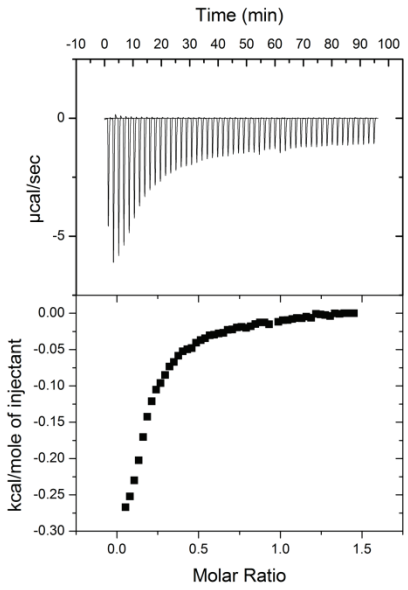

Figure 12: Representative ITC trace obtained for titration of cavitand **4** with octylammonium chloride.

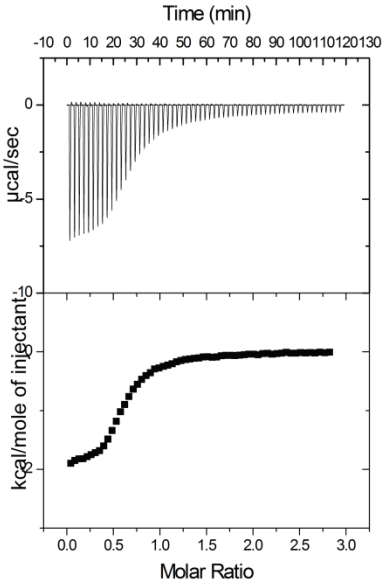

Figure 13: Representative ITC trace obtained for titration of cavitand **4** with octylammonium bromide.

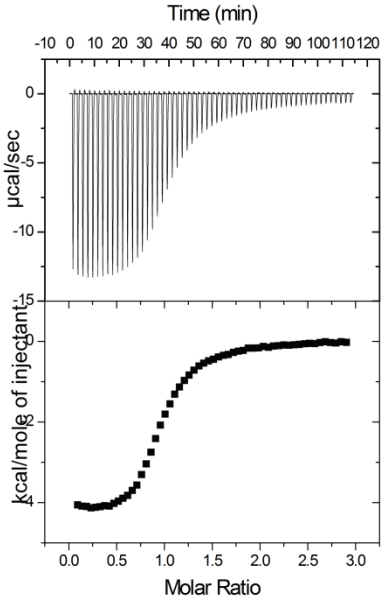

Figure 14: Representative ITC trace obtained for titration of cavitand **4** with octylammonium iodide.

References and Notes.

[1] J. L. Atwood, J. E. D. Davies, D. D. MacNicol, F. Vögtle, J.-M. Lehn in *Comprehensive Supramolecular Chemistry*, vol. 8, (Eds. J. E. D. Davies, J. A. Ripmeester), **1989**, PERGAMON.

[2] (a) A. P. Bisson, C. A. Hunter, J. C. Morales, K. Young, *Chem. Eur. J.* **1998**, *4*, 845-851; (b) C. A. Hunter, *NMRTit HG*, **1998**, University of Sheffield, Sheffield, UK.

[3] *Matlab, version 7.0*, Schrödinger LLc, **2007**, New York, NY ,USA.